Title

Studies of Unimolecular and Bimolecular Reaction Dynamics Via the Molecular Beam Technique

Author

Covinsky, M.H.

Publication Date

1990-11-01

LBL-29950

Lawrence Berkeley Laboratory
UNIVERSITY OF CALIFORNIA

Materials & Chemical Sciences Division

Studies of Unimolecular and Bimolecular Reaction Dynamics Via the Molecular Beam Technique

M.H. Covinsky
(Ph.D. Thesis)

November 1990

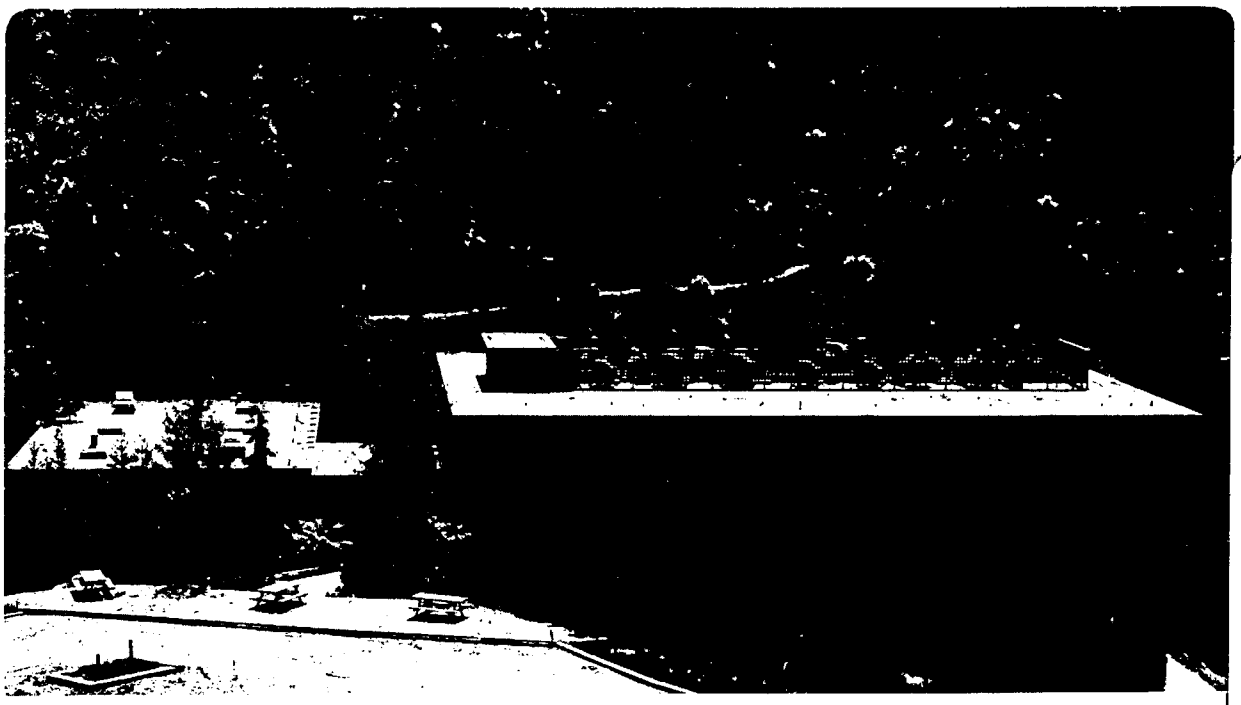

Prepared for the U.S. Department of Energy under Contract Number DE-AC03-76SF00098.

DISCLAIMER

LBL-29950

STUDIES OF UNIMOLECULAR AND BIMOLECULAR REACTION DYNAMICS VIA THE MOLECULAR BEAM TECHNIQUE

Michael Harvey Covinsky

Department of Chemistry
University of California

and

Chemical Sciences Division
Lawrence Berkeley Laboratory
Berkeley, CA 94720 USA

November 1990

This work was supported by the Director, Office of Energy Research, Office of Basic Energy Sciences, Chemical Sciences Division, of the U.S. Department of Energy under Contract No. DE-AC03-76SF00098.

Studies of Unimolecular and Bimolecular Reaction Dynamics via the Molecular Beam Technique

Michael Harvey Covinsky

Lawrence Berkeley Laboratory

and Department of Chemistry

University of California

Berkeley, California 94720

Abstract

Crossed atomic and molecular beams have been used to study the reaction dynamics of ground state and excited sodium atoms. The wide variety of systems studied allows us to make some broad generalizations about the effect of electronic excitation upon the reactivity of sodium atoms.

Crossed molecular and atomic beams have been used to study the photodissociation of NO_2Cl. Insights have been gained into the electronic structure and dynamics of the excited state of this molecule.

Chapter 1 describes the reaction of ground state sodium with ozone at a collision energy of 18 kcal/mole. This reaction occurs via the electron jump mechanism to give forward scattered NaO as a product. The NaO is

formed with a great deal of internal energy. No evidence is seen for NaO_2 formation.

Chapter 2 presents measurements of ground state and excited methyl iodide. This reaction proceeds via the rebound mechanism to produce sodium iodide. The product is back-scattered. Electronic excitation results in an increase in the differential cross section at less backward angles. The extra energy goes into NaI rotation and vibration.

Chapter 3 discusses all the electronically excited sodium atom experiments done in this laboratory. It is demonstrated that examination of electron scattering provides an elementary basis on which to make qualitative predictions of the results of electronically excited sodium reactions. Predictions based on this model are made for systems not yet studied.

Chapter 4 reports the results of the photodissociation of NO_2Cl at 248 and 308 nm. At 248 nm excitation creates a charge transfer state that predissociates mostly to Cl atom and NO_2 in the ground or excited states. The 308 nm transition is centered on the NO_2 group and is vibrationally mediatiated by an out of plane bend. The main products are Cl atom and NO_2 in the ground or B^2B_1 excited state.

Table of Contents

Abstract 1

Acknowledgements v

Chapter 1 The Reaction Dynamics of Sodium with Ozone

A. Introduction 1

B. Experimental 4

1. Primary Source 5

2. Secondary Source 11

3. Data Acquisition 13

C. Results and Analysis 14

D. Discussiion 18

E. Conclusions 23

F. References 24

G. Tables 28

H. Figure Captions 30

I. Figures 32

Chapter 2: The Reaction of Ground State and Excited Sodium Atoms with Methyl Iodide

A: Introduction 43

B: Experimental 48

1: Beam Sources 48

2: Optical Pumping 49

3: Data Acquisition 51

C: Results and Analysis 52

D: Conclusions 56

E: References 58

F: Tables 64

G: Figure Captions 66

H: Figures 69

Chapter 3 Predicting the outcome of Excited State Sodium Reactions

A: Introduction 85

B: Comparison of Reactive and Electron Scattering Data 88

C: Predictions 93

D: Conclusions 97

E: Tables 99

F: References 103

Chapter 4 Photodissociation odf NO_2Cl at 248 and 308 nm

A: Introduction 106

B: Experimental 112

C: Results and Analysis

1: 248 nm 114

2: 308 nm 120

D: Conclusions 121

E: References 123

F: Tables 128

G: Figure Captions 132

H: Figures 137

Acknowledgements

One dictionary definition of acknowledgement is a recognition of something received. In writing this I am supposed to reduce to a few words what someone has meant to me or done for me and how it was important in my getting my Ph.D. Since I do not possess the poet's ability to describe my thoughts and feelings eleoquently and compactly I cannot do justice to the purpose of this section. I can only offer some poor expression of the love I feel for my family, the value I place on the friendships I have made in Berkeley, and the gratitude I feel for the things people have taught me that make me a better scientist and person.

The center of my scientific universe at Berkeley was Yuan T. Lee. There is nothing I can say about his scientific ability, his encyclopedic knowledge of experimental methods, and the inspiration he provides his graduate students that has not already been said. I can only add that among those who know him here at Berkeley, he is held in as much esteem for his personnal qualities as he is held elsewhere for for his scientific ones.

Since I have joined the group the A-Team has been populated by a number of curious inhabitants. Matt Vernon and Hartmut Schmidt broke me in on laser techniques and the workings of crossed molecular beam machines. Paul Weiss laughed at all my jokes. I benefitted from many useful conversations on many subjects with Jean-Michel Mestdagh including

atomic polarization and electron scattering. Barbara Balko joined the experiment and worked on the NO_2 experiments and packed the laboratory up on our own when we were the surprise choice to be the second experiment to move to move to campus. Floyd Davis helped me set up and run the photodissociation experiments and did an outstanding job drafting the drawings for the new seeded high-temperature supersonic metal atom source. Arthur Suits helped me with the ozone experiments and provided a sounding board for my ideas about electron transfer and metal atom dynamics. Hongtau Hou joined the experiment after I started writing my thesis so I have not had the opportunity to work with him but I have seen enough to know that the future of the A-Machine is in very capable hands.

I owe much to other members of the Lee group. I had many interesting conversations wit my office-mates Lisa Yeh and Xinsheng Zhao. Laurie Butler returned after her post-doc and helped get us established on C-level. Rick Brudzynski led us to the all-important chem-league softball championship. Tom Turner and Doug Krajnovich saw to it that I had a proper introduction to the methods of the Lee group. I was the beneficiary of many useful conversations with Gil Nathanson when we started work on photodissociation. I also benefitted from many conversations with Anne-Marie Schmoltner on the idiosyncracies of rotating detector machines. Eric Hintsa was a part of my semi-regular bridge group. Pam Chu and then

James Chesko set up and ran our computer systems. Captain John Price and Jim Myers helped me learn Word-Perfect so I could write this. Bob Continetti deserves special mention for the yeoman work he did in organizing the group's move to campus.

Outside the group I would like to thank John Tromp for helping me through the more obscure parts of quantum mechanics. Daniel Oh of the Johnston group synthesized and purified the NO_2-X compounds used in the photodissociation. Both he and Wade Sisk participated in the photodissociation experiments.

I could not have gotten anything done without the assistance of the LBL and department of chemistry staff. Foremost is the incomparable Ann Weightman. She is the main line of defense against the twin evils of paperwork and bureaucracy. Her knowledge of the dark underside of LBL society saved me countless times. Her assistance in getting my jobs back from the glass shop in a timely fashion is especially appreciated. Tony Moscarelli, formerly of the building 70 student shop, taught me most of what I have forgotten about machining. There were many times when something would break late at night and Tony would ride to the rescue. Fred Vogelsberg and Ed Arnold of the Building 70 electronics shop kept some of our more rickety home-built electonics modules in good working order. Fred Wolfe and Andy Anderson of the chemistry department machine helped me eliminate some of my more naive mistakes in the jobs I

designed. Will Lawrence and Bill Willkie would do our emergency ceramics work with a smile. Finally "Harry" Chiladakis saw to it that we got the electrical, plumbing and other neccesities that we required to get our lab up and running when we moved to campus.

Professor Kelsey Cook gave me my introduction to chemical-research. His encouragement of a hopelessly naive kid just barely out of freshman chemistry is warmly remembered. I had the good fortune to take two high school chemistry courses from Mr. Frank Cardulla. His dedication and enthusiasm for teaching is a large part of the reason I chose to become a chemist.

I appreciate those friends from outside of science who have given me things beyond the ability of a list to enumerate. Josh and Debbie Burton gave me a reminder of home cooking. Josh, Debbie, Dave Brahm, Eric Hintsa, and later Nike Agman and Chad Nelson provided me with many pleasant hours of bad jokes and worse bridge. I should offer some words of encouragement. With just a more few years of practice and study you might be almost as good as I am now.

My grandparents Milton and Hannah Hirsch, Dianne Shatz and Howard Covinsky have always been role models to me. I try to keep their generosity and selflessness in mind. My brother Ken and my sister Maureen through the insults and the yelling and screaming have always supported me and are my best friends.

This work was supported by the Director, Office of Energy Research, Office of Basic Energy Sciences, Chemical Sciences Division, of the U.S. Department of Energy under Contract No. DE-AC03-76SF00098.

This thesis is dedicated to my parents Marvin and Florence Covinsky who have always had faith in me.

Chapter One

The Reaction Dynamics of Sodium with Ozone

Introduction

The reaction of sodium atoms with ozone has been used to model the sodium D line nightglow in the mesosphere and in persistent meteor trains.[1-9] Chapman[1] proposed in 1938 that this reaction was the first step of a two step catalytic mechanism to explain the origin of the nightglow.

$$Na_{(g)} + O_{3(g)} \rightarrow NaO_{(g)} + O_{2(g)} \quad \Delta H_0^0 = -35 \text{ kcal/mole} \quad (1)^{10}$$

$$NaO_{(g)} + O(^3P) \rightarrow Na(3^2P) + O_{2(g)} \quad \Delta H_0^0 = -10 \text{ kcal/mole} \quad (2)^{11}$$

$Na(3^2P) \rightarrow Na\ (3^2S) + h\nu\ (589\ nm)$

For many years the lack of accurate rate constant data hampered the modeling of the sodium layer.[6] Attempts were made to estimate a rate constant based on the $H + O_3$ reaction.[7,8] The rate constant of 6.5×10^{-12} cm^3/sec is too small to allow the Chapman mechanism to be valid. If the rate constant were this small then the three body recombination reaction

$$Na + O_2 + M \rightarrow NaO_2 + M \quad k = 5 \times 10^{-30}\ cm^6/sec^{[12,13]} \quad (3)$$

would provide a major sink for Na. Additionally, incorrect rate constants lead to errors in the prediction of the height of the sodium layer and in the seasonal variation of the atmospheric sodium concentration. It was not until 1975 that Kolb and Elgin[14] pointed out that sodium can react via a long range harpoon mechanism. Using a sodium atom ionization energy of 5.14 eV and an ozone electron affinity of 1.99 eV they calculated a cross-section of $65 Å^2$ for reaction (1) and a corresponding rate constant of 3.3×10^{-10} cm^3/sec at a temperature of 185°K.

The first gas phase measurement of the rate constant was performed by Husain, Marshall, and Plane in 1985.[15] In this experiment the resonance absorption of sodium was monitored following the pulsed

irradiation of NaI in the presence of ozone. They obtained a value of k = 4(+4,–2) x 10^{-10} cm^3/sec for reaction 1.

In 1986 Silver and Kolb[16] used fast flow cell methods to measure the rate constant. Briefly 10^{-4} torr of sodium vapor is generated in an oven and entrained in a helium flow. This mixture is introduced into a flow cell. Ozone is added downstream and the concentration of sodium is monitored by resonance fluorescence or laser induced fluorescence. A value (3.1 ± 0.4) x 10^{-10} cm^3/sec at 295°K was found, in good agreement with the expected harpoon mechanism value.

Using similar methods Ager, Talcott, and Howard[17] derived a rate constant of (7.3 ± 1.4) x 10^{-10} cm^3/sec at 286°K. They also measure a lower limit of 0.95 for $k_1/(k_1 + k_2)$. No explanation is given for this disagreement. However, it is interesting to note that both groups report the same total rate constant for the reaction

$$NaO + O_3 \rightarrow Na + 2O_2 \quad (4)$$

$$\rightarrow NaO_2 + O_2 \quad (5)$$

of 2 x 10^{-10} cm^3/sec which agrees with the harpoon model prediction in which the ionization potential of NaO is 6.5eV.[18]

This chapter presents a crossed molecular beam study of the Na + O_3 reaction. Center of mass angular and translational energy distributions for the products are derived. These distributions are used to understand the dynamics of this reaction.

Experimental

These experiments were carried out in a crossed molecular beams machine that has been described previously.[19-22] A supersonic beam of sodium atoms is crossed orthogonally by a supersonic beam of ozone under single collision conditions at a 3mm x 3mm x3mm collision volume. The collision chamber is liquid nitrogen cooled and pumped to 1 x 10^{-7} torr. (Fig. 1) Product is observed by a triply differentially pumped quadrupole mass spectrometer which has an electron bombardment ionizer and Daly detector. The mass spectrometer rotates in the plane defined by the two beams. A recent change in the detector pumping scheme is that the ion pumps have been removed from all three regions. The Leybold-Heraeus TMP 360 turbomolecular pump that was formerly on region 3 now pumps region 1. Region 2 is pumped by a Seiko-Seiki STP400 a 420 liter/second magnetically suspended turbomolecular pump. Region 3 is pumped with a similar STP300 340 liter/second turbomolecular pump. The replacement of old ion

pumps with pumps that are both cleaner and have a higher pumping speed produces a large decrease in background at masses that correspond to water or to permanent gases i.e. m/e=16,17,18,20,28,32 and (especially important for this experiment) m/e=40.

Another step taken to reduce the detector background is the installation of a copper cold-finger with its base attached to the liquid nitrogen cold shield. The cold finger is positioned so that the detector always views a surface that is at liquid nitrogen temperature. This cuts down on the "straight through" background that arises when a molecule scatters off the surface opposite the detector and passes through all three regions of differential pumping and is ionized in the ionization region. These changes produced a large reduction in the background at m/e=39 (NaO^+). A quantitative measure of the reduction was not possible as a different High-Q head for the quadrupole mass spectrometer was used after the new turbos were installed. However, before the turbos were installed it was not possible to take time of flight data at m/e=39 at angles greater than 20°.

Primary Source

The source of the sodium beam is a resistively heated molybdenum oven that will be described in detail in a later publication.[23] (Fig. 2) As in

the previous stainless steel oven the new oven is divided into three parts.[22] The inlet is a 9 inch long molybdenum tube with an outer diameter of 0.375 inches and an inner diameter of 0.325 inches. A 0.28 inch long molybdenum flow constrictor with a 0.005 inch clearance is placed inside this tube about 0.5 inches from the entrance to the reservoir. This flow constrictor is necessary in order to prevent sodium from backstreaming into the inlet tube and clogging it. The constrictor is held in place by a 0.030 inch tantalum wire that runs the length of the inlet tube and ends in a hook at the inlet tube entrance.

The reservoir consists of two concentric cylinders. The outer one is 2.8 inches long with a 1.75 inch diameter and a 0.30 inch wall thickness. The inner one is 2.6 inches long and has a 1.50 inch diameter. Two 0.031 inch thick semicircular plates are welded to the inside of the inner cylinder at the ends to contain the sodium. This double cylinder wall design serves to ensure that the sodium reservoir is uniformly heated and is the coldest part

of the oven.

The inner nozzle tube is 2.50 inches long with a 0.25 inch diameter and has a 0.050 inch wall. It is concentric with the inlet tube and reservoir. A nozzle cap with a 30° mating surface is welded onto the end of the tube. The nozzle diameter is .008 inches.

The entire oven assembly is designed so as to permit the oven to be removed and replaced without the necessity of realigning the entire source. This is accomplished by rigidly mounting the outer nozzle tube in place. The outer nozzle tube is a 2.00 inch long molybdenum tube with an outer diameter of 0.50 inches and a wall thickness of 0.062 inches. The last 7/16 inches of the outer nozzle is turned down to a diameter of 0.440 inches to ensure that the nozzle tip is the hottest part of the oven. A cap welded to the end of the outer nozzle tube has a 30° mating surface for the inner nozzle tube. A 0.25 inch thick 1.368 inch x 1.250 inch tantalum plate is welded 0.50 inches from the base of the outer nozzle. This plate is bolted to a water cooled copper electrode which is in turn bolted to the aluminum support assembly. The electrode is electrically insulated from the support assembly by alumina spacers and screw collars. The back of the inlet tube is supported by two brackets. These brackets are electrically and thermally insulated by ceramic collars which have a 0.003 inch clearance around the inlet tube. These collars effectively eliminate the transverse movement of the oven. The entire oven is pressed forward by a spring loaded clamp. This forces the inner nozzle tube against the outer nozzle tube and maintains electrical contact and beam alignment through multiple heating and cooling cycles. The second water cooled electrode is just upstream of this clamp. The circuit through the oven can be pictured as going from the

inlet electrode through the inlet tube, the outer cylinder of the reservoir, the inner nozzle, the outer nozzle and the nozzle electrode. The large thickness of the reservoir wall as well as its large radiative area ensures that resistive heating alone will heat the inlet tube and the nozzle more than the reservoir. The temperature of the reservoir can be increased by a radiative graphite heater that surrounds the reservoir. It was not necessary to use the graphite heater for the sodium experiments. Typical oven conditions for sodium were 350 amps at 1.34V a.c. The temperature of the nozzle and reservoir were measured with an optical pyrometer. The temperature of the nozzle was 1100°C and the temperature of the reservoir was 700°C. At this reservoir temperature the vapor pressure of sodium is about 80 torr.

The oven is typically backed with 500 torr of ultrahigh purity helium (99.999%). The Na-He mixture is expanded through the nozzle into the primary source chamber. The chamber is maintained at 2×10^{-4} torr. The mechanical pump which used to back the primary source diffusion pump has been replaced with a SM42/5-50 Leybold-Heraeus roots blower which allows us to use the high backing pressure behind the nozzle.

After the expansion the beam passes through a molybdenum skimmer which is 0.30 inches downstream of the nozzle. The skimmer tip has a diameter of 0.030 inches. The skimmer is heated to 700°C conductively by passing current through four 3/16 inch diameter tantalum rods which pass

through the body of the skimmer. The typical current and voltage is 95 amps at 2.2V a.c. The rods are electrically insulated from the skimmer by alumina tubes.

After the skimmer the beam passes through a differential pumping region which is pumped to 2×10^{-6} torr. The beam then passes into the collision chamber through a collimating slit. The slit is made from four razor blades spot-welded together. These slits define the beam to be 3mm wide by 3mm high at the interaction region. The new oven is an improvement on the old oven in several respects. Most important is the quality of the sodium beam. Using molybdenum instead of stainless steel allows us to run the oven at a higher temperature. This leads to an order of magnitude increase in beam intensity. The higher backing pressures cut the beam spread by almost a factor of two.

The new oven can be run more reliably. The higher temperature used at the nozzle helps prevent sodium and slightly volatile sodium salts from clogging the oven. Additionally molybdenum is much more resistant to corrosion by sodium than is stainless steel.[24,25]

The new oven is easier to use. Previously it was necessary to remove the entire oven assembly whenever the oven was removed. This necessitated completely realigning the source, a time consuming and often

frustrating process. The new oven can be removed even without pulling the source chamber from the machine.

The stainless steel oven could only be used for volatile metals such as alkali metals and mercury. Extensive experiments have been done on the reaction dynamics of barium atoms using this oven. Also seeded beams of transition metals can be created if the oven is made with a boat of the appropriate ceramic material is sealed inside.[26] Beams of manganese and copper have already been made.

There are two drawbacks of this oven as compared to the steel oven. Firstly a full charge of sodium lasts 10-12 hours as compared to 150 hours for the steel oven. However since the beam intensity is now much higher this is enough time to do a complete run on the experiment. Also since the turnaround time is short as discussed above this is not as serious a burden as it would have been before. Secondly molybdenum recrystallizes once it is heated up. This makes the oven very brittle and extremely sensitive to mechanical stresses. This is not a problem if ordinary care is used. More serious is that over the long term the oven tends to develop holes and cracks. Although these can be patched by welding, eventually the nozzle has to be cut off and replaced. It is possible that even this problem can be eased by using annealing techniques.

Secondary Source

The secondary source has been described in great detail previously.[21,22] Briefly it is a stainless steel tube wrapped in heating tape. (Fig. 3) At the end of the tube is a 70 micron platinum electron microscope aperture. This is held and sealed in place with a stainless steel screw-cap and a copper gasket. The source is aligned by a "bird-cage" which keys into place. The temperature is controlled by a copper block heater with thermal coaxial cable hard soldered on. The temperature of the nozzle is measured by a chromel-alumel thermocouple referenced to an ice water bath. The nozzle temperature used in these experiments was 150°C.

The ozone used in this experiment was generated by an OREC model number 03V1-0 auto ozonator and held in a silica gel trap cooled in a dry ice/acetone slush. The trap was transferred to an FTS Systems Multicool model number MC-4-60A-1 constant temperature bath and the gas mixture was generated by passing helium through the trap kept at -77°C. The ozone concentration was monitored by passing the gas mixture through a 1 cm quartz cell and measuring the absorption at 280 nm. This wavelength was chosen rather than the peak of 254 nm. because the gas mixture was too opaque at this wavelength. No attempt was made to remove trapped oxygen. However, since there is not enough energy for O_2 and Na to react

at the beam energies used this was not a problem. The total stagnation pressure of the beam was 240 torr and the mole fraction of ozone behind the nozzle was 0.12. The concentration of ozone was kept constant by adjusting the temperature of the constant temperature bath and continually monitoring the absorption through the quartz cell. The partial pressure of ozone was constant to within ±3% of the mean value. More importantly time of flight measurements of the velocity distribution of the beam taken with the ozone concentration at the extremes of ozone concentration allowed during the experiment varied by ±1% from the mean. The gas mixture was expanded into the source chamber which was maintained at 2×10^{-4} torr. The beam was skimmed by a .023 inch skimmer. After passing through the skimmer the beam entered a region of differential pumping which was typically maintained at $1\text{-}3 \times 10^{-7}$ torr. The beam was modulated by a 150 Hz. tuning fork chopper (Bulova) for the angular distribution experiments. The chopper was attached to a water cooled copper block that was mounted on the front face of the secondary source. The beam passes from the differential region into the main chamber through collimating slits. These slits define the beam to be 2.8 mm high and 2.1 mm wide when the beam reaches the collision region.

Data Acquisition

Data is acquired with programs run on an LSI-11/23 computer interfaced to a camac crate.[22] There are two types of experiments performed to paint a complete picture of the reaction dynamics. The first type of experiment is the measurement of the product angular distribution. In this experiment the ozone beam is modulated by the 150 Hz tuning fork chopper on the secondary source. The pulses from the detector are filtered by a quad discriminator (Lecroy model 821) and from there fed into a quad scaler. (Joerger model S1). Two types of signal are measured, the total signal with the ozone beam blocked and the total signal with the ozone beam unblocked. The gating is provided by a waveform taken from the chopper. Signal is measured with the detector kept at a particular angle for 80 seconds. The signal at a particular angle is simply the counts with the chopper open minus the counts with the chopper closed. At the end of the countdown interval the detector is moved to the next angle in sequence. The angular range for this measurement was −15° to −10° and 15° to 80° in 2.5° degree steps where 0° is looking straight into the sodium beam and 90° is looking straight into the ozone beam. To correct for long-term drifts the detector is moved to 30° degrees after every 10 measurements and data is taken at this angle twice. The data can then be normalized by taking a linear

interpolation based on the time a given angle is measured and the time between normalization measurements.

The second type of experiment is the time-of-flight measurement of the velocity distribution of products. In this experiment a cross-correlation wheel with two identical 255 bit sequences is mounted in front of the detector and spun at 392 Hz.[27-29] The wheels were photoetched by PCM Products based on artwork drawn for Lee group specifications. These wheels give a resolution of 5 microseconds in the flight time of the reaction products. The detector is stationed at a particular angle for about 15 minutes to measure reaction product flight times. Data is accumulated for at least a total of one hour at all angles measured.

Beam velocity profiles are also measured with the time of flight technique however, single-shot wheels are used. The peak velocities and beam spreads of the sodium and ozone beams are listed in table 1.

Results and Analysis

Angular and time of flight distributions were recorded at a collision energy of 18 kcal/mole. The newton diagram for this collision energy is shown in figure 4. The angular distribution (Fig. 5) is very broad and peaked forward of the center of mass. This angular distribution was recorded at m/e = 39 which corresponds to NaO^+ thus unambiguously

identifying the signal as being the result of reactive scattering. The signal is strong at all angles. This distribution is diagnostic of a long range electron transfer with the forward scattering of the NaO product.

The time of flight distributions at m/e=39 are shown in figure 6. The distributions are fit using program GM an updated version of program CMLAB.[30] This program fits the data using the forward convolution method. It is assumed that the center of mass product flux distribution can be expressed as a product of P(E), the center of mass translational energy distribution and T(θ), the center of mass angular distribution. P(E) and T(θ) are assumed to be independent of each other. The program uses these input distributions to calculate time of flight and angular distributions averaging over the two beam velocity and angular spreads and the ionizer length. Both distributions are adjusted to get the best fit between the measured and calculated energy and angular distributions.

The P(E) and the T(θ) used to fit the data are shown in figures 7 and 8. One feature of the P(E) that becomes apparent is the unusual behavior at low translational energy. The distribution looks as if it has been cut away. The explanation is that we are detecting a diatomic product with a fragmentation ratio $I(NaO^+)/I(Na^+)$ that is very sensitive to the internal energy of the NaO product. Since NaO usually fragments to Na^+ upon ionization a small change in the fragmentation ratio will produce a large

change in the intensity of NaO^+ detected. We assume in fitting the data that $I_{cm}(\theta,E) = P(E)\times T(\theta)$. However since fragmentation is important this is properly written

$$I_{cm}(m,\theta,E) = [F_m(E)\times P(E)]\times T(\theta)$$

where $F_m(E)$ is the ratio of the number of ions produced at fragment mass m to the total number of product molecules ionized as a function of the total relative translational energy of the products. In writing this equation an extra assumption is made in addition to the usual one about the separability of P(E) and $T(\theta)$. The extra assumption is that for a given relative translational energy E the state distributions of the products do not change drastically as a function of the center of mass angle θ such that the fragmentation ratio will be angular dependent. If for example NaO were backscattered with relative translational energy E and all the available internal were in NaO vibration, then it would be expected that NaO ionization would strongly favor Na^+ production. If NaO were forward scattered with the same relative translational energy but the internal energy of NaO is much less with most of the internal energy stored in O_2 then NaO ionization would produce more NaO^+ than in the previous example. It is likely that any such breakdown in this assumption would also accompany a corresponding breakdown in the separability assumption. Therefore, it is unlikely that, for a given translational energy, there are

large enough differences in the NaO quantum states produced as a function of the center of mass angle to cause a significant additional error.

To measure $F_m(E)$ times of flight were taken 45° at both m/e=23 and m/e=39. This angle was chosen for two reasons. First this angle is very close to the center of mass and therefore times of flight taken at this angle sample the entire range of translational energies down to below one kcal/mole. Second this laboratory angle corresponds to a wide center of mass scattering angle for the elastic scattering of sodium off ozone. This wide scattering angle would require a low impact parameter collision. Since it is known that this reaction has a very large cross-section as discussed in the introduction, these low impact parameter collisions will most likely lead to reaction rather than elastic scattering. Therefore the m/e=23 time of flight at 45° contains negligible contribution from elastic scattering.

The times of flight at 45° were taken at by alternating between m/e=23 and m/e=39 after short intervals. The quadrupole resolution was set low to ensure that the transmission function was the same at both masses. The time of flight spectra were normalized to their counting time and added. The m/e=23 times of flight had to be shifted to be five microseconds slower to account for the different ion flight times. The resulting sum is shown in figure 9. The $T(\theta)$ is derived from the m/e=39 data. The P(E) derived is shown in figure 10. The salient features of this

distribution are shown in table 2. The integrated intensities of the normalized m/e=23 and m/e=39 times of flight were used to normalize the areas under the curves for both the m/e=39 P(E) and the total P(E). The m/e=39 P(E) was divided by the total P(E) to obtain $F_m(E)$ for m=39. It should be emphasized that $F_m(E)$ is a function only of the total translational energy and thus it is a quantity that averages over the range of combinations of O_2 internal energies and NaO vibrational and rotational energies that occur at a given relative translational energy. It is expected that $F_m(E)$ should also be dependent on the electron bombardment energy which was 200 volts in this experiment.

Discussion

The center of mass angular distribution of NaO is very strongly forward peaked. Additionally although the translational energy distribution extends out to the maximum allowed by conservation of energy the energy distribution peaks at low values. These distributions are characteristic of a reaction that proceeds via a long range harpoon mechanism[31]. This mechanism is possible when the initial covalent surface is crossed by an attractive ionic surface. The separation at which this crossing occurs is given by

$$r(\text{Å}) = 4.35/(\text{I.P.(Na)} - \text{E.A.}(O_3)) = 4.6\text{Å}$$

where I.P.(Na) is the 5.1 eV ionization potential of Na and E.A.(O_3) is the 1.99 eV electron affinity of O_3. This is the distance at which the coulombic attraction of Na^+ and O_3^- counterbalances the difference between the ionization potential of Na and the electron affinity of O_3. As will be discussed later, similar to halogen molecules, O_3^- can dissociate into O_2 and O^-. The Na^+ then "reels in" an O^- and NaO proceeds in the same direction as the initial Na velocity thus yielding a forward distribution. If there is only a small interaction between the departing NaO and O_2 molecules then this reaction approaches the forward stripping limit. In this limit the velocity of O_2 formed is the same as the initial velocity of O_3. Under the conditions used in this experiment the stripping limit would result in a product translational energy of 7 kcal/mole. Support for this mechanism can be found in the large gas phase rate constants previously measured for this reaction.[13-15] Additionally the proposed charge transfer state $Na^+O_3^-$ has been detected in rare gas matrices.[32,33]

Bates and Ojha[34] argued that in the gas phase reaction once the electron is transferred from Na to O_3 a hard collision takes place between the Na^+ and the O_3^- exciting the internal modes of the anion. Our results suggest another possible model. NaO is strongly forward scattered which implies that Na and O_3 spend less than 1/2 a rotational period together. This means that the oxygen-oxygen bond must be broken very quickly. In

the course of this group's work on ground and excited state sodium reactions it has been found that the course of a reaction between sodium and a given molecule can be predicted in a very rough and broad manner by examining the gas phase electron scattering data of the molecule in question.[35] The feature that has proved most important is the existence of broad low energy dissociative attachment resonances. Such processes have been seen in ozone.[36,37] The processes in question are

$O_3 + e^- \rightarrow O_2 + O^-$ $\Delta H = -9$ kcal/mole (4)

$O_3 + e^- \rightarrow O + O_2^-$ $\Delta H = 15$ kcal/mole (5)[38]

The threshold for reaction 4 was found to be at an electron kinetic energy of 0 eV. The threshold for reaction 5 was 0.4 eV within experimental error. The cross-section for O^- production was found to be greater than the cross-section for O_2^- production at the peaks of the resonances. The existence of the broad zero volt resonance implies that when an electron is transferred from Na to O_3 the O_3^- will fall apart into O_2 and O^- rapidly and without any need for a subsequent hard collision. The bond can then be formed between the Na^+ and the O^- ion. The higher threshold for the production of O_2^- is consistent with the fact that no NaO_2 was seen. Of course at the maximum

crossing distance, once the electron attaches to O_3 there is no energy to excite the O_3^- vibrations. However, the O_3^- is formed in the strong field of the Na^+. The manner in which this can drive the dissociation in can be thought of in two ways. First, the Na^+ creates a 6.7 x 10^7V/cm field at a distance of 4.6Å. As pointed out by Birely and Hershbach this can initiate the field-induced dissociation of O_3^-.[39],[40] Additionally, as the electron is transferred the Na^+-O^- coulombic interaction can provide the energy necessary to dissociate the O_3^-. This interaction represents the nascent Na-O bond.

The Bates and Ojha model might still be consistent with the data. It is possible for Na^+--O_3^- to have a strong collision after electron transfer occurs at long distance and for the reaction to be complete in less than one rotational period. However it seems likely that O_3 will behave like a halogen and dissociate without the hard collision.

The fact the translational energy distributions are so broad might indicate strong coupling between the departing NaO and O_2. The NaO formed by the "harpoon" with high vibrational energy can relax with the energy going into translation as the molecules separate.

Normally it is difficult to make conclusions about the distributions of excess energy between two product molecules and the partitioning of the internal energy between vibrational and rotational degrees of freedom in

crossed molecular beam experiments that make only angular and time of flight distribution measurements. For all but the lightest molecules in triatomic reactions the rovibrational energy levels are too closely spaced to be resolved. These conditions are true in this experiment. However, the fragmentation pattern results do allow us some qualitative insights into the internal energy distribution. If all the internal energy went into O_2 the $F_m(E)$ would be flat. The fact that it is strongly dependent on the product translational energy means that there is considerable variation in the internal excitation of the NaO bond. In other words, O_2 formed might not contain as much variation in the internal excitation. At very low translational energies the $F_m(E)$ turns slightly upward in favor of m/e=39. If NaO is formed in a state with electronically excited character then it can fluoresce during the 125 microsecond flight time and thus increase the probability of NaO^+ production upon electron impact ionization. NaO fluorescence from an electronically excited state has been found by Gole and coworkers in an Na + O_3 flame at 6700Å.[41,42] The high background of m/e=32 and m/e=16 in the detector precluded us from making any measurements of the O_2 distribution. However our proposed mechanism allows us to make predictions of what the measured distributions would be. The bond length in ozone is 1.278Å and the bond angle is 116.8° whereas the bond length in O_2 is 1.208Å.[38] If the dissociation of O_3 is initiated by a

rapid electron transfer then O_2 might have substantial vibrational and rotational excitation. Hapgood observed persistent IR emission in a meteor train which he assigned to emission from excited oxygen ($B^1\Sigma^g \rightarrow X^3\Sigma^g$).[43] He hypothesized that the source of the excited oxygen as being due to reaction 2 of the Chapman mechanism. This experiment implies that the first step may also give rise to this emission.

Conclusions

The reaction of Na + O_3 yields only NaO + O_2. It occurs via a long range electron transfer with the NaO forward scattered. Although the translational energy distribution extends out to the maximum allowed by energy conservation there is a great deal of energy in the internal modes of the products a substantial amount of which is in NaO vibration.

Endnotes

1. S. Chapman, Journal of Astrophysics 90, 309, (1939)
2. See e.g. V.W.J.H. Kirchoff, B.R. Clemensha and D.M. Simonich, Journal of Geophysical Research 86, 6892, (1981)
3. N.D. Sze, M.K.W. Ko, W. Swider, and Edmond Murad, Geophysical Research Letters 9, 1187, (1982)
4. S.C. Liu and G.C. Reid, Geophysical Research Letters 6, 283, (1979)
5. Alice L. Newman, Journal of Geophysical Research 93 #A5, 4067, (1988)
6. See e.g. W.J. Baggaley, Nature 257, 567, (1975)
7. J.E. Blamont and T.M. Donahue Journal of Geophysical Research 69, 4093, (1964)
8. Theodore L. Brown, Chemical Reviews 73, 645, (1973)
9. Donald M. Hunten, Space Sci. Rev. 6, 493, (1967)
10. Donald L. Hildebrand and Edmond Murad, Journal of Chemical Physics 53, 3403, (1970)
11. All thermodynamic data in this thesis are taken from the Journal of Physical and Chemical Reference Data, Volume 11, (1982), Supplement No. 2, The NBS Tables of Chemical Thermodynamic Properties unless otherwise noted
12. D. Husain, and John M.C. Plane, Journal of the Chemical Society Faraday Transactions 2, 78, 163, (1982)

13. D. Husain, Paul Marshall, and John M.C. Plane, Journal of the Chemical Society Faraday Transactions 2, 81, 301, (1985)

14. C.E. Kolb and J.B. Elgin, Nature, 263, 488, (1976)

15. David Husain, Paul Marshall, and John M.C. Plane, Journal of the Chemical Society Chemical Communications, 18, 1216, (1985)

16. Joel A. Silver and Charles E. Kolb, Journal of Physical Chemistry, 90, 3263-3266

17. Joel W. Ager III, Carol L. Talcott, Carleton J. Howard, Journal of Chemical Physics, 85, 5584, (1986)

18. Hildebrand and Murad op. cit.

19. Y.T. Lee, J.D. McDonald, P.R. LeBreton, and D.R. Hershbach, Review of Scientific Instruments 40, 1402,(1969)

20. P.E. Siska, J.M. Parson, T.P. Schaefer, and Y.T. Lee, Journal of Chemical Physics 55, 5762, (1971)

21. M.F. Vernon Ph.D. Thesis, University of California, Berkeley, (1983)

22. P.S. Weiss Ph.D. Thesis University of California, Berkeley, (1986)

23. H.F. Davis III, M.H. Covinsky, A.G. Suits, and Y.T. Lee, manuscript in preparation.

24. Donald Peckner and I.M. Bernstein Handbook of Stainless Steels, McGraw-Hill Book Company, New York, (1977)

25. William G. Moffatt The Handbook of Binary Phase Diagrams, General Electric Company, Corporate Research and Development, Technology Marketing Operation, Schenectady, New York, (1981-)

26. G.V. Samsonov The Oxide Handbook, IFI/Plenum, New York, (1982)

27. G. Comsa, R. David, and B.J. Schumacher, Rev. Sci. Inst., 52, 789, (1981)

28. K. Skold, Nucl. Instum. Methods, 63, 114, (1968)

29. V.L. Hirschy and J.P. Aldredge, Rev. Sci. Inst., 42, 381, (1971)

30. R. J. Buss Ph.D. Thesis, University of California, Berkeley, (1979)

31. J.L. Magee Journal of Chemical Physics, 8, 687, (1940)

32. D.R. Bates and P.C. Ojha, Nature, 286, 790, (1980)

33. Frank J. Adrian, Vernon A Bowers, and Edward L. Cochran, Journal of Chemical Physics, 61, 5463, (1974)

34. Robert C. Spiker Jr. and Lester Andrews, Journal of Chemical Physics 59, 1851, (1973)

35. A discussion of the application of electron scattering to this group's sodium atom scattering experiments can befound in chapter 3 of this thesis.

36. R.K. Curran Journal of Chemical Physics, 35, 1849, (1961)

37. D. Stelman J.L. Moruzzi, and A.V. Phelps, Journal of Chemical Physics, 56, 4183, (1971)

38. The electron affinities of O-and O_2^- were taken from the CRC Handbook of Chemistry and Physicss 64th Ed., CRC Press Inc. Boca Raton, Florida, (1979)

39. Examples of field induced dissociation of an ion can be found in A.C. Riviere and D.R. Sweetman, Phys Rev. Lett. **5**, (1960) or Alan Carrington, Iain R. McNab and Christine A. Montgomerie, Chemical Physics Letters, 151, 258

40. J.H. Birely and D.R. Hershbach, Journal of Chemical Physics, 44, 1690, (1966)

41. Joerg Pfeifer and J.L. Gole, Journal of Chemical Physics, 80, 565, (1984)

42. R. Woodward, J.S. Hayden, and J.L. Gole unpublished results

43. M.A. Hapgood, Nature, 286, 582, (1980)

Table 1

Beam Parameters

	peak velocity (cm/sec)	beam spread $v/\Delta v$
Na	2.80×10^5	11.3
O_3	1.43×10^5	10.4

Table 2

P(E) Features

	$<E_{trans}>$	E_{peak}
m/e=39	28.7 kcal/mole	38 kcal/mole
m/e=23 + m/e=39	22.4 kcal/mole	10 kcal/mole

Figures

Figure 1: Schematic of the crossed molecular beams apparatus.

Figure 2: Schematic of the seeded supersonic metal atom source. (1) Teflon insulator, (2) Ceramic Collar, (3) Outer reservoir cylinder, (4) Na reservoir, (5) Graphite resistance heater for reservoir, (6) Copper containment and support can, (7) Inner reservoir cylinder, (8) Copper cooling water line, (9) Tantalum plate, (10) Water cooled nozzle electrode, (11) Inner nozzle tube, (12) Outer nozzle tube, (13) Molybdenum skimmer, (14) Skimmed sodium beam, (15) Primary source wall, (16) Reservoir end plates, (17) Molybdenum flow constrictor (18) Stainless steel support (19) water cooled inlet tube electrode, (20) Springs to force entire oven forward, (21) Tantalum wire, (22) Inlet tube.

Figure 3: Schematic of the secondary source.
(1) nozzle cap, (2) inlet tube heating tape, (3) "birdcage" keying device, (4) Copper block nozzle heater, (5) Copper pre-heater, (6) thermocouple, (7) skimmer. adapted from reference 22

Figure 4: Newton diagram for the reaction $Na + O_3 \rightarrow NaO + O_2$

E_{coll} = 18 kcal/mole

Figure 5: Laboratory angular distribution at m/e=39. The points are the measured distribution. The line is the best fit to the distribution.

Figure 6: Time of flight distributions at m/e=39. The dots are the data. The lines are the best fit to the data.

Figure 7: P(E) m/e=39 used for best fit

Figure 8: T(θ) m/e=39 used for best fit

Figure 9: Time of flight for the sum of m/e=23 and m/e=39

_____ total calculated fit. ----- contribution from m/e= 23

___..__ contribution from m/e=39

Figure 10: P(E) derived for the sum of m/e=23 and m/e=39

Figure 11: $F_m(E)$ Fragmentation of NaO to NaO^+ as a function of total translational energy.

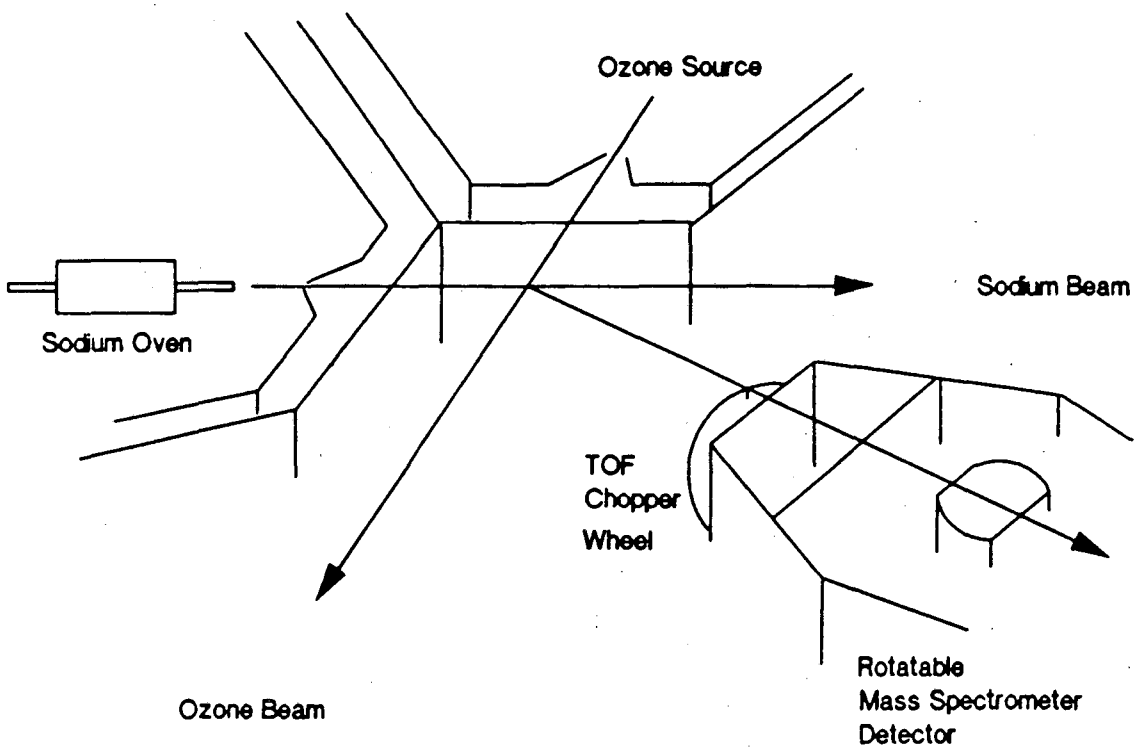

Crossed Beams Apparatus

XBL 9011-3707

Figure 1

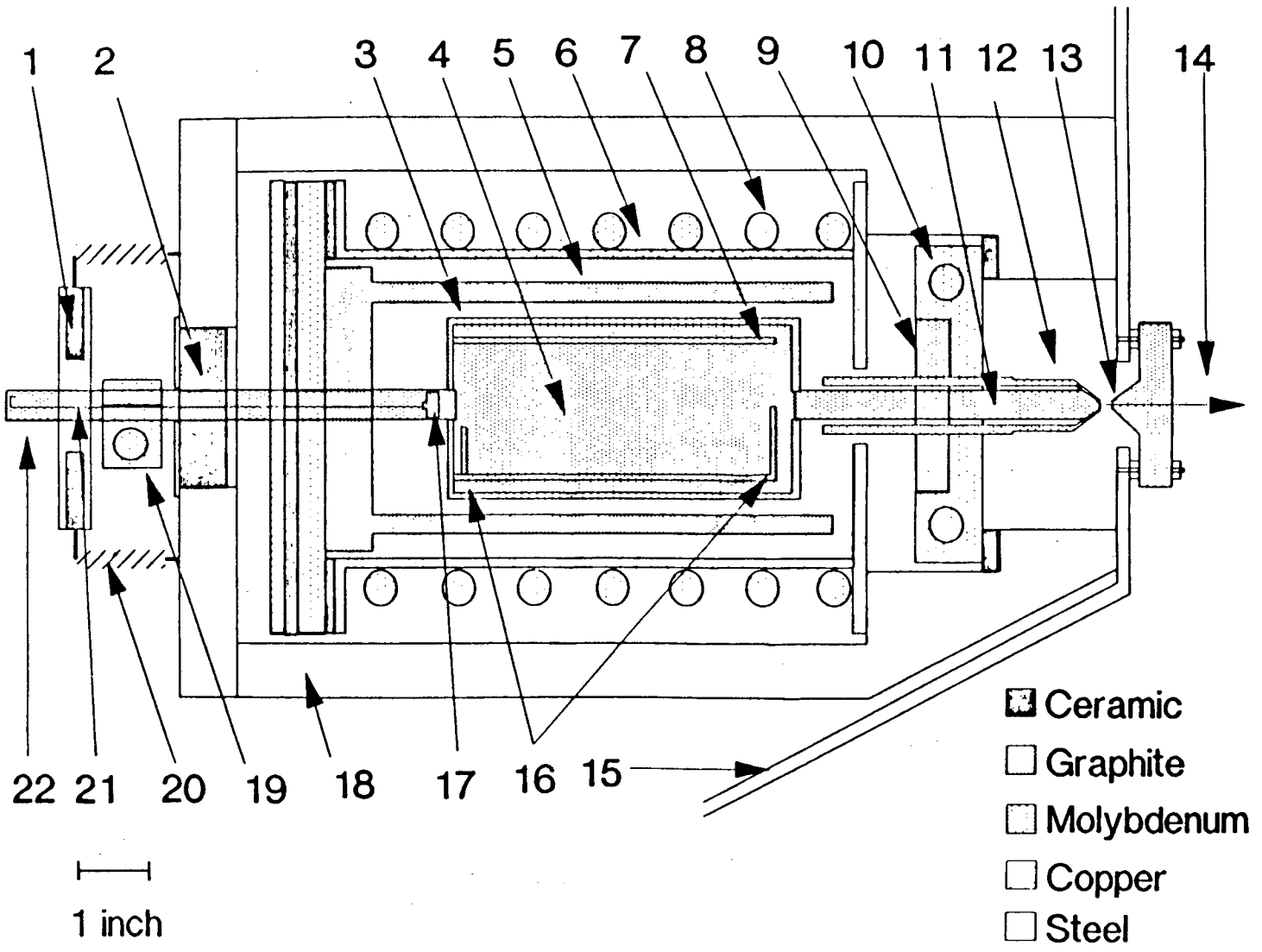
1
2
3
4
5
6
7
8
9
10
11
12
13
14
22
21
20
19
18
17
16
15
1 inch
Ceramic
Graphite
Molybdenum
Copper
Steel
XBL 9011-3708

Figure 2

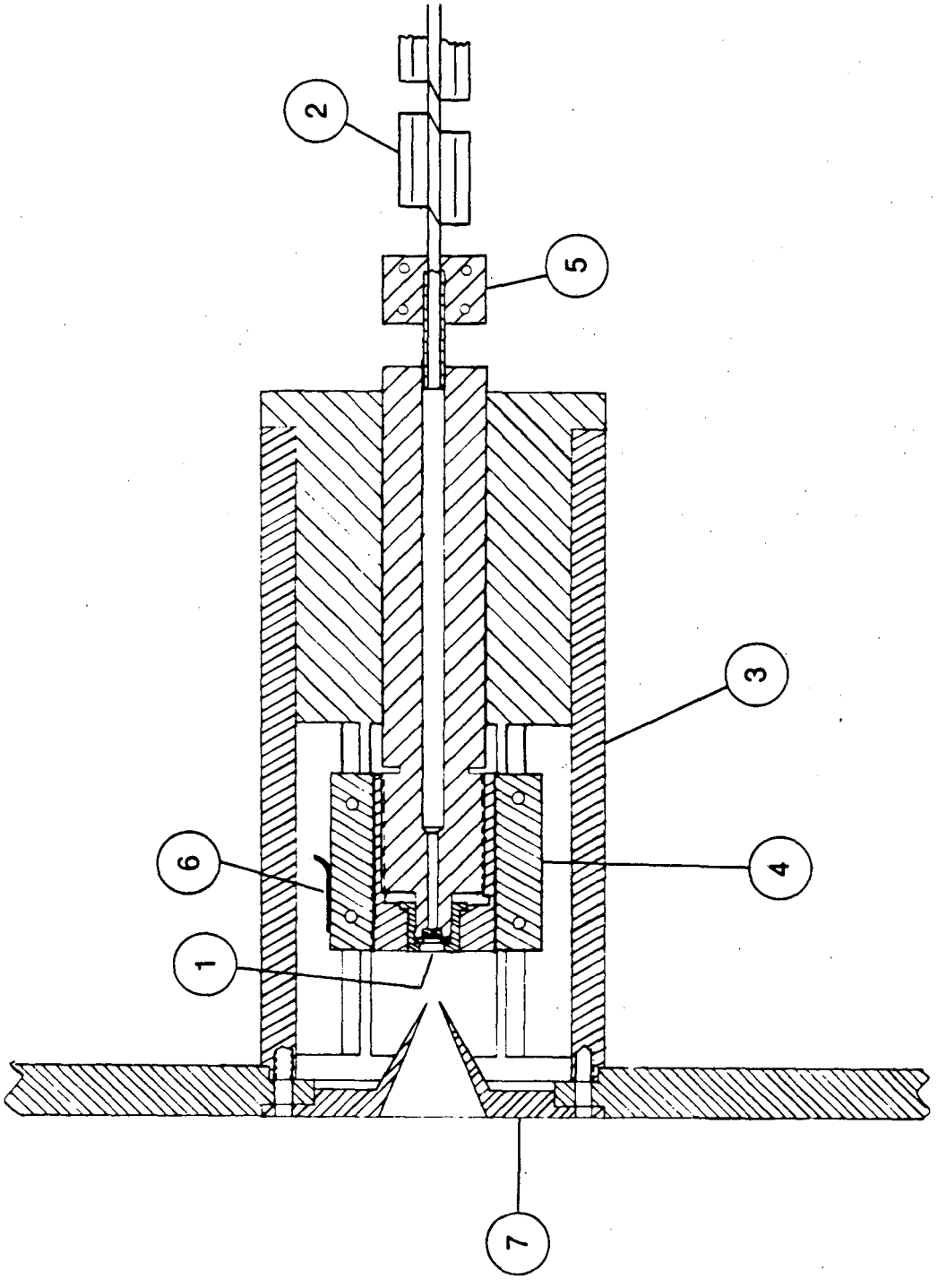

XBL 834-9474A

Figure 3

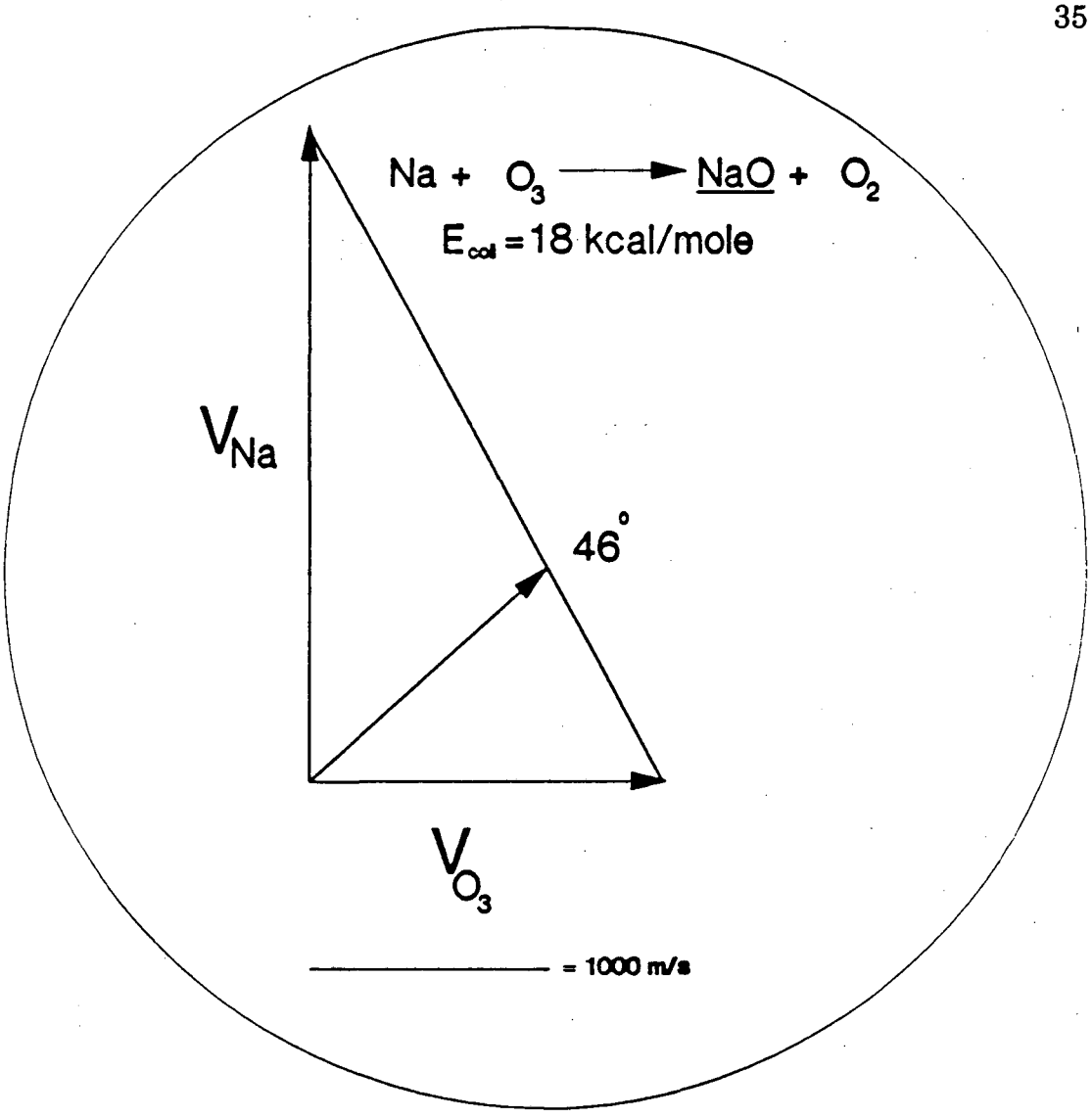

XBL 9011-3709

Figure 4

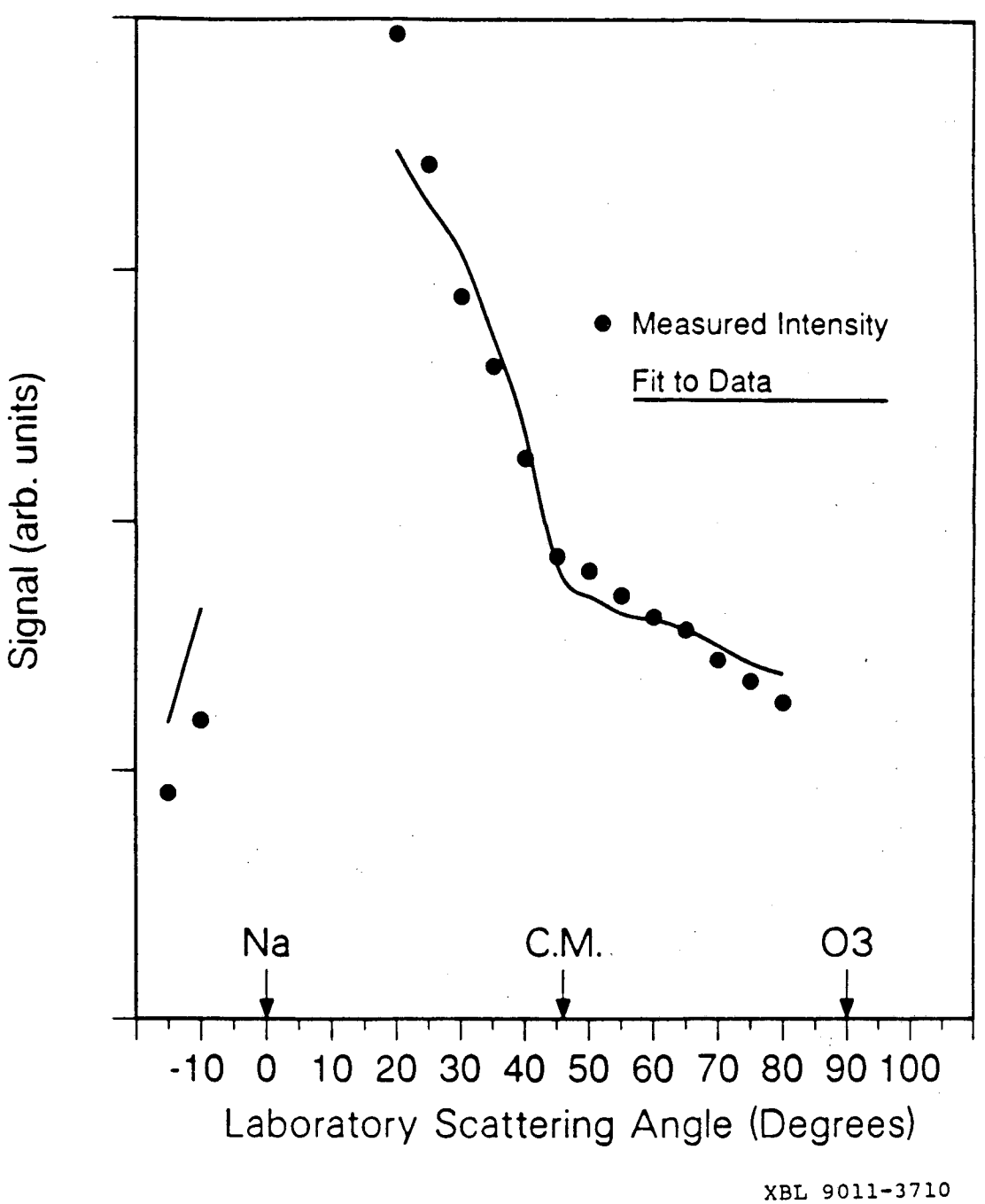
Laboratory Angular Distribution
Signal (arb. units)
Measured Intensity
Fit to Data
Na
C.M.
O3
-10 0 10 20 30 40 50 60 70 80 90 100
Laboratory Scattering Angle (Degrees)
XBL 9011-3710

Figure 5

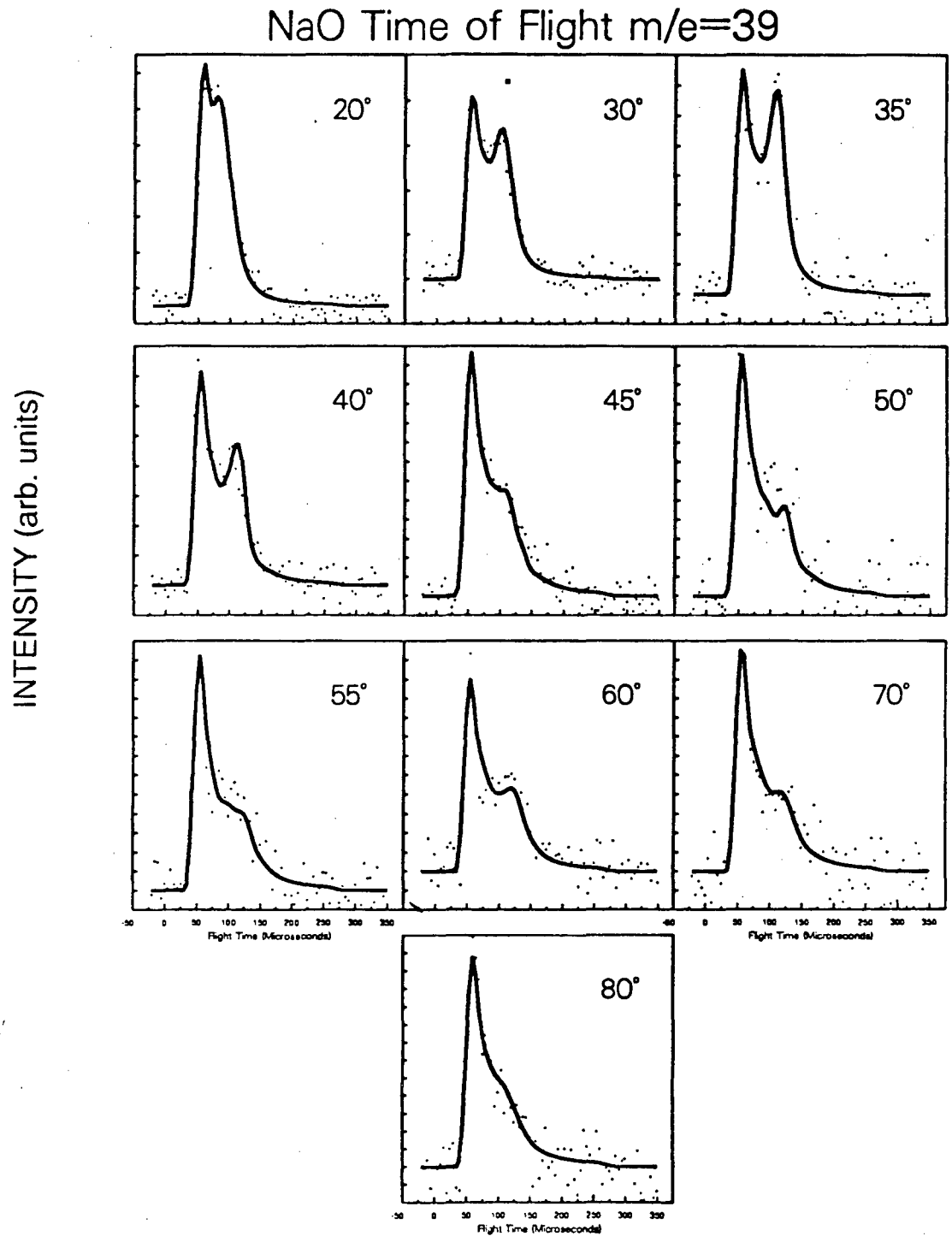
NaO Time of Flight m/e=39
INTENSITY (arb. units)
20°
30°
35°
40°
45°
50°
55°
60°
70°
80°
Flight Time (Microseconds)

Figure 6

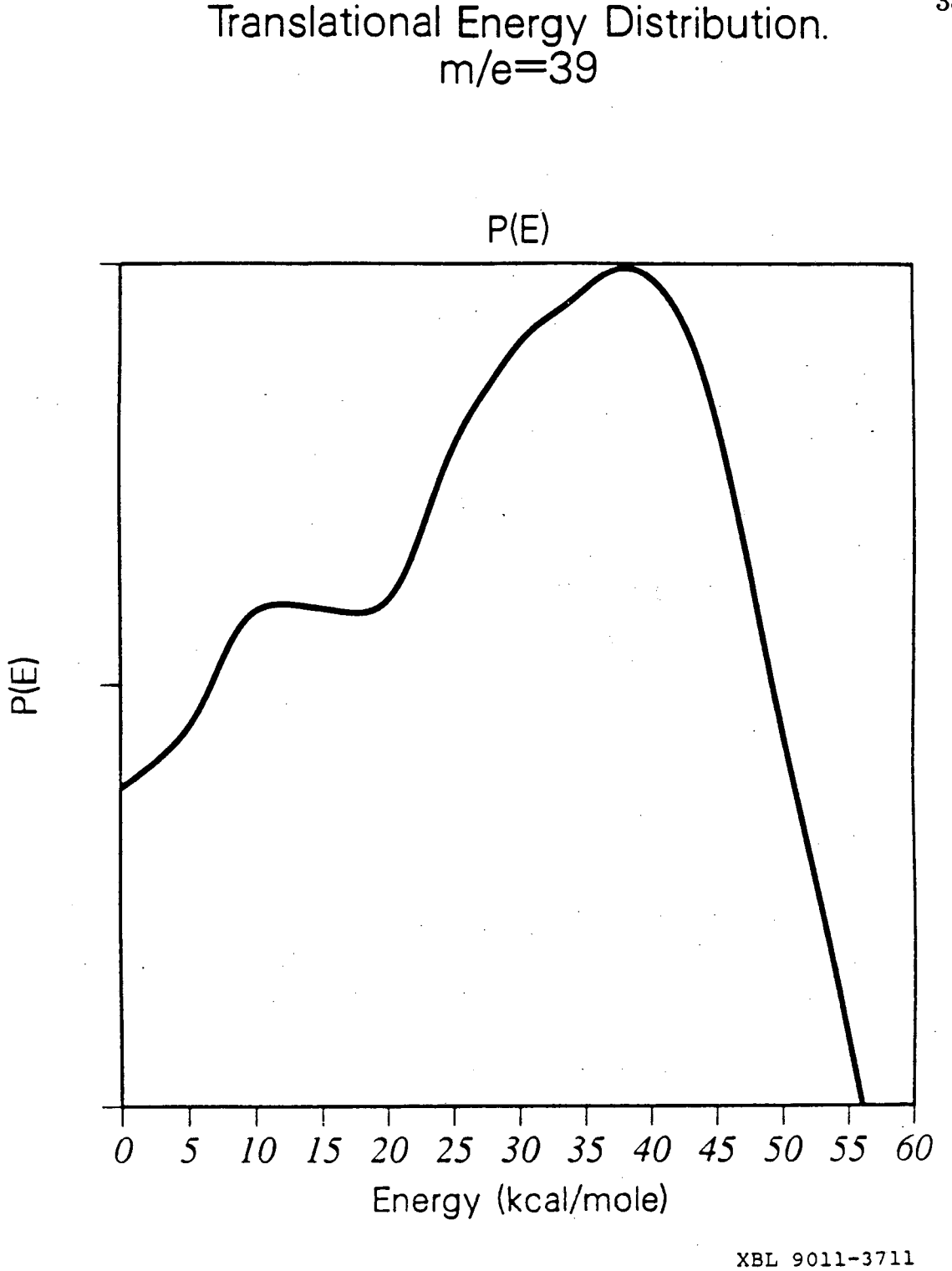
Translational Energy Distribution.
m/e=39
P(E)
P(E)
0
5
10
15
20
25
30
35
40
45
50
55
60
Energy (kcal/mole)
XBL 9011-3711

Figure 7

Center of Mass Angular Distribution.

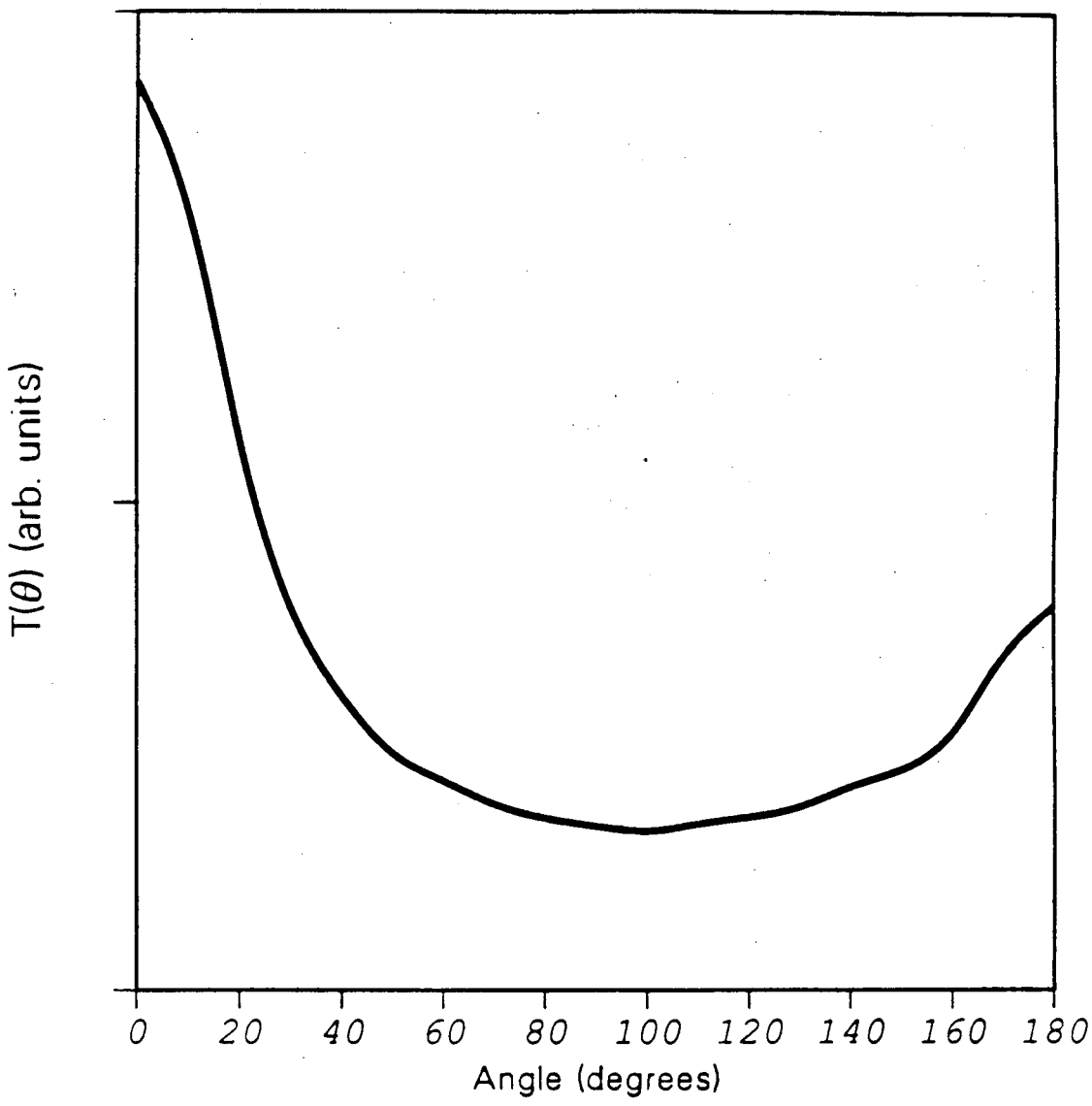

Figure 8

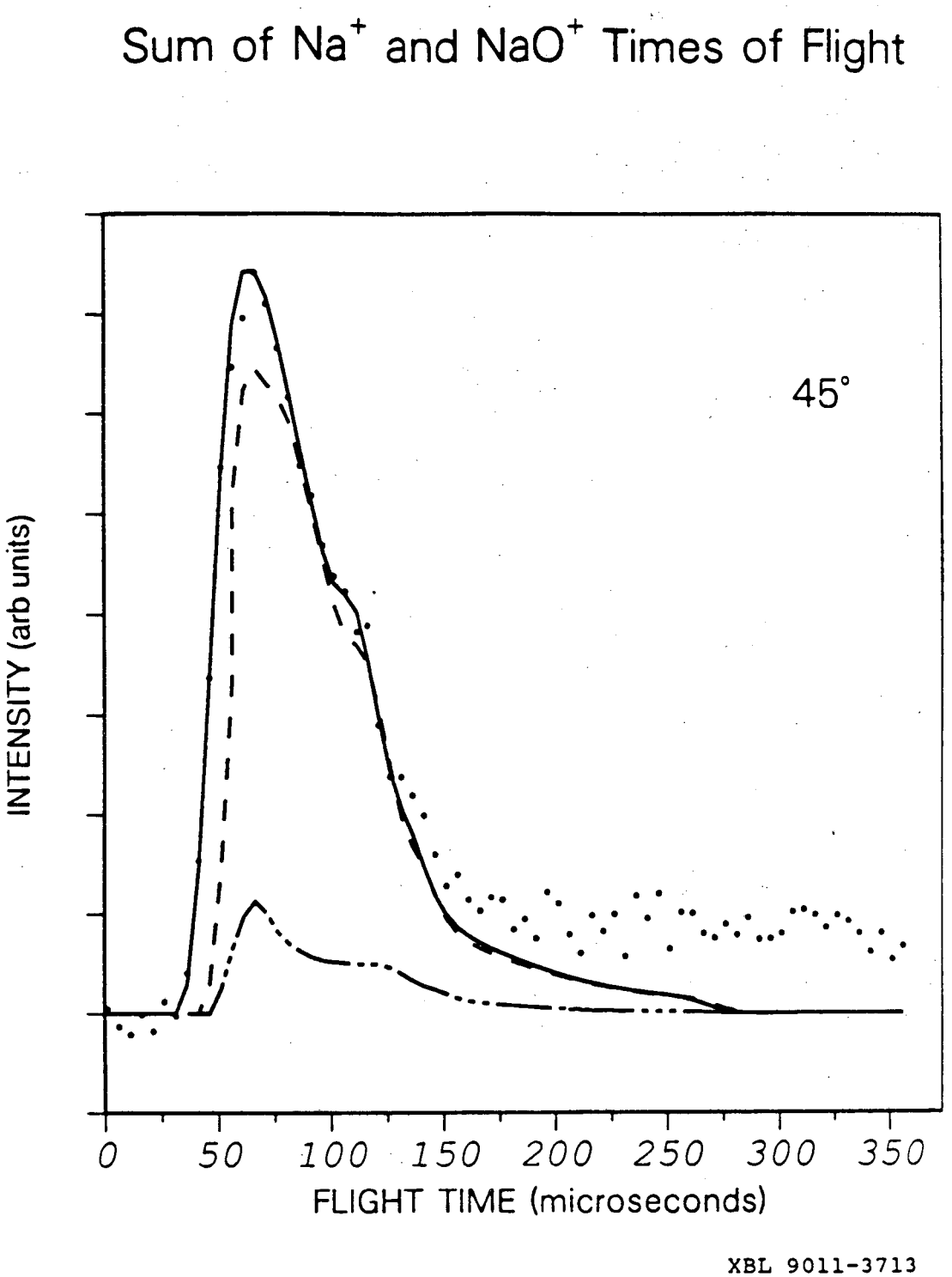
Sum of Na^+ and NaO^+ Times of Flight
45°
INTENSITY (arb units)
0
50
100
150
200
250
300
350
FLIGHT TIME (microseconds)
XBL 9011-3713

Figure 9

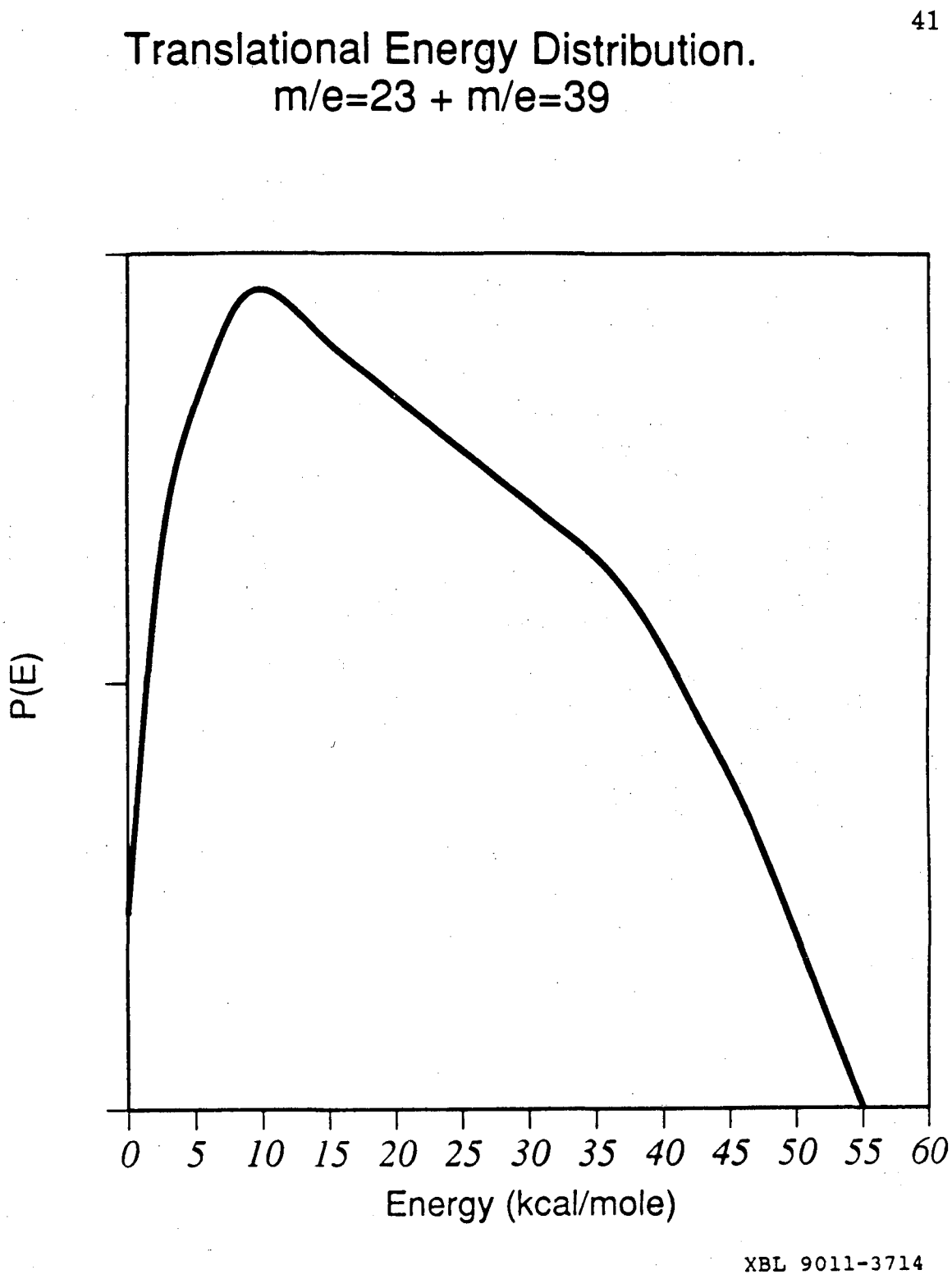
Translational Energy Distribution.
m/e=23 + m/e=39
P(E)
0
5
10
15
20
25
30
35
40
45
50
55
60
Energy (kcal/mole)
XBL 9011-3714

Figure 10

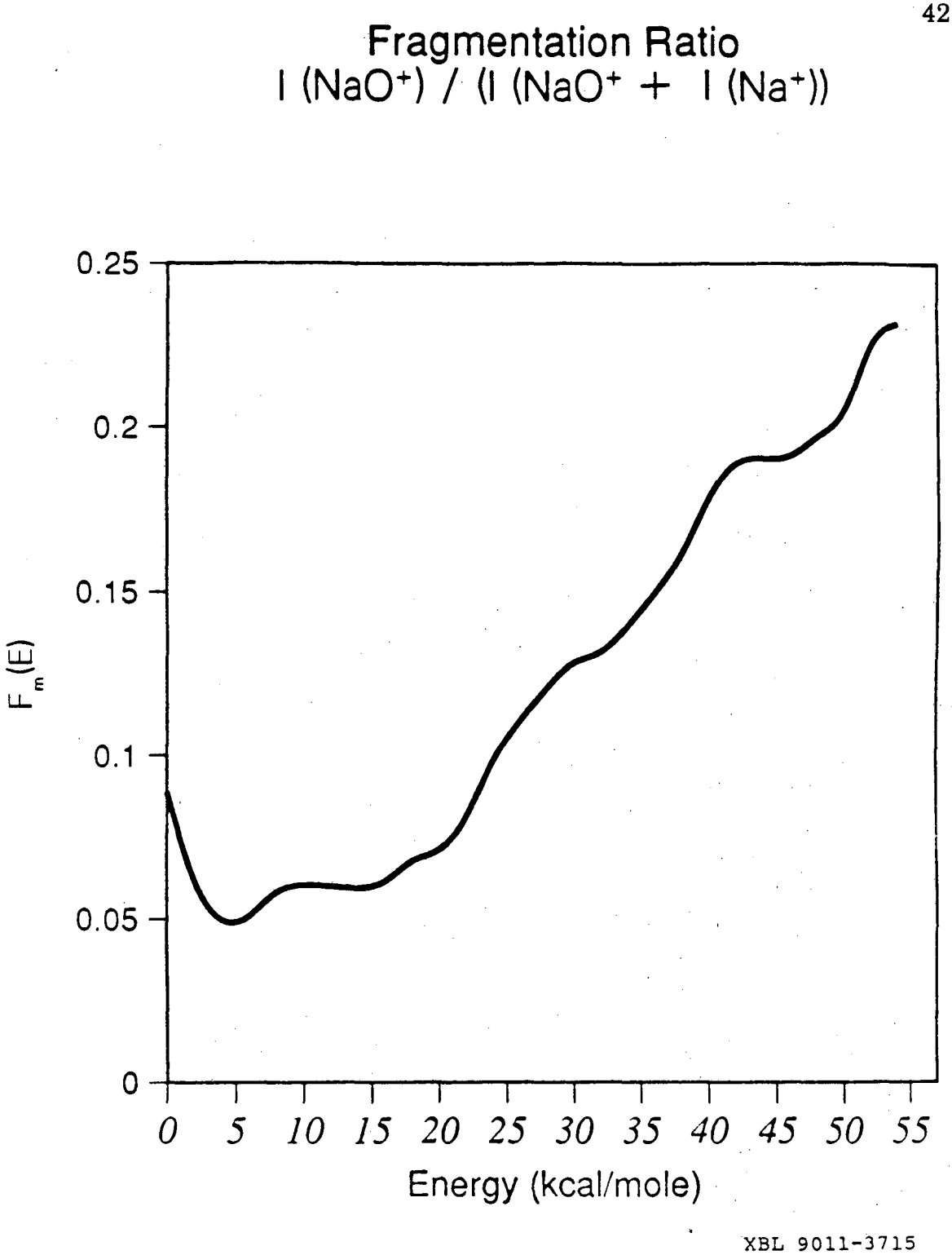
Fragmentation Ratio
I (NaO+) / (I (NaO+ + I (Na+))
0.25
0.2
0.15
0.1
0.05
0
F_m(E)
0 5 10 15 20 25 30 35 40 45 50 55
Energy (kcal/mole)
XBL 9011-3715

Figure 11

Chapter 2

The Reaction of Ground State and Electronically Excited Sodium Atoms with Methyl Iodide

Introduction

The reactions of alkali atoms with alkyl halides are possibly the most studied family in reaction dynamics. The angular distribution of K + CH_3I was the first ever measured in a crossed molecular beam experiment.[1] This reaction was the prototype for the rebound mechanism that has been found for all alkali atom plus alkyl monohalides and pseudohalides.[2-12]

Bernstein[13-16] and Brooks[17] have done a series of classic experiments in which a beam of alkyl halides are selected by a hexapole field for $\langle KM/J^2+J \rangle$ where J is the total angular momentum quantum number, K is the projection of **J** upon the symmetry axis and M is the projection of **J** on a space fixed axis. By changing the orientation of the dipole moment

Bernstein, Brooks and coworkers were able to determine the steric opacity function for this reaction. In agreement with chemical intuition they found that in order for reaction to occur the alkali atom must approach the iodine end of the molecule. The reaction probability is zero if the atom approaches the methyl end.

There have been a number of crossed beam studies of alkali atoms and methyl halide molecules.[1-12,18-21] All the angular distributions are peaked in the backwards direction with respect to the alkali atom. This is consistent with orientation studies. If for those collisions that lead to reaction the preferred orientation of the methyl iodide molecule is with the iodine atom facing the incoming sodium atom then the reaction product will most likely be scattered in the backwards hemisphere. This effect will be the most pronounced for low impact parameter collisions. As the collision energy of the alkali atom plus methyl halide systems are increased the alkali halide product becomes less backwards scattered.

The product translational energy distributions are typically broad and the peak of these distributions for this family of reactions increases linearly with the collision energy. For the reaction of Na and CH_3I $(dE'_T/dE_T) = 0.73$ where E'_T is the product translational energy and E_T is the collision energy.[10] This is the same value as was found for K + CH_3I[7,19] as well as for K and Rb + CH_3Br.[9] The value for Rb + CH_3I was 0.5.

The translational energy dependence of the total reactive cross section of Na + CH_3I[22] as well as K and Rb + CH_3I has been measured.[6,19,20,23-25]. All three systems behave similarly. The Na cross section rises from an estimated threshold at 0.05 eV to a maximum at 0.14 eV. The K cross section peaks at 0.18 with a value of 38Å^2. It drops rapidly to less than a factor of two of this value by 0.3 eV and declines slowly to ⅓ of the peak value by 1.0 eV. The Rb cross section declines from a value of 38Å^2 at the lowest energy measured to a shallow minimum at 0.9 eV at which energy the cross section is 35% of the maximum. The cross section increases to 40% of the maximum at 1.7 eV, the highest energy measured.

The cross section of K + CH_3Br has been measured to be 3Å^2[5]. It has a threshold of 0.2 eV and appears to increasing up to a maximum at 0.9 eV the highest energy measured. Rb + CH_3Br has a threshold of 0.1 eV. No obvious maximum was seen below 1.4 eV.[9]

Bulk rate constants have been measured for alkali metal plus methyl halide systems.[26-28] They confirm two trends. For M + CH_3X the cross section increases through the sequence F < Cl < Br < I and Na < K < Rb. See Table 1.

Fluendy etal. has looked at the inelastic collisions of high energy potassium atoms with alkyl halides especially methyl iodide.[29-31] They measured the energy loss spectrum of K and assigned peaks either to

electronic excitation of K or the vibrational or mainly electronic excitation of RX. They modelled their results in terms of an electron transfer either into the σ^* orbital on the C-I bond or a higher energy orbital. This transfer was followed by the subsequent recapture of an electron either from the excited orbital, the highest occupied molecular orbital in the neutral molecule or from an inner orbital.[44] Recapture in one of these last two cases created an excited CH_3I and appeared as a translational energy loss of K.

There is a large body of theoretical work that has been done on M + CH_3X systems.[32-51] Each of the phenomena discussed above has been addressed at least obliquely by theory.

The primary model for these systems is that an electron jumps from the alkali atom to the methyl halide. The lowest available molecular orbital in methyl halides is the σ^* antibonding orbital on the C-X bond. If an electron is transferred into this orbital the C-X bond will break forming nascent $CH_3 + X^-$. The X^- will bond with the M^+ to form MX. To describe the dynamics of this system Kuntz, Mok and Polanyi proposed the DIPR (Direct Interaction Product Repulsion) model.[34,35] In this model after the electron is transferred there is a monotonically decreasing C-X repulsion which operates predominantly along the C-X axis. They ran simulations in which either the charge was allowed to migrate from CX^- to C^-X or it was fixed on the X. In the free migration case the angular distributions were forward scattered à la M + X_2. However in the fixed case, the one

applicable to methyl halides the angular distributions are backwards scattered.

The angular distributions have been the subject of many studies.[36,46–48,50,51] There is an orientation dependent barrier that is a minimum for the head on collision and rises until the methyl end cuts off the possibility for reaction. The cones of reactance and non-reactance are what yield the backward scattering. As the collision energy is increased the more repulsive initial angles are accessed. This, combined with the impulsive effects of a high energy collision would result in more forward scattering as well as a greater release of translational energy with an increase of the reagent collision energy.

There are several models extant which try to explain the maximum in dependence of the reactive cross section upon collision energy and the post-maximum decline. Shin proposed a model in which reactant trajectories are reflected back into the reagent valley.[37,39,43] LaBudde etal[36] proposed a model in which the post-maximum decline was due to the recrossing of trajectories from the ionic to the covalent potential. Gonzalez Ureña proposed a transition state model in which the transition state moved as a function of collision energy. As the collision energy increased the transition state would move into the product valley.

The experiment Na(3S,3P,4D) + CH_3Br was performed in our laboratory.[18,52] The only product found was NaBr. In the ground state the

product was strongly back-scattered. Most of the available energy went into product translation with the distribution going out to the maximum allowable by conservation of energy. As the electronic energy of Na increased there was more scattering in the forward direction. The 3P translational energy distribution was virtually the same as the 3S distribution. The 4D translational energy distribution was broader, extending to both higher and lower energies.

Experimental

Beam Sources

These experiments have were performed using two crossed seeded beams. The laser used to excite the sodium atoms passed through the collision region in the third perpendicular direction (fig. 1). The sodium beam was generated with the old stainless steel oven which has been described previously. The oven has three separately heated chambers. (Fig. 2) The sodium reservoir was heated with thermal coaxial cable to a temperature of 525°C.

The upper part of the oven has a mini-conflat flange. The inlet tube has a mating flange and the two flanges are sealed with a nickel gasket. Seed gases were introduced through the inlet tube. This part of the oven

was radiatively heated by a tungsten ribbon wound around ceramic support posts. The operating temperature of the top oven was 550°K.

A He-Na gas mixture at a total pressure of 450 torr was expanded out a 0.007" nozzle. The nozzle tube was heated by thermal coaxial cable to a temperature of 630°K. After the expansion the beam was collimated by a stainless steel skimmer. To prevent clogging the skimmer was heated by thermal coaxial cable. The beam was defined by 0.53 mm x 1.90 mm collimating slits on the primary differential wall. This yielded a 1.1 mm high by 3.0 mm wide beam at the crossing center. This reduced height was necessary to reduce the transverse doppler broadening of the beam when Na was optically pumped.

The secondary beam was made in a similar manner to what was described in chapter 1. For the experiments conducted at a collision energy of 23.9 kcal/mole 500 torr of helium was bubbled through CH_3I kept at 20°C. For the 28.4 kcal/mole experiment the 500 torr of helium was bubbled through CH_3I kept at -26°C. In both cases the nozzle temperature was 201 °C.

Optical Pumping

The $Na(3^2P_{3/2} \leftarrow 3^2S_{1/2})$ transition was pumped by the output of a Coherent 699-21 cw single frequency ring dye laser. The dye used was Rhodamine 6G. The laser was pumped at 5145Å by a Spectra-physics 171

argon ion laser. It was possible to get 900 mW of power at 5892Å when pumping with 6W at 5145Å. With effort over 1000 mW was possible. However at these powers saturation effects occurred so that the laser was typically run at 200 mW.

The laser light entered through the main door of the machine. It propagated counter-parallel to and 10 inches below the secondary beam. The laser light was reflected up through the scattering center and perpendicular to both beams. This arrangement minimized the longitudinal Doppler broadening in the sodium beam.

Fluorescence was monitored at an angle of -12.5° from the Na beam. The monitor was used to ensure that both the laser and the Na beam were stable. It was possible to fix the laser frequency at the peak of the Na transition by locking the frequency to the peak of the fluorescence using a lock-in stabilizer.

There are two ports on the machine that allow the laser to pass at a 45° angle with respect to the Na beam. About once an hour a fraction of the laser light would be split off and allowed to pass through the 45° while the laser would be scanned. The fluorescence from the 45° crossing would be Doppler shifted from the fluorescence from the orthogonal crossing. The size of the shift would give us the peak velocity of the beam. The ratio of the width of the Doppler shifted peak to the amount of the Doppler shift would give us the speed ratio of the beam.

The Na 3S and 3P energy levels are shown in figure 3. The laser was tuned to excite Na from the F=2 hyperfine level of the ground state to the F=3 hyperfine level of the $3^2P_{3/2}$ excited state. Since the selection rule for fluorescence is $\Delta F = 0,\pm 1$ atoms in the F=3 hyperfine level of the $3^2P_{3/2}$ excited state can radiatively decay only to the F=2 level of the $3^2S_{1/2}$ ground state. Thus we have an isolated two level system.

The fluorescence lifetime of the 3P state is 16.9 nanoseconds.[53] This means that a sodium atom can cycle through the ground and excited states many times as it passes through the collision region. The residence time in the collision region for a sodium atom for the beam conditions used in this experiment is one microsecond. This cycling causes the Na beam to become polarized if polarized light is used.[54,55]

Data Acquisition

Data is acquired in the same manner as described in chapter 1 with the following changes. The gate generator drives a stepping motor to block and unblock the laser at a rate of 3 Hz. There are now 4 detector channels. These are Laser on, secondary beam on (ON_+); Laser on, secondary beam off (ON_-); Laser off, secondary beam on (OFF_+); and laser off, secondary beam off (OFF_-). For a given measurement at a particular angle the laser on signal is given by

$$ON_{SIG} = ON_+ - ON_-$$

The laser signal due to the presence of Na^* in the beam is

$$EX = \frac{ON_{SIG} - [(1-f)OFF_{SIG}]}{f}$$

where f is the fraction of Na electronically excited. Since it was not possible to find an angle at which there is no excited state signal but there is ground state signal it is hard to determine f. In these experiments a value of 0.2 is assumed.[52]

Results and Analysis

The reactions

$$Na(3S) + CH_3I \rightarrow NaI + CH_3 \quad \Delta H = -13.8 \text{ kcal/mol}^{56} \quad (1)$$

$$Na(3P) + CH_3I \rightarrow NaI + CH_3 \quad \Delta H = -62.3 \text{ kcal/mol} \quad (2)$$

were studied. Both reactions (1) and (2) were studied at a 23.9 kcal/mole collision energy. Reaction (1) was also studied at 28.4 kcal/mole. The beam parameters are shown in table 2. The newton diagrams are shown in figures 4 and 5. Due to poor kinematics lower energies were not tried.

The angular distributions are shown in figures 6 and 7. These angular distribution were measured at m/e = 23. It is apparent the distributions at both energies are back-scattered. Electronic excitation of Na leads to no change at the most back-scattered angles. At more forward angles there is significant increase in signal. The statistics achieved here are better than what was achieved in the Na + CH_3Br experiments with only 1/4 the counting time. (Unfortunately that still translates into 18 hours.) Time of flight measurements were not done as the difference between the ground state signal and the excited state signal was so small compared to the signal to noise ratio that it would have rendered those experiments intractable.

The angular distributions were fit using program GM. The fits to the angular distributions are shown in figures 8-10. The center of mass angular distributions derived [T(θ)] are shown in figures 11-13. As expected these T(θ)'s are more forward scattered than those measured for Na + CH_3Br. The 28.4 kcal/mol T(θ) is more forward scattered than the ground state 23.9 kcal/mole distribution. The amount of forward scattered NaI is significantly greater for the excited Na the for ground state Na.

The center of mass translational energy distributions [P(E)] are shown in figures 14-16. The ground state distributions for 23.9 and 28.4 kcal/mole are nearly the same. What is more surprising is that the P(E)'s for the ground and excited state reactions at 23.9 kcal/mole are similar

maximum translational energy releases in spite of the fact the excited state reaction has 48.5 kcal/mole more energy available to it. In fact the translational energy distribution for the electronically excited sodium atom reaction peaks 10 kcal/mole lower than the ground state distribution.

The similarity of the energy distributions in consistent with the model of an electron transfer from Na to CH_3I. If after the electron transfer occurs the interaction between CH_3 and I^- is governed only by the repulsion between the two then this interaction should be unchanged when going from ground state Na to excited Na. Furthermore if the interaction between CH_3 and I^- is unchanged, then the final velocity of CH_3, and by conservation of momentum, the final velocity of NaI would be the same for both the ground and excited states. For small impact parameters electronic excitation would lead to vibrationally excited molecules scattered in the backward direction. For higher impact parameter collisions this would lead to rotationally excited molecules scattered in the more forward directions. The lowering of the peak of the translational energy distribution with increasing electronic energy is analogous to what was seen in Na(3S,3P,4D,5S) + HCl.[57,58] Increasing the electron transfer distance allows the methyl radical to separate from the I^- ion before the NaI bond is formed thus lowering the repulsion between the radical and the closed shell molecule and trapping the extra electronic energy in the internal energy of NaI.

The increase in forward scattering is consistent with what is predicted by the DIPR model.[34,35] For molecules in which there is no charge migration increasing r_x, the electron transfer distance, leads to more forward scattering. The fact that the CH_3I reaction is more forward scattered than the CH_3Br reaction is consistent with the intuitive feeling that the larger I atom is easier to attack than a Br atom. Additionally the DIPR model predicts an increase in forward scattering for lower $C\text{-}X^-$ repulsion. Herschbach[59] modified the DIPR model to approximate this repulsion. The DIPR-DIP (Distributed as in Photodissociation) uses photodissociation data to model the repulsion and generate energy distributions. From photodissociation data it is possible to predict that the $C\text{-}I^-$ repulsion should be lower than the $C\text{-}Br^-$ repulsion and therefore the CH_3I reaction should be more forward scattered than the CH_3Br reaction. An alternative explanation is that increasing the electron transfer distance means that the cone of acceptance for CH_3I increases. This would occur because an excited sodium atom would not have to climb as far up the repulsive wall outside the cone of acceptance as would a ground state atom.

The biggest difficulty with this experiment is the lack of time of flight data. It is predicted that the $T(\theta)$ and the $P(E)$ might be coupled. Comparing the ground and excited state laboratory angular distributions it is seen that both distributions are identical at the most backwards angles. This suggests that the center of mass angular and energy distributions

might similar for extreme back scattering. If this is true then the lower translational energy component of the excited state distribution appear only at the more forward angles. It is impossible to test this without time of flight experiments. There would also be the obvious benefit of more accurate energy and angular distributions especially at high translational energies.

Since this experiment was done major improvements have been made in the machine as discussed in chapter 1. The new molybdenum oven has provided a large increase in primary source intensity. The new turbo pumps caused a large reduction in the detector background. These improvements should make it possible to get angular distributions better than those presented here with less than 4 hours counting time and very probably less than 1 hour. The improved signal to noise ratio should make TOF measurements quite feasible.

Conclusions

The reactions of Na(3S,3P) + CH_3I proceed via a rebound mechanism. The electronic energy is most likely channelled into the internal energy of NaI. There is an increase of scattering to forward angles with the increase of electronic energy. Both of these features are predicted by the DIPR

model. The next step if this system were revisited would be to do time of flight measurements to see if there is coupling between the center of mass angular and translational energy distributions.

Endnotes

1. D.R. Herschbach, G.H. Kwei, and J.A. Norris, Journal of Chemical Physics, 34, 1842, (1961)
2. Michael E. Gersh and Richard B. Bernstein, Journal of Chemical Physics 56, 6131, (1972)
3. Alan M. Rulis and Richard B. Bernstein, Journal of Chemical Physics 57, 5497, (1972)
4. R.B. Bernstein and A.M. Rulis, Faraday Discussions of the Chemical Society, 55, 293, (1973)
5. Richard H. Goldbaum and L. Robbin Martin, Journal of Chemical Physics, 62, 1181, (1975)
6. H.E. Litvak, A. Gonzalez Ureña and R.B. Bernstein, Journal of Chemical Physics 61, 4091, (1975)
7. A. Gonzalez Ureña and R.B. Bernstein, Journal of Chemical Physics 61, 4101, (1974)
8. Charlotte M. Sholeen and Ronald R. Herm, Journal of Chemical Physics 65, 5398, (1976)
9. H.F. Pang, K.T. Wu and R.B. Bernstein, Journal of Chemical Physics, 69, 5627, (1978)

10. V. Saez Rabanos, E. Verdasco, A. Segura and A. Gonzalez Ureña, Molecular Physics 50, 825, (1983)

11. V. Saez Rabanos, F.J. Aoiz, V.J. Herrero, E. Verdasco and A. Gonzalez Ureña, Molecular Physics 59, 707, (1986)

12. J.L. Kinsey, G.H. Kwei, and D.R. Herschbach, Journal of Chemical Physics, 64, 1914, (1976)

13. D.H. Parker, K.K. Chakravorty, and R.B. Bernstein, Journal of Physical Chemistry, 85, 466, (1981)

14. Seung E. Choi and Richard B. Bernstein, Journal of Chemical Physics, 83, 4463, (1985)

15. Richard B. Bernstein, Journal of Chemical Physics, 82, 3656, (1985)

16. Seung Choi and Richard B. Bernstein, Journal of Chemical Physics, 85, 150, (1986)

17. George Marcelin and Philip R. Brooks, Journal of the American Chemical Society, 97, 1710, (1975)

18. P.S. Weiss, J.M. Mestdagh, H. Schmidt, M.H. Covinsky, and Y.T. Lee, submitted to the Journal of Physical Chemistry 1990

19. G. Rotzoll, R. Viard, and K. Schügerl, Chemical Physics Letters, 35, 353, (1975)

20. M. Pauluth and G. Rotzoll, Zeitschrift für Physikalische Chemie Neue Folge, 136, 171-185, (1983)

21. E. Verdasco, V. Saez Rabanos, F.J. Aoiz, and A. Gonzalez Ureña, Molecular Physics, 62, 1207, (1987)

22. V. Saez Rabanos, E. Verdasco, V.J. Herrero, and A. Gonzalez Ureña, Journal of Chemical Physics, 81, 572, (1984)

23. Michael E. Gersh, and R.B. Bernstein, Journal of Chemical Physics, 56, 6131, (1972)

24. S.A. Pace, H.F. Pang and R.B. Bernstein, Journal of Chemical Physics, 66, 3635, (1977)

25. K.T. Wu, H.F. Pang and R.B. Bernstein, Journal of Chemical Physics, 68, 1064, (1977)

26. David Husain and Paul Marshall, International Journal Of Chemical Kinetics, 18, 83, (1986)

27. D. Husain and Y.H. Lee, International Journal Of Chemical Kinetics, 20, 223, (1988)

28. David Husain and Bing Ji, Journal of Photochemistry and Photobiology A, 48, 1, (1989)

29. Malcolm A.D. Fluendy, Kenneth P. Lawley, John McColl, Charlotte Sholeen, and David Sutton, Faraday Discussions of the Chemical Society, 67, 41, (1979)

30. F. Castano, M.A.D. Fluendy, K.P. Lawley, C. Sholeen, and D. Sutton, Chemical Physics Letters, 65, 26, (1979)

31. Malcolm A.D. Fluendy, Kenneth P. Lawley, Charlotte Sholeen, and David Sutton, Molecular Physics, 42, 1,(1981)

32. I. M. Raff and M. Karplus, Journal of Chemical Physics, 44, 1212, (1966)

33. P.J. Kuntz, Molecular Physics, 23, 1035 (1972)

34. P.J. Kuntz, E.M. Nemeth, and J.C. Polanyi, Journal of Chemical Physics, 50, 4607, (1968)

35. P.J. Kuntz, M.H. Mok, and J.C. Polanyi, ibid., 4623

36. R.A. Labudde, P.J. Kuntz, R.B. Bernstein, and R.D. Levine, Journal of Chemical Physics, 59, 6286, (1973)

37. Hyung Kyu Shin, Chemical Physics Letters, 38, 253, (1975)

38. Donald L. Bunker, and E.A. Goring-Simpson, Faraday Discusions of the Chemical Society, 55, 93, (1973)

39. Hyung Kyu Shin, Chemical Physics Letters, 34, 546, (1975)

40. A. Cabello and A. Gonzalez Ureña, Chemical Physics Letters, 35, 255, (1975)

41. J.L. Kinsey, G.H. Kwei, D.R. Herschbach, Journal of Chemical Physics, 64, 1914, (1976)

42. James Stone, Donald J. Kouri, Jeong-long Lin, Journal of Chemical Physics, 67, 477,(1977)

43. Hyung Kyu Shin, Chemical Physics Letters, 45, 533, (1977)

44. E.E.B. Cowan, M.A.D. Fluendy, A.M.C. Moutinho, and A.J.F. Praxedes, Molecular Physics, 52, 1125, (1984)

45. A. Gonzalez Ureña, Molecular Physics, 52, 1145, (1984)

46. Seung Choi and R.B. Bernstein, Journal of Chemical Physics, 83, 4463, (1985)

47. Normand C. Blais and Richard B. Bernstein, Journal of Chemical Physics 85, 7030, (1986)

48. Maurice H.M. Janssen, and Steven Stolte, Journal of Physical Chemistry, 91, 5480, (1987)

49. J. Alonso, L. Banares, M. Menendez, and A. Gonzalez Ureña, Canadian Journal Of Chemistry, 66, 1410, (1988)

50. Yu-Ran Lup, and Sidney W. Benson, Journal of Physical Chemistry, 92, 1107, (1988)

51. I. Schecter and R.D. Levine, Chemical Physics Letters, 153, 527, (1988)

52. Paul S. Weiss, Ph.D. Thesis, University of California at Berkeley, (1986)

53. O.S. Heavens J. Optical Society, 51, 1058, (1961)

54. A. Fischer and I.V. Hertel, Zeitschrift für Physik A, 304, 103, (1982)

55. I.V. Hertel and W. Stoll, Adv. At. Mol. Phys., 13, 113, (1978)

56. Journal of Physical and Chemical Referenece Data, 11, 2, (1982) Supplement No. 2. The NBS tables of chemical thermodynamic properties

57. P.S. Weiss, J.M. Mestdagh, M.H. Covinsky, B.A. Balko, and Y.T. Lee, Chemical Physics, 126, 93, (1988)

58. M.F. Vernon, H. Schmidt, P.S. Weiss, M.H. Covinsky, and Y.T. Lee, Journal of Chemical Physics, 84, 5580, (1986)

59. D.R. Herschbach Faraday Discussions of the Chemical Society, 55, 233, (1973)

Table 1

Kinetic data for M + CH_3X reactions

Reactants	T(°K)	k($cm_3molecule^{-1}sec^{-1}$)
Na + CH_3F	804	$(2.8 \pm 0.2) \times 10^{-15}$
Na + CH_3Cl	801	$(2.32 \pm 0.12) \times 10^{-13}$
Na + CH_3Br	817	$(9.9 \pm 0.7) \times 10^{-12}$
K + CH_3F	822	$(3.75 \pm 0.52) \times 10^{-14}$
K + CH_3Cl	817	$(2.7^{+4.7}_{1.7}) \times 10^{-12}$
K + CH_3Br	804	$(1.64 \pm 0.13) \times 10^{-11}$
Rb + CH_3Cl	788-820	$(7.1 \pm 0.7) \times 10^{-12}$
Rb + CH_3Br	782-871	$(2.5 \pm 0.3) \times 10^{-11}$

Table 2

Beam Parameters

Beam	velocity cm/sec	v/Δv	E_{coll}
Na/He	3.1×10^5	6.0	Both
CH_3I @+20°C/He	7.0×10^4	10.4	23.9 kcal/mole
CH_3I @−26°C/He	1.5×10^5	11.1	28.4 kcal/mole

Figures

Figure 1: Schematic of the crossed molecular beam machine

Figure 2: Schematic of the stainless steel seeded supersonic sodium atom source. (1) Noble gas inlet tube, (2) Molybdenum flow constrictor, (3) Mating mini-conflat flanges with nickel gasket, (4) Top oven, (5) Stainless Steel Nozzle heat shield, (6) Nozzle thermocouple, (7) Nozzle disc with .007' nozzle, (8) Nozzle thermal coaxial cable heaters, (9) Nozzle tube, (10) Stainless steel sodium reservoir heat shields, (11) Sodium reservoir, (12)Sodium reservoir thermocouple, (13) Sodium reservoir thermal coaxial cable heaters, (14) Sodium oven support rods.

Figure 3: Hyperfine structure of the $Na(^2P_{3/2} \leftarrow ^2S_{1/2})$ transition

Figure 4: Newton diagram for $Na(3S,3P) + CH_3I \rightarrow \underline{NaI} + CH_3$ at a collision energy of 23.9 kcal/mole

Figure 5: Newton diagram for $Na(3S) + CH_3I \rightarrow \underline{NaI} + CH_3$ at a collision energy of 28.4 kcal/mole

Figure 6: NaI m/e=23 laboratory angular distribution for Na(3S,3P) + CH_3I at a collision energy of 23.9 kcal/mole

Figure 7: NaI m/e=23 laboratory angular distribution for Na(3S) + CH_3I at a collision energy of 28.4 kcal/mole

Figure 8: The best fit to the NaI laboratory angular distribution for Na(3S) + CH_3I at a collision energy of 23.9 kcal/mole. The solid line shows the fit to the data.

Figure 9: The best fit to the NaI laboratory angular distribution for Na(3P) + CH_3I at a collision energy of 23.9 kcal/mole. The solid line shows the fit to the data.

Figure 10: The best fit to the NaI laboratory angular distribution for Na(3S) + CH_3I at a collision energy of 28.4 kcal/mole. The solid line shows the fit to the data.

Figure 11: Center of mass angular distribution for Na(3S) + $CH_3I \rightarrow \underline{NaI} + CH_3$ E_{coll} = 23.9 kcal/mole

Figure 12: Center of mass angular distribution for Na(3P) + $CH_3I \rightarrow \underline{NaI}$ + CH_3 E_{coll} = 23.9 kcal/mole

Figure 13: Center of mass angular distribution for Na(3S) + $CH_3I \rightarrow \underline{NaI}$ + CH_3 E_{coll} = 28.4 kcal/mole

Figure 14: Center of mass translational energy distribution for Na(3S) + $CH_3I \rightarrow NaI + CH_3$ E_{coll} = 23.9 kcal/mole

Figure 15: Center of mass translational energy distribution for Na(3P) + $CH_3I \rightarrow NaI + CH_3$ E_{coll} = 23.9 kcal/mole

Figure 16: Center of mass translational energy distribution for Na(3S) + $CH_3I \rightarrow NaI + CH_3$ E_{coll} = 28.4 kcal/mole

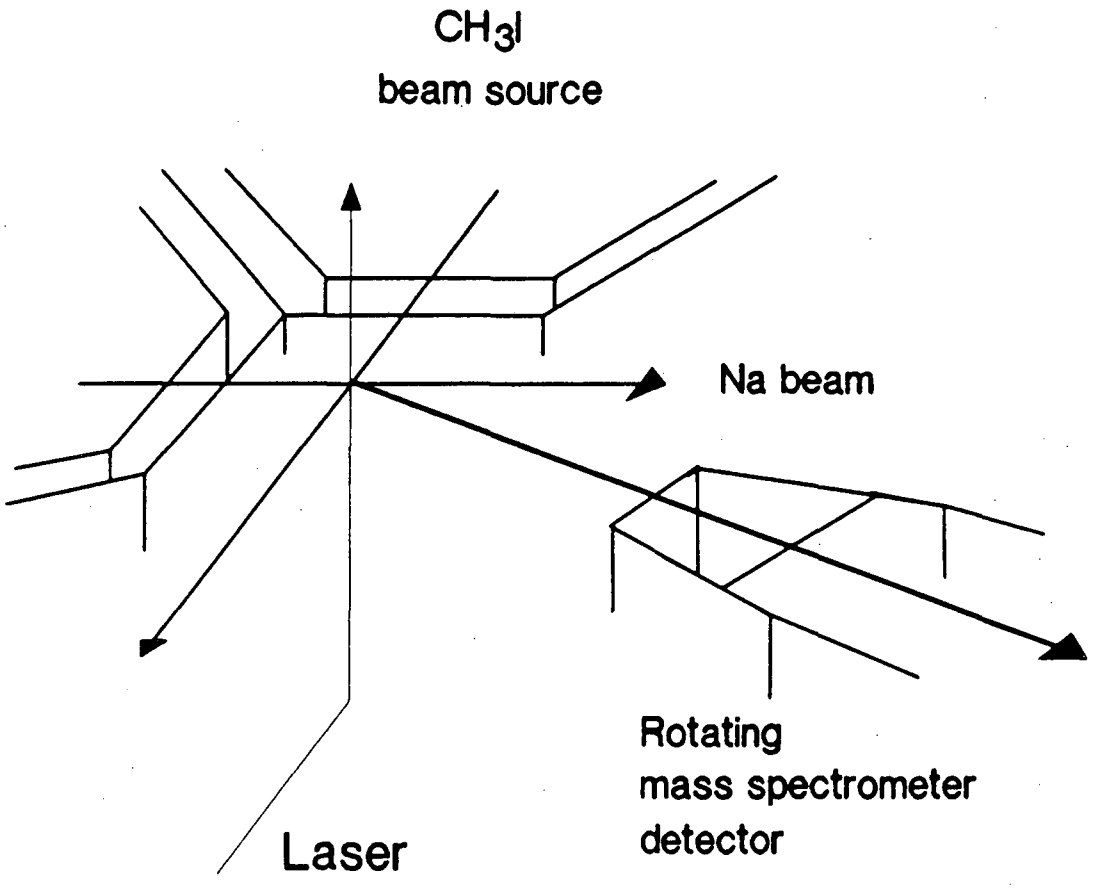
CH_3I
beam source
Na beam
Rotating
mass spectrometer
detector
Laser
XBL 9011-3716

Figure 1

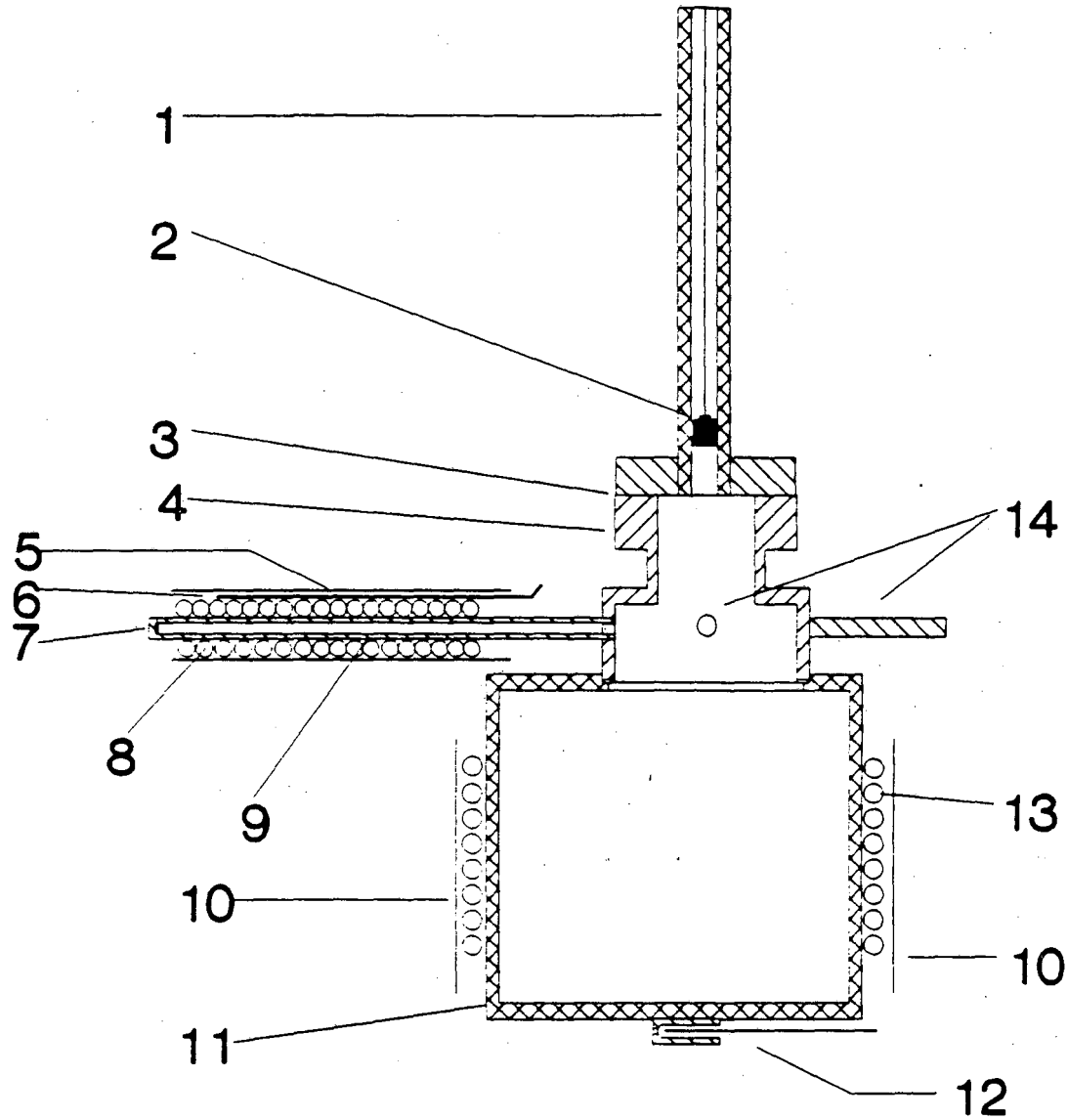

XBL 9011-3717

Figure 2

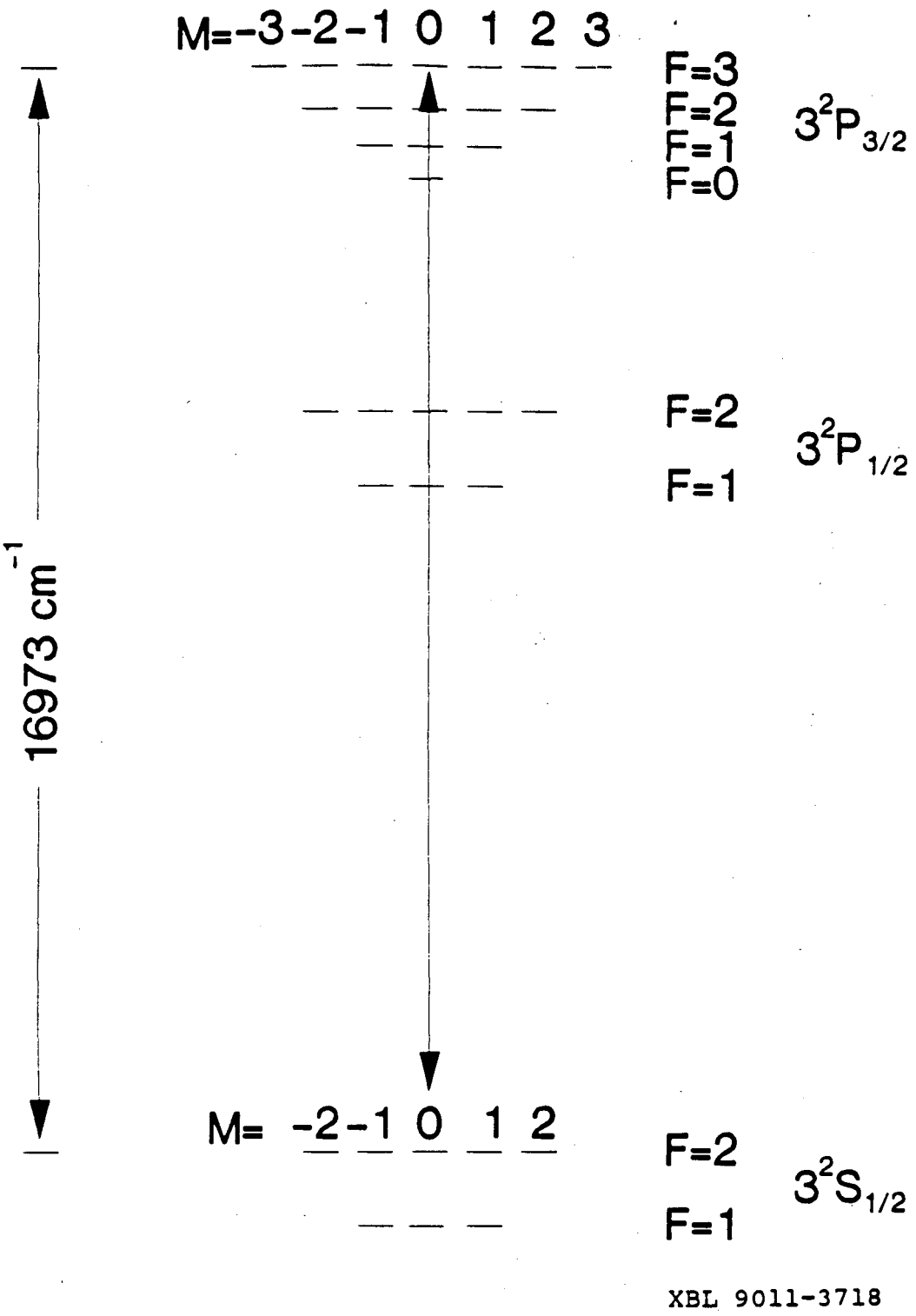
M=-3 -2 -1 0 1 2 3
F=3
F=2
F=1
F=0
$3^2P_{3/2}$
F=2
F=1
$3^2P_{1/2}$
16973 cm^{-1}
M= -2 -1 0 1 2
F=2
F=1
$3^2S_{1/2}$
XBL 9011-3718

Figure 3

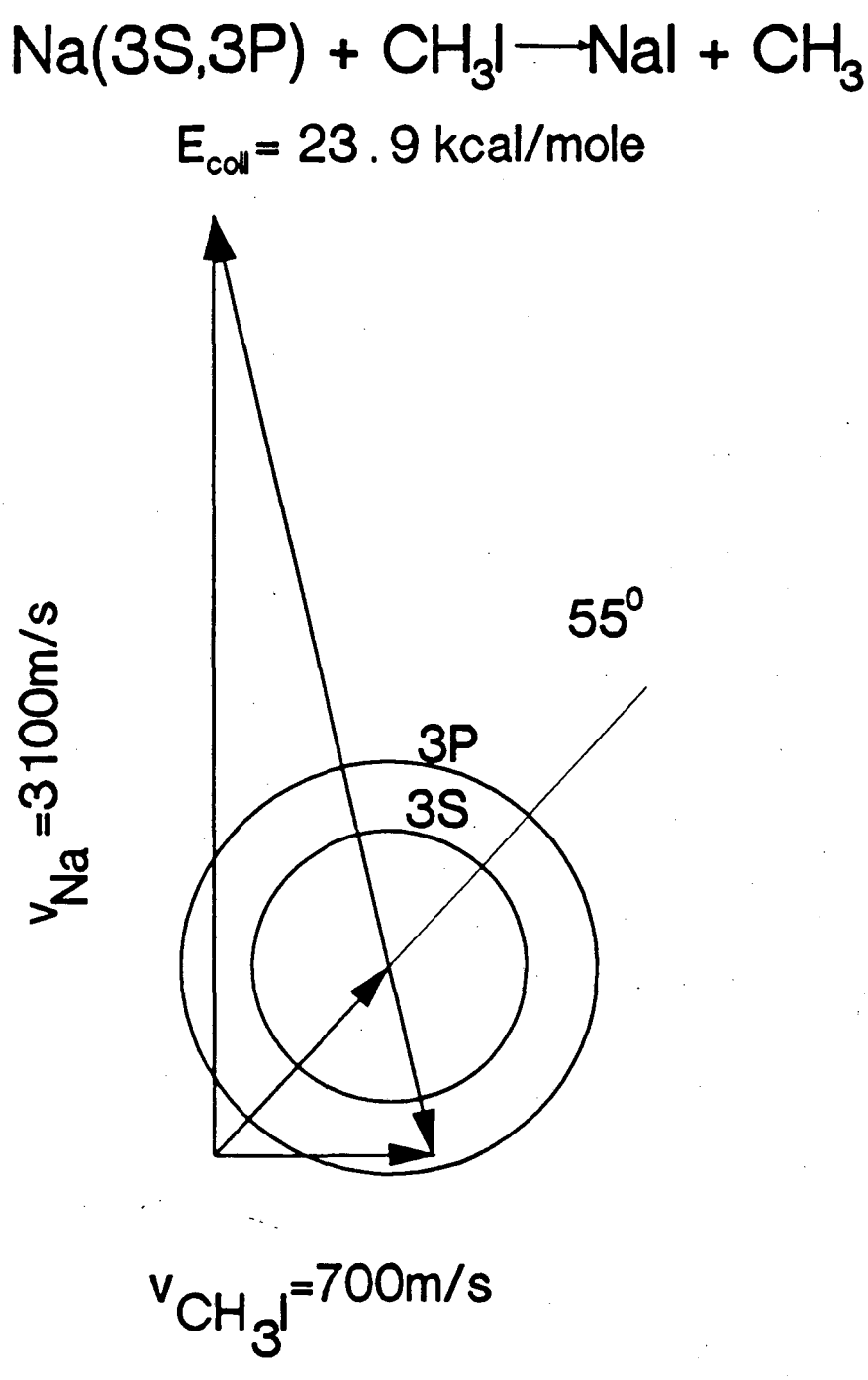
Na(3S,3P) + CH3I → NaI + CH3
Ecoll = 23.9 kcal/mole
55°
3P
3S
vNa=3100m/s
vCH3I=700m/s
=1000 m/s
XBL 9011-3719

Figure 4

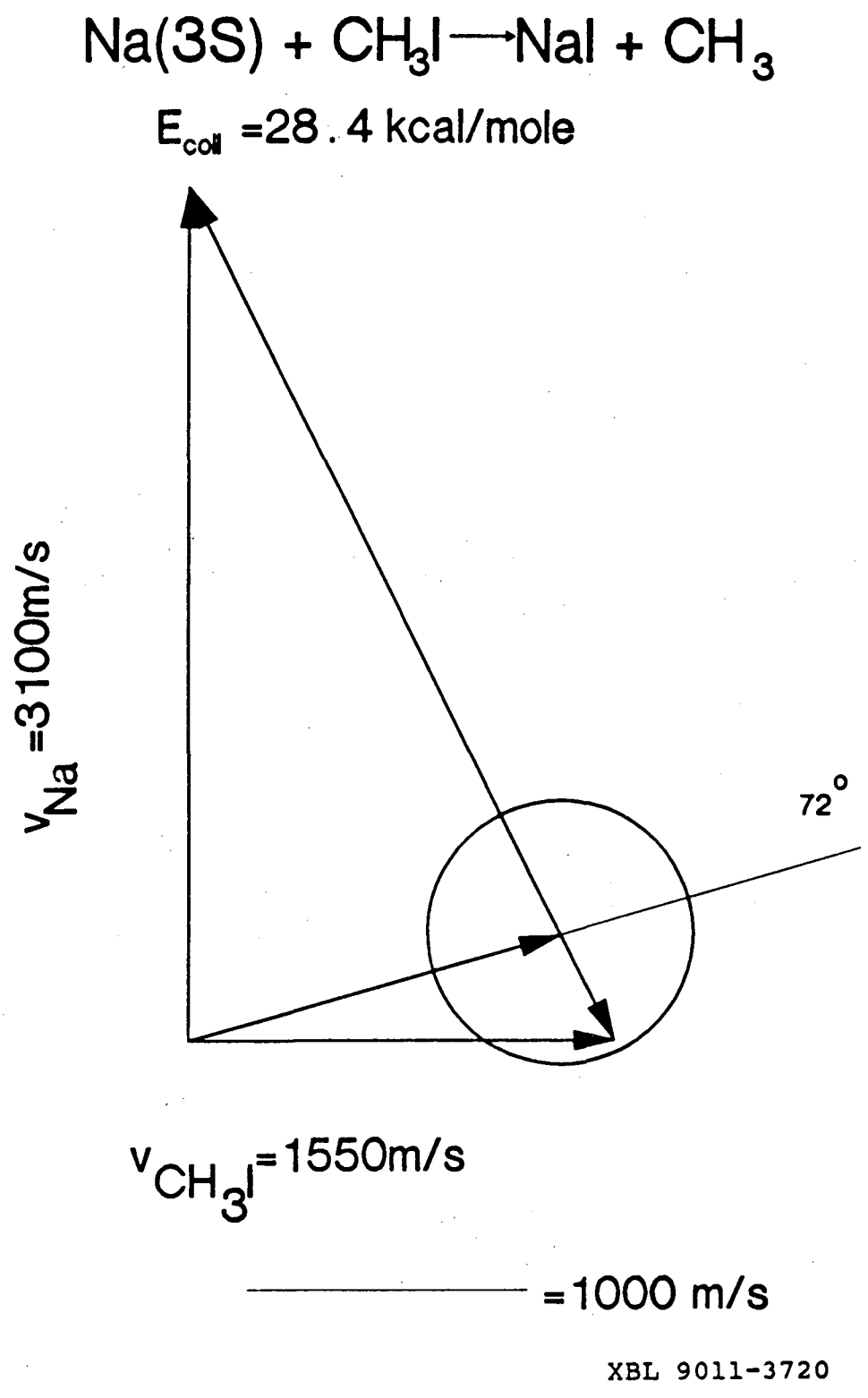
Na(3S) + CH3I → NaI + CH3
Ecoll =28.4 kcal/mole
vNa=3100m/s
72°
vCH3I=1550m/s
=1000 m/s
XBL 9011-3720

Figure 5

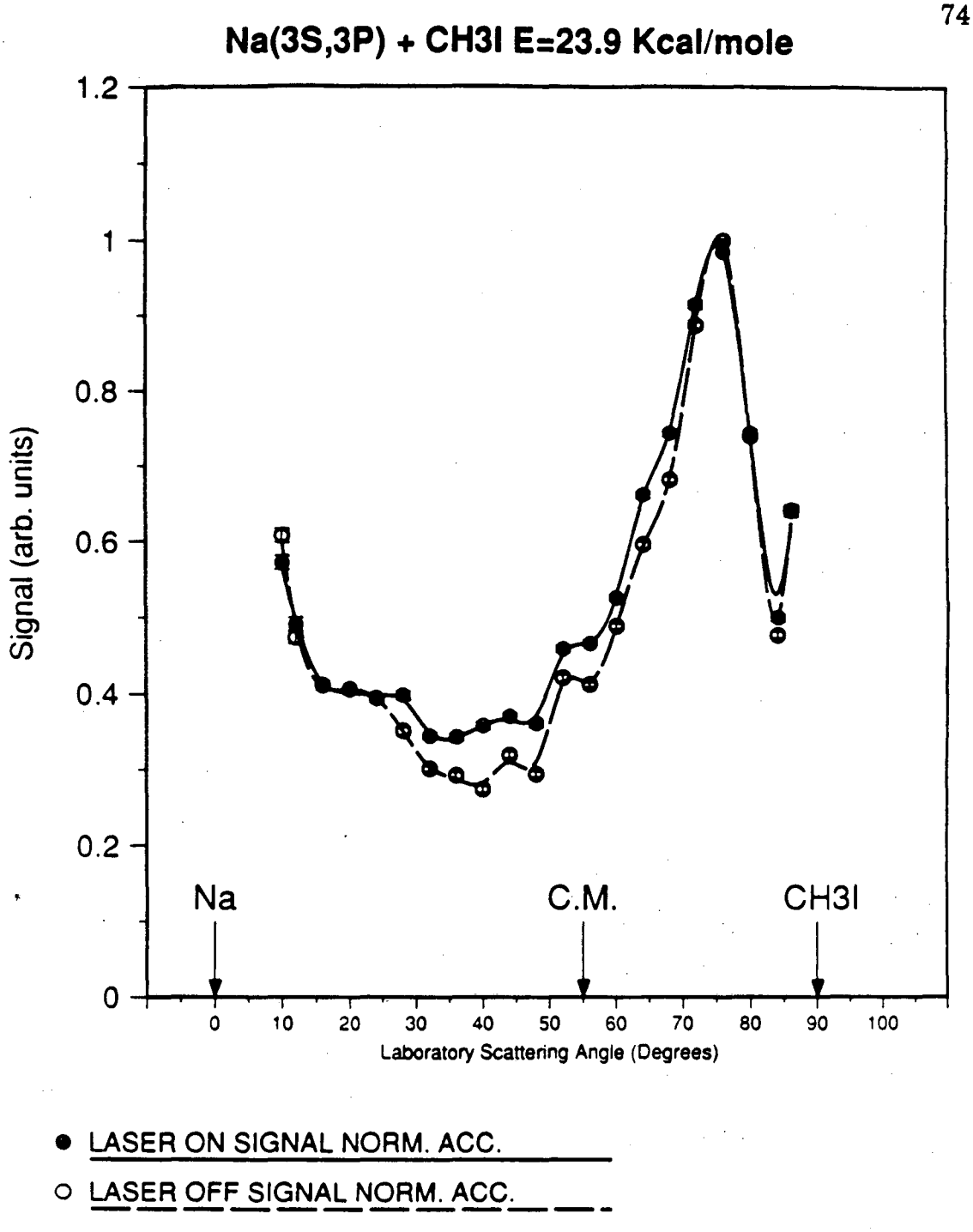
Na(3S,3P) + CH3I E=23.9 Kcal/mole
Signal (arb. units)
1.2
1
0.8
0.6
0.4
0.2
0
Na
C.M.
CH3I
0
10
20
30
40
50
60
70
80
90
100
Laboratory Scattering Angle (Degrees)
LASER ON SIGNAL NORM. ACC.
LASER OFF SIGNAL NORM. ACC.
XBL 9011-3721

Figure 6

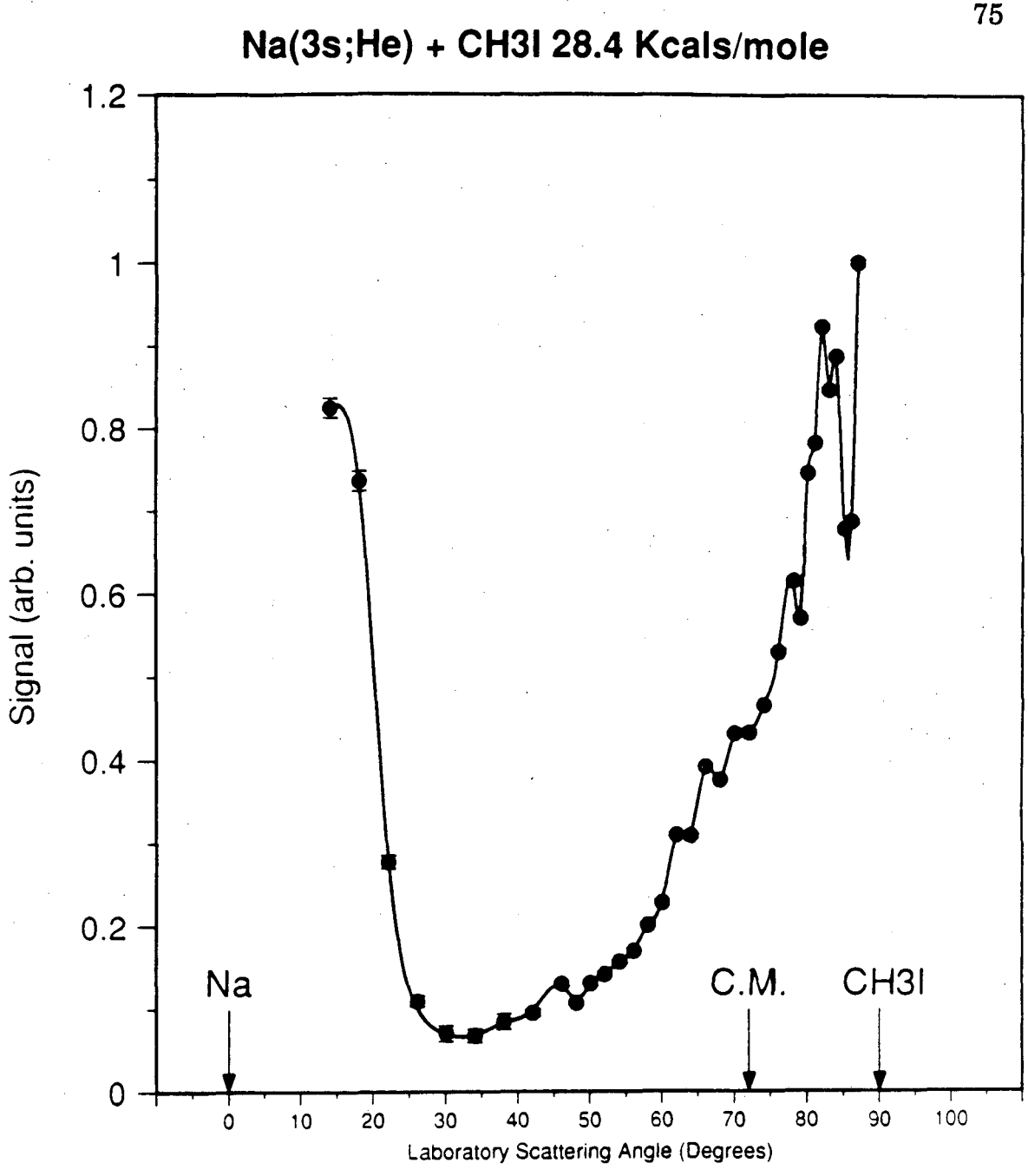
Na(3s;He) + CH3I 28.4 Kcals/mole
Signal (arb. units)
1.2
1
0.8
0.6
0.4
0.2
0
Na
C.M.
CH3I
0
10
20
30
40
50
60
70
80
90
100
Laboratory Scattering Angle (Degrees)
SIGNAL NORM. ACC.
XBL 9011-3722

Figure 7

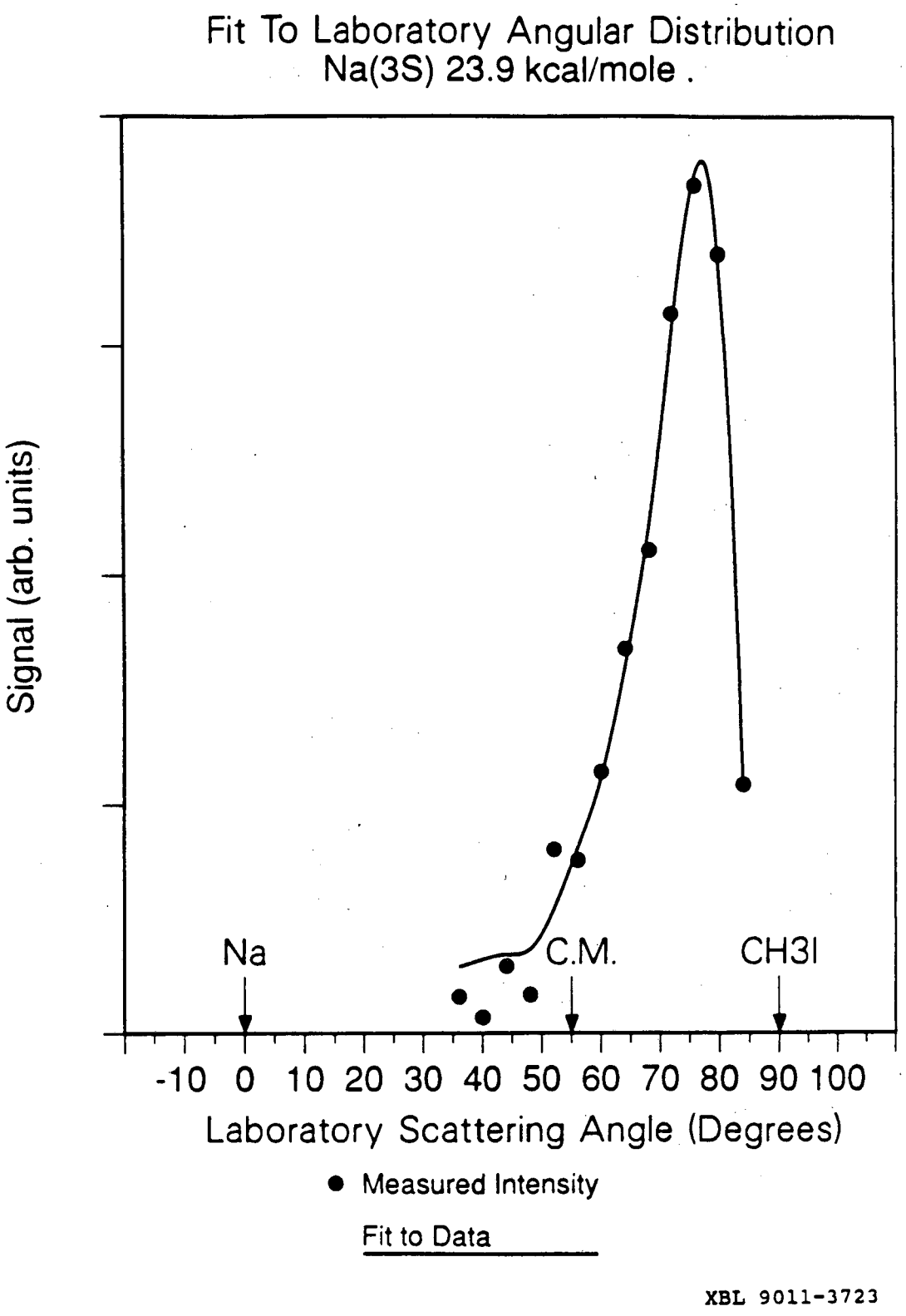
Fit To Laboratory Angular Distribution
Na(3S) 23.9 kcal/mole .
Signal (arb. units)
Na
C.M.
CH3I
-10 0 10 20 30 40 50 60 70 80 90 100
Laboratory Scattering Angle (Degrees)
Measured Intensity
Fit to Data
XBL 9011-3723

Figure 8

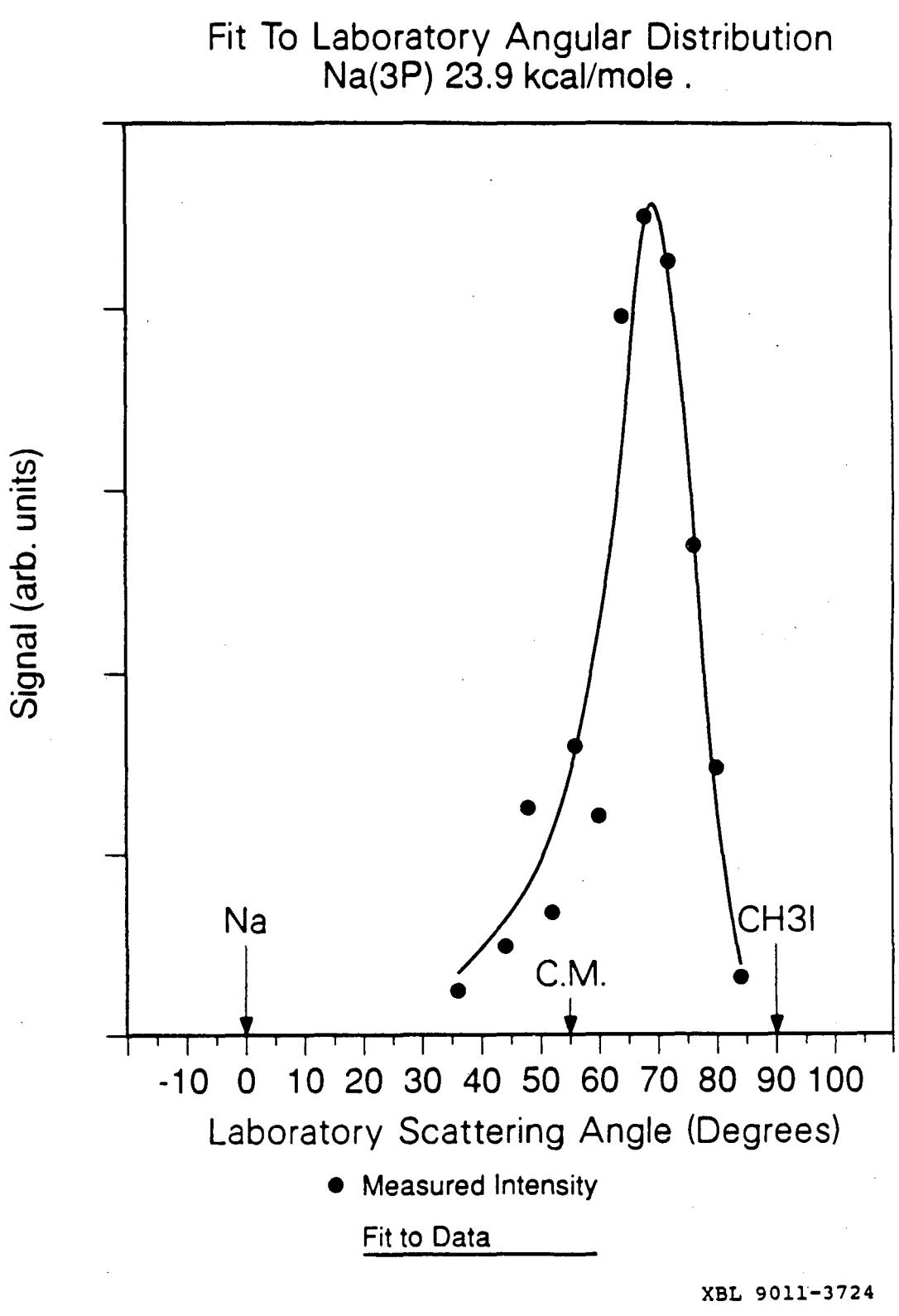
Fit To Laboratory Angular Distribution
Na(3P) 23.9 kcal/mole .
Signal (arb. units)
Na
C.M.
CH3I
-10 0 10 20 30 40 50 60 70 80 90 100
Laboratory Scattering Angle (Degrees)
Measured Intensity
Fit to Data
XBL 9011-3724

Figure 9

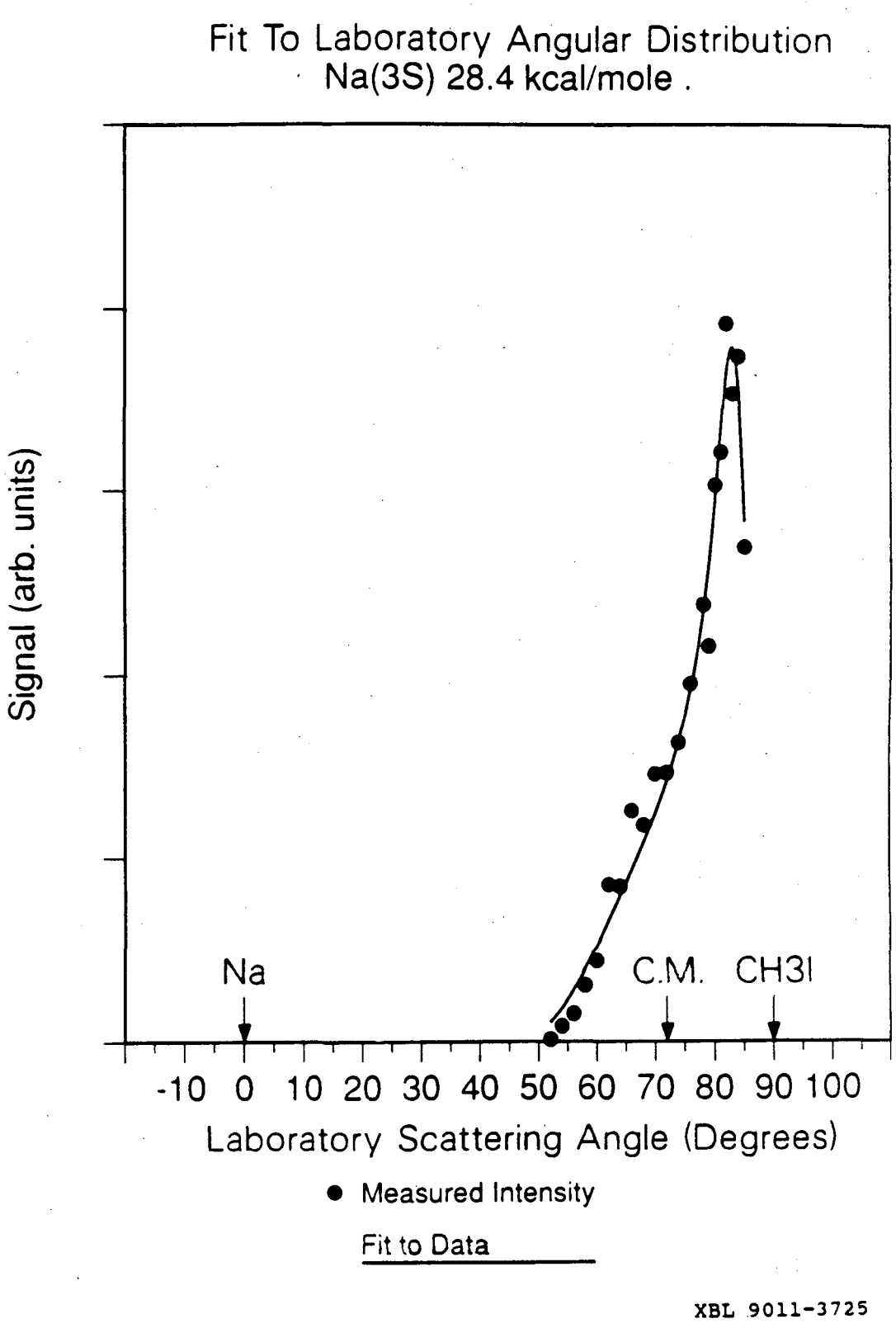
Fit To Laboratory Angular Distribution
Na(3S) 28.4 kcal/mole .
Signal (arb. units)
Na
C.M.
CH3I
-10 0 10 20 30 40 50 60 70 80 90 100
Laboratory Scattering Angle (Degrees)
Measured Intensity
Fit to Data
XBL 9011-3725

Figure 10

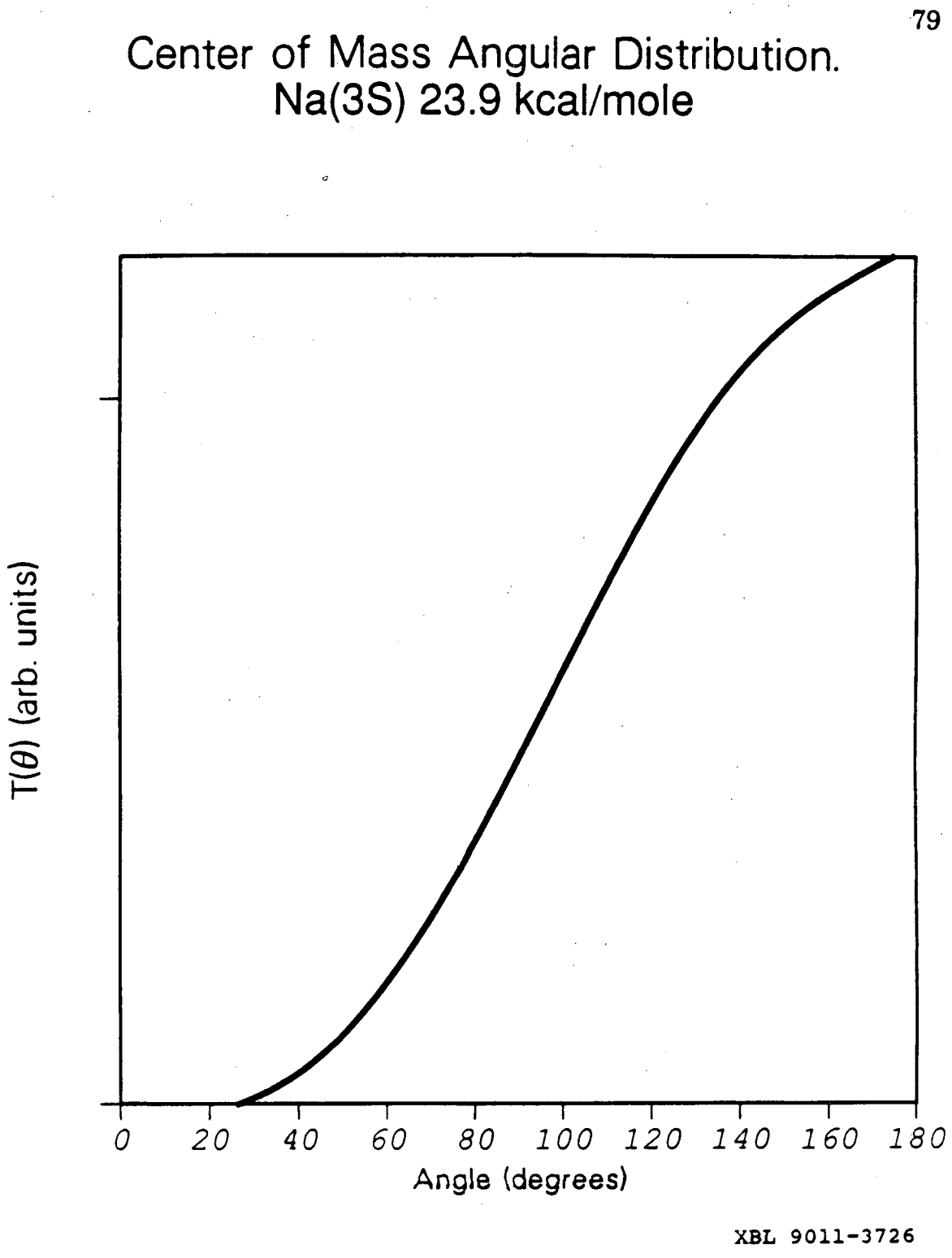
Center of Mass Angular Distribution.
Na(3S) 23.9 kcal/mole
T(θ) (arb. units)
0
20
40
60
80
100
120
140
160
180
Angle (degrees)
XBL 9011-3726

Figure 11

Center of Mass Angular Distribution. Na(3P) 23.9 kcal/mole

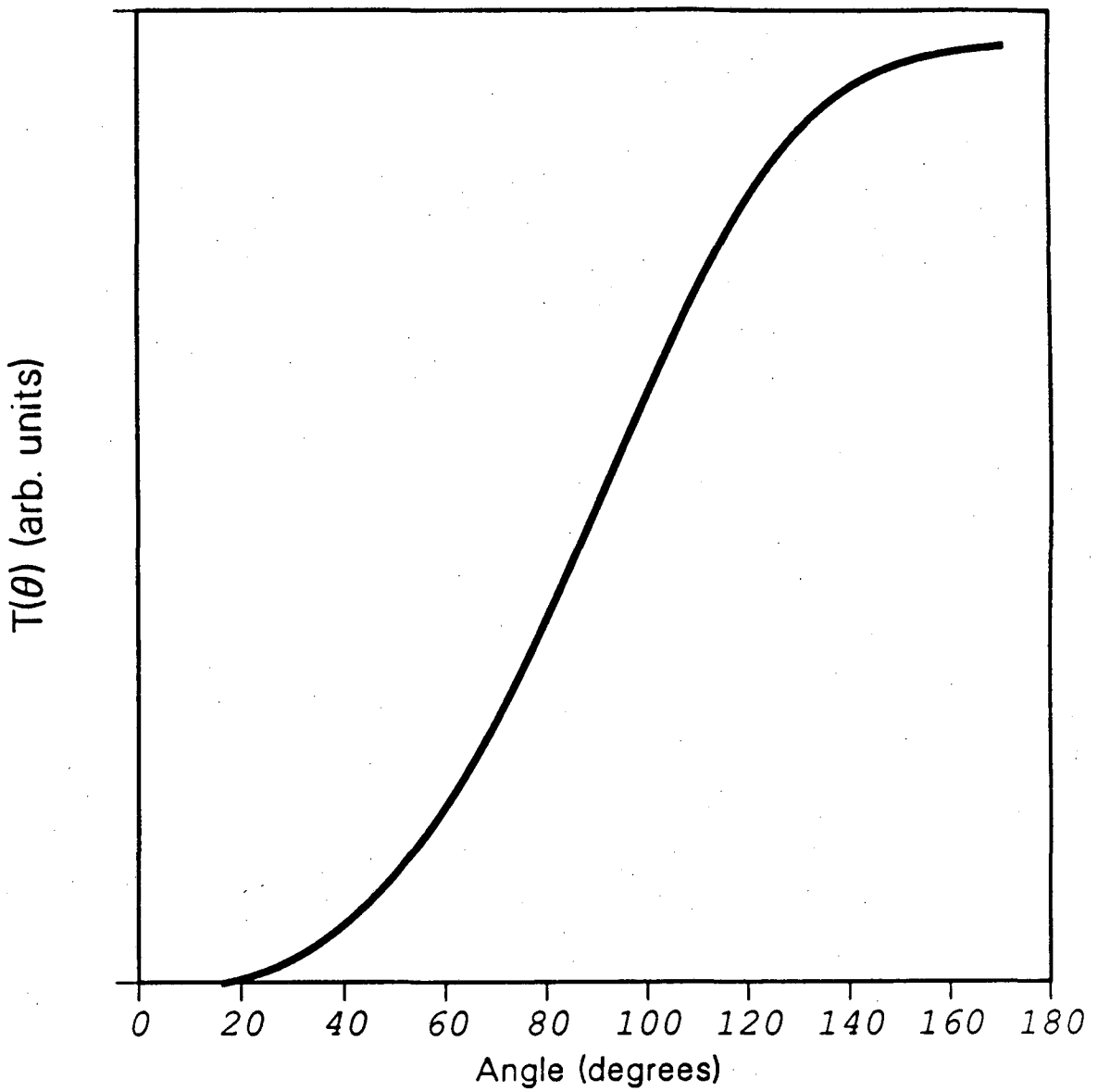

XBL 9011-3727

Figure 12

Center of Mass Angular Distribution.
Na(3S) 28.4 kcal/mole

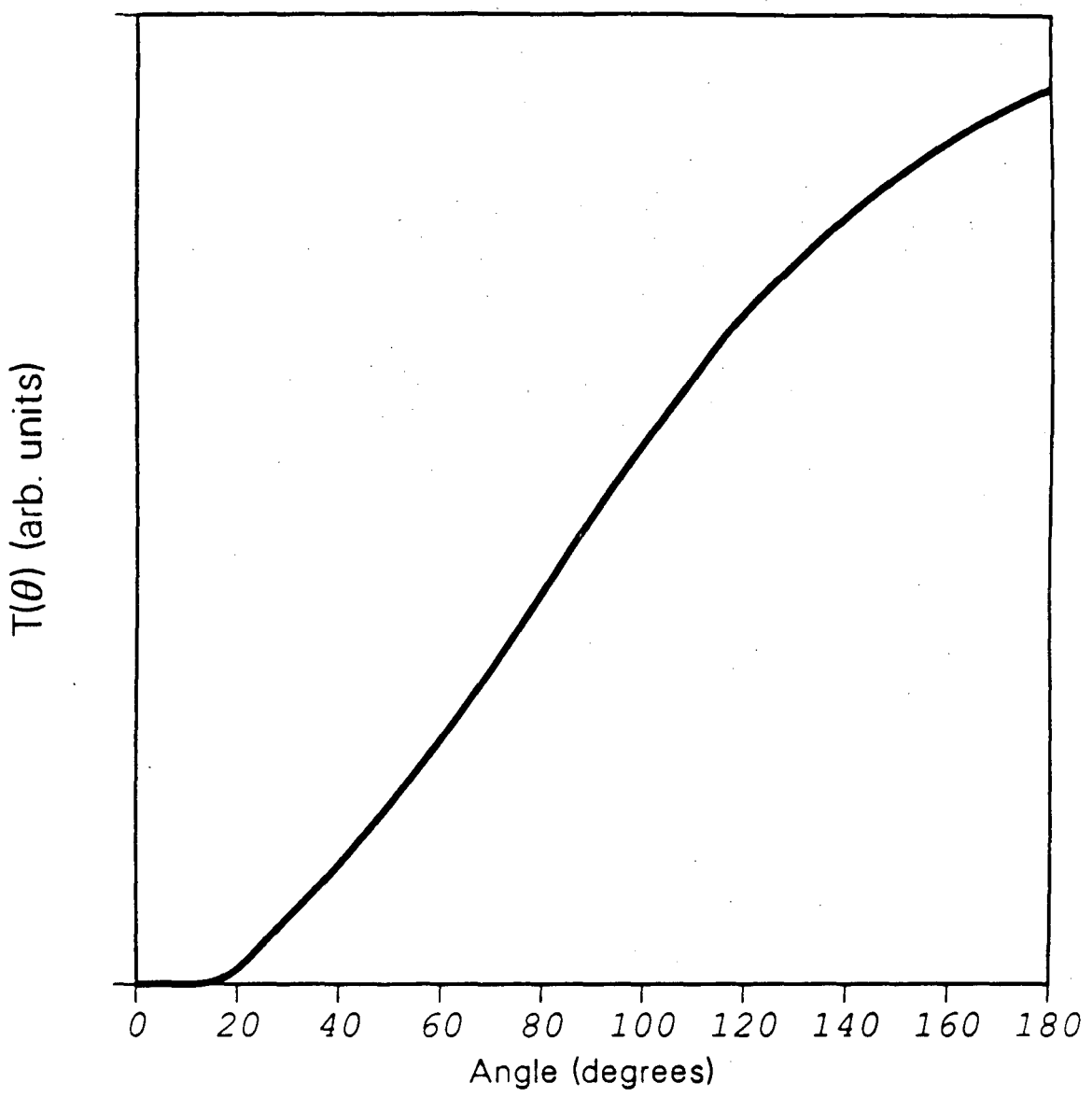

XBL 9011-3728

Figure 13

Translational Energy Distribution.
Na(3S) 23.9 kcal/mole

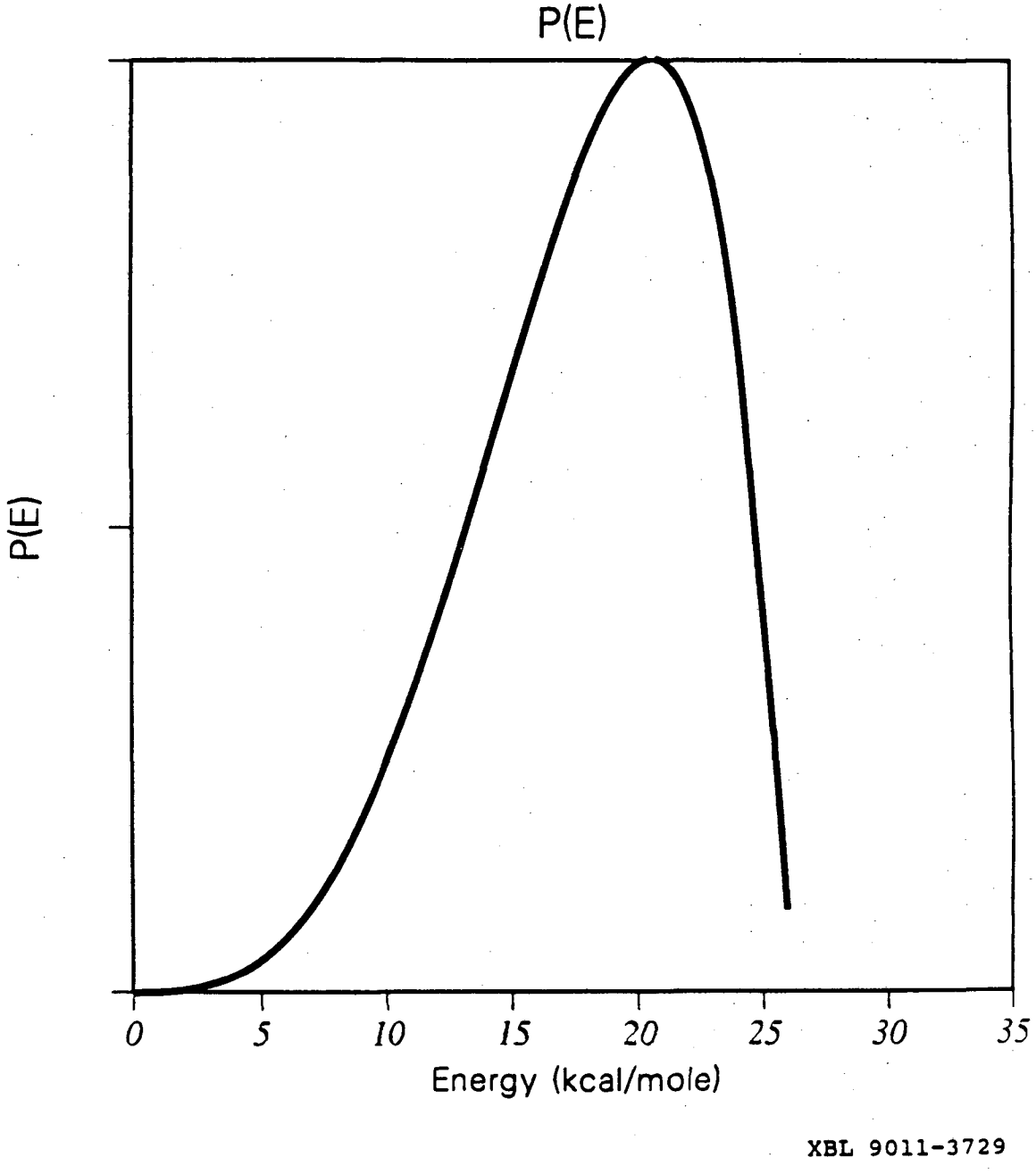

Figure 14

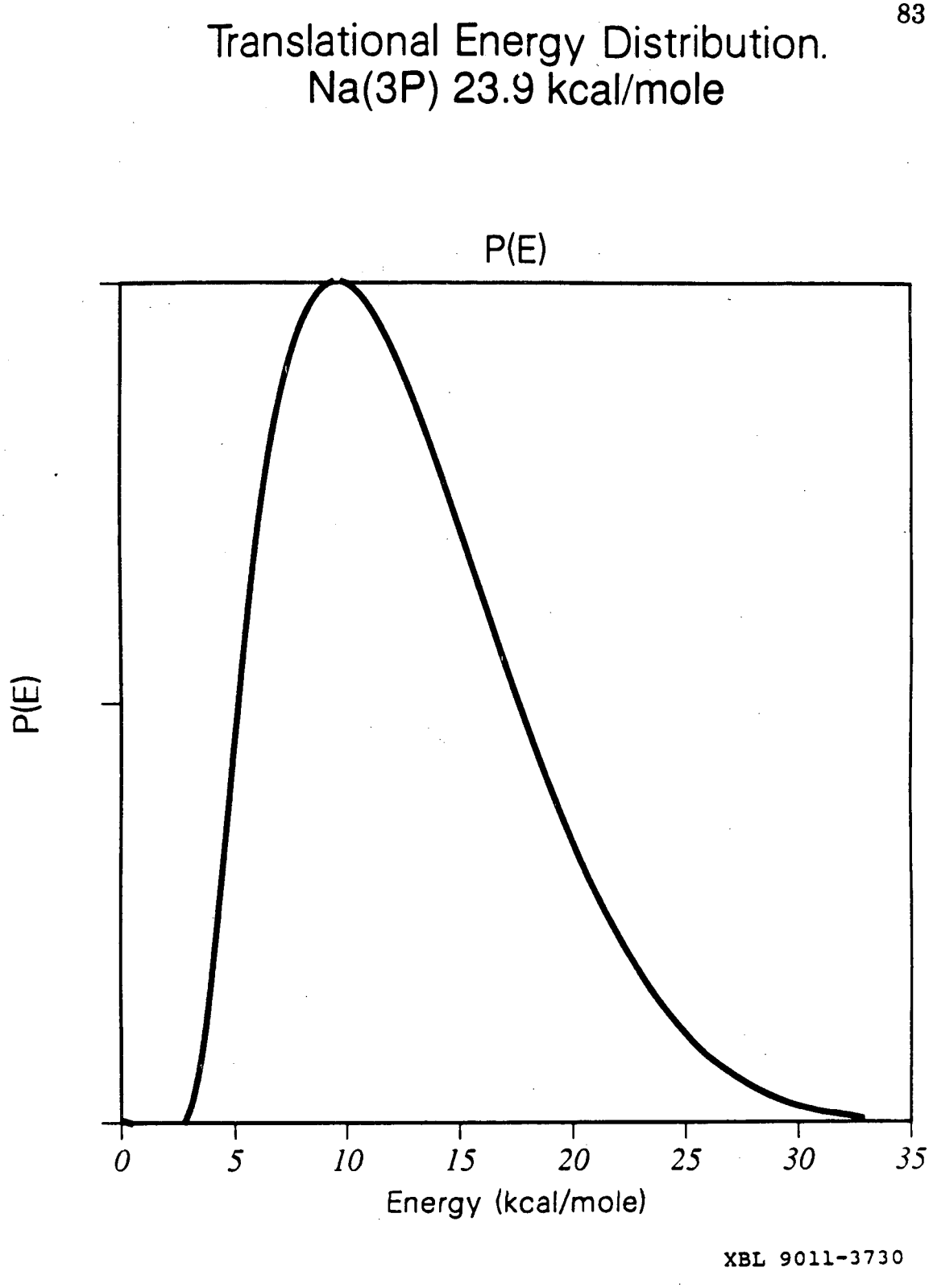
Translational Energy Distribution.
Na(3P) 23.9 kcal/mole
P(E)
P(E)
0
5
10
15
20
25
30
35
Energy (kcal/mole)
XBL 9011-3730

Figure 15

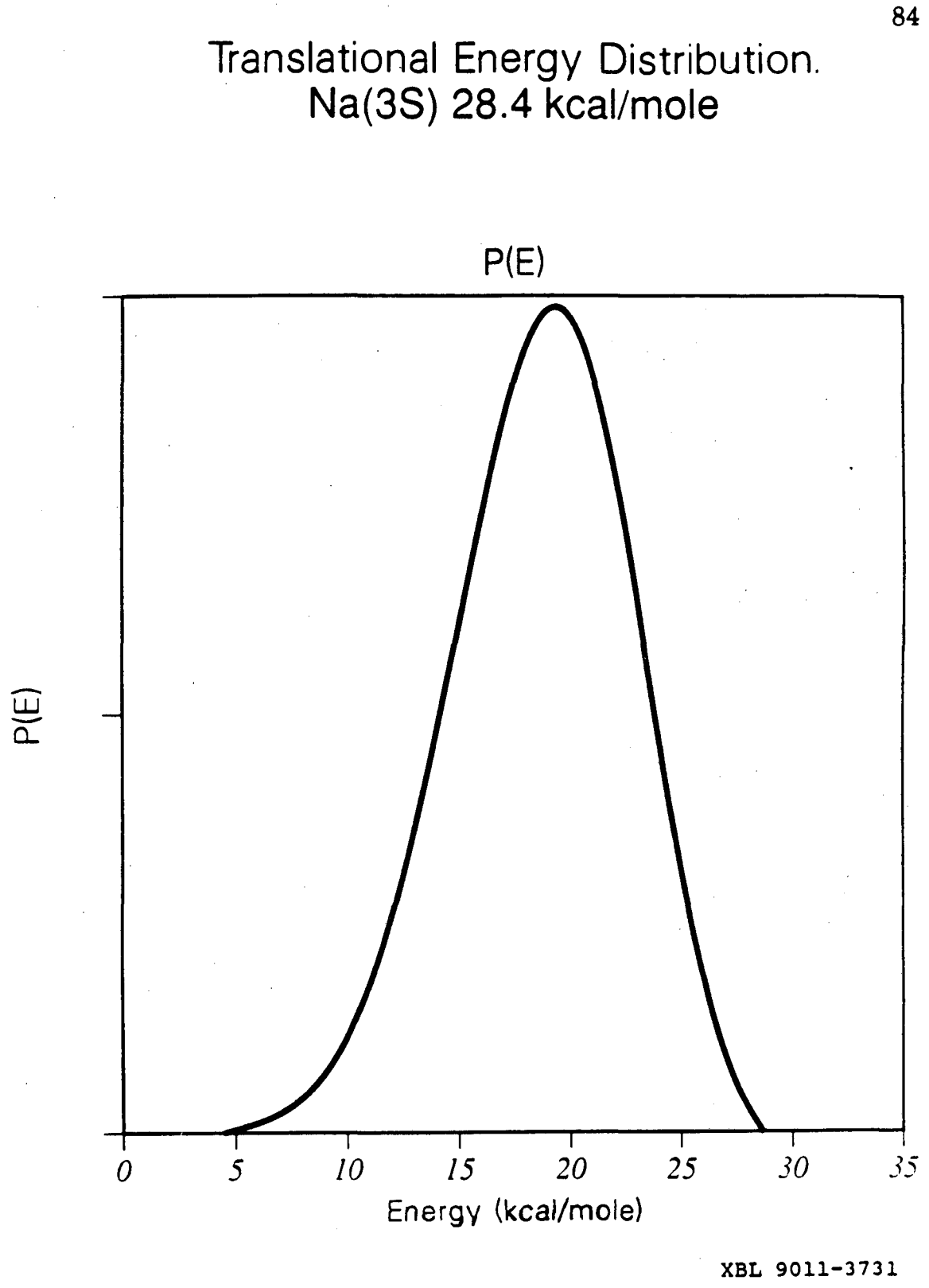
Translational Energy Distribution.
Na(3S) 28.4 kcal/mole
P(E)
P(E)
0
5
10
15
20
25
30
35
Energy (kcal/mole)
XBL 9011-3731

Figure 16

Chapter 3

Predicting the Outcome of Excited State Sodium Reactions

Introduction

When the studies of the reactions of excited sodium began one of the goals was to see how putting in a large amount of energy into the reactants and changing the potential surface the reactants begin on would affect the course of the reaction. The simple harpoon relation[1]

$$\sigma = \pi * (\frac{14.4}{I.P.-EA})^2$$

where I.P. is the ionization energy of the donor atom in eV and E.A. is the electron affinity of the electron acceptor in eV predicted that the cross sections should grow rapidly with electronic energy and approach infinity when the ionization energy approached the electron affinity. One difficulty with this model is the value of the electron affinity. There are three commonly used definitions for the electron affinity. One value is the

vertical electron affinity. This value is the energy difference between the neutral potential curve and the anionic potential curve taken at the equilibrium bond distance of the neutral molecule. These values tend to underestimate the value of the ground state cross section. A second value that can be used is the adiabatic electron affinity which is the energy difference between the minima of the neutral and anionic potential curves. The third value used is the reactive electron affinity. This is similar to the vertical electron affinity but is taken at the outer turning point of the neutral molecule.[2] This produces a result intermediate between the two other electron affinities.

All three models suffer from the same problem. As the electron excitation of the donor atom increases the cross section should approach infinity. One reason the cross section does not go up as rapidly is that as the crossing radius between the covalent and ionic surfaces increases the overlap between the electronic wave function on the donor atom and the electronic wave function on the acceptor molecule decreases. There are a number of methods of calculating the coupling constant.[3,4] These methods suffer the problem of either requiring knowledge of the anionic potentials to calculate the proper coupling constants or requiring the proper value of the electron affinity.

When these studies began it was hoped to see a reaction that did not occur in the ground state "turn on" in the excited state. Although

enhancements were seen in the reactivity of systems in which there was a small signal seen in the ground state, no non-reactive systems turned themselves on with the exception of $Na(4^2D) + O_2$. Additionally the enhancements seen were much smaller than those predicted by harpoon models.[5]

Table 1 is a listing of all the sodium atom systems studied in our laboratory. The Na electronic energy levels for which signal was seen are shown in bold face. As can be seen some systems remained non-reactive even when 100 kcal/mole of electronic energy was added. The ground state thermodynamics of each system are shown in Table 2.[6] As can be seen there is no simple correlation between ΔH and reactivity.

A very broad range of systems has been studied. What is desired is a freshman chemistry level model that will in a broad way predict the reactivity of Na^* + AB systems. In particular an experimentalist would like a way of predicting which systems will not react. A great deal of effort went into studying the non-reactive systems listed. It was necessary to be certain that the lack of signal was due to the system being studied and not an error in the setup of the experiment. If it is possible to predict whether or not reactive signal will be seen then we will have a guide to help us decide which systems ought to be looked at.

The analogy between long-range electron transfer and dissociative attachment in electron scattering in electron scattering has been previously

noted.[5,7] Electronically excited sodium atoms can be thought of as a source of low energy electrons. In a sufficiently excited atom one might consider the interaction between the excited atom and the molecule to be independent of the ion core. If a molecule AB has a low energy dissociative attachment resonance leading to A^- + B then transfer of an electron from Na^* to the molecule should be facile resulting in Na^+A^- + B products. Dunning and coworkers[8,9] have studied the collisions of potassium atoms in high Rydberg states. They found for the reaction:

$$K(nd) + C_2Cl_4 \rightarrow Cl^- + K^+ + C_2Cl_3 \quad 12 \leq n \leq 100$$

that the cross section rises until n=40 and the levels off. The authors show that this behavior is what is expected if the Rydberg atom collision corresponds to s-wave of free electrons. This demonstrated that collisions of sufficiently excited atoms with molecules can be thought of as collisions between a molecule and a low energy electron with the ion core acting as a spectator. For most of the cases discussed below it is those molecules with low energy dissociative attachment resonances that will be reactive.

Comparison of Reactive and Electron Scattering Data

Cl_2

Cl_2 has a zero eV resonance for Cl^- production with a cross section of 1 x 10^{-16} cm^2.[10] This large dissociative cross section at zero eV is in line with the large reactive cross sections.

Hydrogen Halides

Dissociative Attachment Resonances

	ε(eV)	σ(cm^2)
HF/(F^-)	>2.4[11]	N.A.
HCl/(Cl^-) [12]	0.84	$2.7x10^{-17}$
HBr/(Br^-) [13]	0.	$2.7x10^{-16}$
HI/(I^-) [13]	0.	$2.3x10^{-14}$

The large thermodynamic threshold for dissociative attachment to HF is consistent with the fact that no reaction was seen for this system. The lower threshold for attachment to HCl is consistent with the fact that we saw reaction for this system. The signal seen for HBr was much larger than that seen for HCl. HI was not studied but according to the dissociative attachment data the reactive cross section should be enormous.

Methyl Halides

Dissociative Attachment Resonances

	ε(eV)	σ(cm^2)
CH_2Cl_2/(Cl^-)[14]	0.	$\sigma<1x10^{-19}$
CH_3Cl/(Cl^-)	0.	$\sigma<1x10^{-20}$
CH_3NO_2/(NO_2^-)	0.6	N.A.
CH_3I/(I^-)	0.	$3x10^{-17}$

$CH_3Br/(Br^-)$	0.	$2x10^{-18}$
$CH_3CN/(CN^-)$	0.	$\sigma<1x10^{-21}$

The only methyl halides in which reaction was unequivocally seen were CH_3I and CH_3Br. In these systems the resonance energies are all very low but the magnitudes of the cross sections vary. CH_3Cl reaction was seen but the signal was not strong enough to take an angular distribution. These data are consistent with the molecular beam studies of Goldbaum and Martin for K atom reactions[15] and the data presented in Table 1 of Chapter 2 of this thesis.

Oxygen and Ozone

	ε(eV)	$\sigma(cm^2)$
$O_3(O^-)$	0.	N.A.(see chapter 1)
$O_2(O^-)$[16]	Threshold 4.5 Max 6.7	$1.3x10^{-18}$

Of the systems studied the O_2 system is the most difficult to understand. Reactive scattering was seen only when Na is excited to the $4^2D_{5/2}$ state.[5,17,18] The $5^2S_{1/2}$ state did not react even though it has nearly the same electronic energy. It is important to note that in addition to the dissociative attachment resonance O_2 has extensive transmission resonance structure corresponding to both elastic and inelastic scattering of electrons. This reactive system can nonetheless be explained in terms of electron scattering data. When an electron is transferred from Na^* to O_2 into a state

corresponding to a transmission resonance a long lived $Na^+O_2^-$ complex is formed. Since the ground state reaction is strongly endothermic the complex decays back into the $Na(3^2S) + O_2$ channel. Any electron transfer into a state corresponding to a transmission resonance will yield the quenching channel rather than the reactive channel. Thus in order for reaction to occur the electron must not be transferred at long range. When the sodium atom is excited to the 4^2D level with the d orbital polarized perpendicular to the relative velocity vector and undergoes a collinear collision with O_2, the electronic state of the Na^*-O_2 system has Δ symmetry. This enables the excited electron to avoid being transferred to O_2. If the Na^* can undergo an impulsive collision the electron can be transferred at close range to the σ_u^* antibonding orbital of O_2 yielding the repulsive $^2\Pi_u$ state of O_2^-.[19] It should be noted that short range effects of this type are really beyond the scope of this simplistic model.

Other Oxygen Containing Molecules

	ε(eV)	σ(cm^2)
$NO_2/(O^-)$[20]	1.61	N.A.
$NO_2/(NO^-)$	3.11	N.A.
$NO_2/(O^2)$	4.03	N.A.
$H_2O/(H^-)$[21]	7.0	$1.2x10^{-21}$
$H_2O/(O^-)$	7.0	$1.0x10^{-19}$

$H_2O/(OH^-)$	6.5	$1.3x10^{-18}$
$N_2O/(O^-)$	2.3	$1x10^{-17}$
$CO_2/(O^-)$[22]	4.4	$1.43x10^{-19}$

The reaction of ground state sodium with NO_2 yields NaO + NO. This reaction proceeds via a long lived complex. Since this reaction is only slightly endothermic the complex can decay to NaO + NO. No evidence of transmission resonances was found in the literature. However since the highest occupied molecular orbital in NO_2 is the half-occupied $6a_1$ orbital it is likely that such resonances exist. These resonances would most likely attach smoothly to the O^- dissociative attachment resonance at 1.61 eV. This comparatively low lying resonance rationalizes the reactivity of NO_2 and the NaO product.

H_2O and CO_2 did not react because the resonances at 4.4 and 6.5 eV are too high to contribute to reactions. Signal was seen for the very exothermic N_2O reactions however the signal seen was very weak. The fact that the resonance is at 2.3 eV makes it appear that the only reason that we can see a reaction is the large cross section for this resonance.

<u>D_2/H_2</u>

	ε(eV)	$\sigma(cm^2)$
$D_2/(D^-)$[16]	3.8	$1.7x10^{-22}$

$H_2/(H^-)$	3.8	$8x10^{-24}$

These molecules have high energy dissociative attachment resonances with minuscule cross sections. This is consistent with the fact that no long range electron transfer reaction was seen with this system.

Predictions

If this model is valid then it should be possible to predict the outcome of experiments on systems that have not been tried.

	ε(eV)	σ(cm^2)
$NF_3/(F^-)$[23]	0.	$2.1x10^{-18}$
$SF_6/(F^-)$[24]	2.4	$5.8x10^{-18}$
$SF_6/(F^-)$	0.	$4.5x10^{-16}$
$SF_6/(SF_6^{*-})$	0.	$4x10^{-14}$
$SO_2/(O^-)$	4.5	$8x10^{-18}$
$SO_2/(S^-)$	4.0 (2.5 eV onset)	$3x10^{-19}$
$SO_2/(SO^-)$	4.6	$1x10^{-17}$
$CS_2/(S^-)$[25]	2.5eV onset	N.A.
$COS/(S^-)$[26]	1.15	N.A.
$(CN_2)_2/(CN^-)$[27]	2.7 (1.5 eV onset)	10^{-14}-10^{-15}

The reaction $Na^* + NF_3 \rightarrow NaF + NF_2$ should occur because NF_3 has a low lying resonance with a large cross section. There should either be no reaction or only a small reaction with CS_2 because the resonance is too high in energy. There is the possibility of see the reaction $Na^* + COS \rightarrow NaS + CO$ because the resonance is only at 1.15 eV. The new sodium oven discussed in chapter 1 might allow this experiment to be successful. The SO_2 should not react because the onset of its lowest energy resonance is 2.5 eV and because that resonance has a small cross section. There should only be a weak reaction with the pseudohalogen $(CN_2)_2$ due to its high dissociative attachment threshold. It is possible that a sensitive experiment might see the reaction

$Na(4^2D) + (CN_2)_2 \rightarrow NaCN + CN^*$ because the peak of the resonance has been correlated with the process

$(CN_2)_2 + e^- \rightarrow CN^- \; CN^*(^2\Pi)$

There are two likely reaction channels for $Na^* + SF_6$. The most important one would correlate to the enormous cross section for electron attachment to SF_6 producing SF_6^-. The angular distribution for this channel should have substantial forward-backward character for very high electronic energies. There should also be a substantial amount of the channel $Na^* + SF_6 \rightarrow NaSF_5 + F$ corresponding to the zero energy dissociative attachment resonance. This channel should have a forward-scattered

angular distribution. As a practical matter unless $NaSF_5$ can be detected at the parent mass or at a mass other than m/e=23(Na^+) or m/e=42(NaF^+) this channel is likely to be overwhelmed by the NaF channel.

Vinyl Halides and Halobenzenes[28]

Vinyl Chlorides

	ε(eV)
$C_2Cl_4/(Cl^-)$	0.
$C_2Cl_3H/(Cl^-)$	0.6
1,1-$C_2Cl_2H_2/(Cl^-)$	0.8 (broad)
trans-$C_2Cl_2H_2/(Cl^-)$	0.9 (narrow)
cis-$C_2Cl_2H_2/(Cl^-)$	1.1
$C_2ClH_3/(Cl^-)$	1.3

The first four compounds should be reactive and produce NaCl. The signal should decrease as you move down the table. There are no absolute cross sections published for these resonances but it may be possible to see reaction if the cross section is large enough.

Vinyl Monohalides

	ε(eV)
$C_2H_3I/(I^-)$	0.
$C_2H_3Br/(Br^-)$	0.9

$C_2H_3Cl/(Cl^-)$	1.3
$C_2H_3F/(F^-)$	2.2

From this data one would predict σ_r $C_2H_3I>>C_2H_3Br>C_2H_3Cl$. There should be no reaction with C_2H_3F.

Halobenzenes and paradihalobenzenes

	ε(eV)
$C_6H_5I/(I^-)$	0.
$C_6H_5Br/(Br^-)$	0.8
$C_6H_5Cl/(Cl^-)$	1.0
$p\text{-}C_6H_4I_2/(I^-)$	0.
$p\text{-}_6H_4Br_2/(Br^-)$	0.
$p\text{-}C_6H_4Cl_2/(Cl^-)$	0.4

This data suggests that reaction with $p\text{-}C_6H_4I_2$, C_6H_5I, $p\text{-}C_6H_4Br_2$ and $p\text{-}C_6H_4Cl_2$ should be easily seen. There should also be a reaction with C_6H_5Br and C_6H_5Cl but with a smaller cross section. No resonances were seen with either C_6H_5F or $p\text{-}C_6H_4F_2$ so these molecules should not react.

It is interesting to consider what other phenomena this model predicts. There are isotope effects in the dissociative attachment of

hydrogen halides.[13] In particular $\sigma(HI/I^-)/\sigma(DI/I^-)\approx 2$. Therefore there should be an isotope effect in the reaction

$Na(3S,3P,5S,4D) + HI(DI) \rightarrow NaI + H(D)$

This effect should increase with increasing electronic energy.

Conclusions

It has been shown that there is a strong correlation between the reactive scattering of Na^* and electron scattering. In particular reactive scattering of Na^* will be seen with a molecule if that molecule has a dissociative attachment resonance below ~1.5 eV with a cross section greater than $1x10^{-18}$ cm^2. The new oven may lower the latter number. Additionally if a molecule has a low lying transmission resonance then that molecule will react if the ground state reaction is exothermic or mildly endothermic.

In short comparison with electron scattering subsumes the problems of the proper electron affinity, the potential curves of the ions, and the coupling constants.

Some weaknesses in this model should be pointed out at this time. This model only addresses long range electron transfer. If the reaction is impulsive, if the reaction proceeds via a neutral-neutral adduct, or if the electron transfer is a gradual one occurring smoothly over a range of M^*-AB

distances and configurations then this model is no longer applicable. Additionally we are exciting only the n=4 and n=5 electronic energy levels. The electron still has a high expectation value for its kinetic energy. We are not yet in the regime where the interaction of the ion core may be entirely ignored. This is a very simple construct designed to give a qualitative feel for a wide range of reactions. It is not intended to be a substitute for more sophisticated theoretical methods.[29]

Table 1

Na^* Systems Studied

(continued on the next page)

Molecule	Levels Studied Reactive Levels Underlined	Product
HCl	3S,3P,5S,4D	NaCl
HBr	3S,3P	NaBr
CH_3Cl	3S,3P	N.R.
CH_3Br	3S,3P,4D	NaBr
CH_3I	3S,3P	NaI
Cl_2	3S,3P	NaCl
NO_2	3S,3P,5S,4D	NaO, NaO_2
CO_2	3S,3P	N.R.
H_2O	3S,3P,4D	N.R.

Table 1 Continued

Molecule	Levels Studied	Products
NO	3S,3P,4D	N.R.
N_2O	3S,3P,4D	NaO
D_2	3S,3P,4D	N.R.
O_2	3S,3P,5S,4D	NaO
O_3	3S	NaO
CH_3CN	3S,3P	N.R.
CH_2Cl_2	3S,3P	N.R.

Table 2 Thermodynamic Properties[6]

	Energy(eV)
$Na\ (3^2S_{1/2}) \rightarrow Na\ (3^2P_{3/2})$	2.1
$\rightarrow Na\ (4^2D_{5/2})$	4.3
$\rightarrow Na\ (5^2S_{1/2})$	4.1
$\rightarrow Na^+ + e^-$	5.14
$Na\ (3^2S_{1/2}) + HCl \rightarrow NaCl + H$	0.20
$+ HBr \rightarrow NaBr + H$	0.0
$+ HF \rightarrow NaF + H$	0.56
$+ HI \rightarrow NaI + H$	0.05
$+ CH_3Cl \rightarrow NaCl + CH_3$	−0.60
$+ CH_3Br \rightarrow NaBr + CH_3$	−0.89
$+ CH_3I \rightarrow NaI + CH_3$	−0.60
$+ CH_2Cl_2 \rightarrow NaCl + CH_2Cl$	−0.60(est.)
$+ CH_3CN \rightarrow NaCN + CH_3$	0.80
$+ N_2O \rightarrow NaO + N_2$	−0.90
$+ NO \rightarrow NaO + N$	4.0
$+ NO_2 \rightarrow NaO + NO$	0.3
$\rightarrow NaO_2 + N$	2.8
$+ H_2O \rightarrow NaO + H_2$	2.5
$\rightarrow NaOH + H$	1.5

Table 2 continued

	ε(Ev)
+ $Cl_2 \rightarrow NaCl + Cl$	−1.7
+ $O_2 \rightarrow NaO + O$	2.5
+ $CO_2 \rightarrow NaO + CO$	2.9
+ $D_2 \rightarrow NaD + D$	2.5

ENDNOTES

1. J.L. Magee, Journal of Chemical Physics, 8, 687, (1940)
2. Eric A. Gislason in Alkali Halide Vapors, pp. 415-438, P.Davidovits and D.L. McFadden eds., Academic Press Inc., 111 Fifth Ave., New York, New York, 10003, (1979) and references therein.
3. R.E. Olson, F.T. Smith, and E. Bauer, Applied Optics, 10, 1848, (1971)
4. R.W. Anderson and D.R. Hershbach, Journal of Chemical Physics, 62, 2666, (1975)
5. Paul S. Weiss, Ph.D. Thesis, University of California at Berkeley, (1986)
6. Journal of Physical and Chemical Reference Data, 11, Supplement 2, (1982) The NBS Tables of Chemical Thermodynamic Properties
7. D.R. Hershbach, Faraday Discussions of the Chemical Society, 55, 233, (1973)
8. R.W. Marawar, C.W. Walter, K.A. Smith, and F.B. Dunning, Journal of Chemical Physics, 88, 1, (1988)
9. C.W. Walter, C.B. Johnson, A. Kalamarides, K.A. Smith, and F.B. Dunning, Journal of Chemical Physics, 86, 4945, (1987)
10. Estimated from the rate constant at 213° for 0.054 electrons in D.L. McCorkle, A.A. Christodoulides, and L.G. Christophorou, Chemical Physics Letters, 109, 276, (1984)
11. This is the thermodynamic threshold for this process.

12. O.J. Orient, and S.K. Srivastava, Phys. Rev. A 32, 2678, (1985)

13. L.G. Christophorou and J.A.D. Stockdale, Journal of Chemical Physics, 48, 1956, (1968) or

L.G. Christophorou, J.G. Carter, P.M. Collins and A.A. Christdoulides, Journal of Chemical Physics, 54, 4706, (1971)

14. H.U. Scheunemann, E. Illenberger, and H. Baumgartel, Ber. Bunsenges. Phys. Chem. 84, 580, (1980)

15. Richard Goldbaum and L. Robbin Martin, Journal of Chemical Physics, 62, 1181, (1975)

16. George Schulz, Reviews of Modern Physics, 468, (1973)

17. H. Schmidt, P. S. Weiss, J. M. Mestdagh, and M. H. Covinsky, and Y. T. Lee, The State Specific Reaction of Electronically Excited Sodium Atoms with Oxygen Molecules. Chem. Phys. Lett. **118**, 539-543 (1985). LBL-19763

18. Paul S. Weiss, Jean-Michel Mestdagh, Hartmut Schmidt, Matthew F. Vernon, Michael H. Covinsky, and Barbara A. Balko, and Yuan T. Lee, Reaction Dynamics of Electronically Excited Alkali Atoms with Simple Molecules. In "Recent Advances in Molecular Dynamics," edited by R. Vetter and J. Vigue (Centre Nationsl de la Recherche Scientifique, Paris, (1986) p.15-26. J. Chin. Chem. Soc. (Taipei) **32**, 179-85 (1985). LBL-19719

19. J.M. Mestdagh, D. Paillard, and J. Berlande, Journal of Chemical Physics, 88, 2398, (1988)

20. R. Abouaf, R Paineau, and F. Fiquet Fayard, J. Phys. B Atomic and Molecular Physics, 9, 303, (1978)

21. R.N. Compton, and L.G. Christophorou, Phys. Rev., 150, 110, (1967)

22. O.J. Orient and S.K. Srivastava, Chemical Physics Letters, 96, 681, (1983)

23. G.D. Sides and T.O. Tiernan, Journal of Chemical Physics, 67, 2382, (1977)

24. Marita Fenzlaff, Rolf Gerhard, Eugen Illenberger, Journal of Chemical Physics, 88, 149, (1988)

25. Rainer Dressler, Michael Allan, and Michel Tronc, J. Phys. B. At. Mol. Phys. 20, 393, (1987)

26. Michel Tronc, Laurance Malegat, and Roger Azria, Chemical Physics Letters, 92, 551, (1982)

27. Alexander Kühn, Heinz-Peter Fenzlaff, and Eugen Illenberger, Chemical Physics Letters, 135, 335, (1987)

28. James K. Olthoff, John A. Tossell, and John H. Moore, Journal of Chemical Physics, 83, 11, (1985)

29. Mary M. Gallo and David R. Yarkony, Journal of Chemical Physics, 86, 4990, (1987)

Chapter 4

The Photodissociation of NO_2Cl at 248 and 308 nm

Introduction

Compounds of the type NO_2X especially NO_2Cl and HNO_3 (NO_2-OH) are important to the study of ozone in the atmosphere and to the study of photochemical smog.[1-9] HNO_3 is a major sink for OH and NO_2 both of which can destroy ozone catalytically. The photodissociation cross sections and the probabilities and natures of the photodissociation channels are required to model the effect of these compounds on the ozone layer and in the chemistry of smog.

The structure of NO_2Cl is shown in figure 1.[10] NO_2Cl is a molecule of C_{2v} symmetry. The absorption spectrum is shown in figure 2.[11,12] The assignments shown are based on an analogy to the HNO_3 spectrum[13,14] and are taken from Oh[15]. The transition at 248 nm is a $n \rightarrow \pi^*$ transition whereas

the 308 nm transition is a $\sigma \rightarrow \pi^*$ transition. Both transitions are located on the NO_2 moiety.

There has been very little work done on the photodissociation of NO_2Cl. Nelson[12] measured the quantum yield of Cl atom at 351 nm to be 0.93 ± 0.15 and the quantum yield of O atom to be less than .02.

In a series of experiments that are complementary to the work reported here Oh[15] and Sisk[16] measured the photolysis induced fluorescence (PIF) of NO_2Cl at 193, 248, and 266 nm. They found that the quantum yield for electronically excited NO_2 (NO_2^* = A^2B_2, B^2B_2) is 0.03 ± 0.03, 0.70 ± 0.20 and 0.90 ± 0.50 respectively. The decrease in the NO_2^* yield at high energy is attributed to the formation of the NO + O + Cl channel. This channel may be arrived at in three ways

1) The secondary dissociation of NO_2

$$NO_2Cl + 193\ nm \rightarrow Cl + NO_2(X,A,B) \rightarrow Cl + NO + O$$

2) The secondary dissociation of NOCl

$$NO_2Cl + 193\ nm \rightarrow NOCl + O \rightarrow NO + O + Cl$$

3) The three body dissociation of NO_2Cl

$$NO_2Cl + 193\ nm \rightarrow NO + O + Cl$$

By dispersing the fluorescence from NO_2^* Oh and Sisk obtained internal energy distributions for NO_2^* (figure 3).

There is much more data available for the photodissociation of NO_2Cl analogues especially HNO_3.[17-27] Johnston etal.[19] studied the

photodissociation of HNO_3 at wavelengths ranging from 200 nm to 300 nm. They concluded that the photodissociation occurred through the channel

$$HNO_3 + h\nu \rightarrow OH + NO_2$$

with a quantum yield of one. A later measurement by Jolly etal[22] found a quantum yield of 0.89 ± 0.08 for NO_2 at 222 nm.

More recent measurements have uncovered other channels.[24-27] In a series of measurements Stuhl and coworkers discovered that the channel

$$HNO_3 + 193\ nm \rightarrow HONO + O$$

occurs. They concluded that HONO is formed in the triplet state. They were also the first to observe the production of NO_2^*. However they concluded that this was a minor channel. Nelson etal[26] found that the quantum yield for OH at 193 nm was .42. They did not identify what the other channels were.

The photodissociation of HNO_3 at 193 nm was studied in our laboratory. The analysis of the data is incomplete but the HONO channel has been tentatively identified and the quantum yield is on the order of 0.5. HNO_3 was also studied at 248 nm. This data is unanalyzed but there is no evidence of HONO formation at this energy.

Crim and coworkers have studied the vibrationally mediated photodissociation of HNO_3.[28-32] By using a 755 nm photon to excite the third OH stretching overtone and a 355 nm photon to dissociate the molecule they were able to compare the dynamics of a vibrationally excited

molecule with that of a vibrationally cold molecule excited with an energetically equivalent 241 nm photon. They found that both excitation schemes deposited over three-quarters of the available energy into NO_2. Direct photolysis resulted in more NO_2 internal energy than vibrationally mediated photodissociation. The two-color experiment directed more energy into translation. This was ascribed to the fact that direct photodissociation accesses a potential energy surface that correlates to electronically excited NO_2 whereas vibrationally mediated photodissociation will more often excite a potential energy surface that correlates to ground state NO_2.

August etal[33,34] has done some highly detailed studies of correlation effects at 280 nm. They found the value of β, the anisotropy parameter to be 0.4, $1.0 > \beta > -0.5$ Simple consideration of the symmetries of the molecular orbitals involved in this electronic transition shows that this should either be a perpendicular or forbidden transition. The authors resolve this conflict by pointing out that Walsh's rules predict a pyramidal configuration for the excited state. If the excitation is mediated by the O–N–O(H) out of plane bend then the vibronic transition will become parallel.

The photolysis of N_2O_5 has been studied by several groups.[11,35–37] It was found that the quantum yield of NO_3 was one at all wavelengths. Oh[37] found that by changing the wavelength the relative contributions of the following three channels changed

$N_2O_5 + h\nu \rightarrow NO_3 + NO_2$

$N_2O_5 + h\nu \rightarrow NO_3 + NO_2^*$

$N_2O_5 + h\nu \rightarrow NO_3 + NO + O$

The third channel was predominant at 248 nm with a quantum yield of 0.72 and non-existent at 305 nm. The second channel rose from a yield of .03 at 305 nm to .25 at 266 nm. The energy distribution of NO_2^* was smooth. The presence of the channel 3 is ascribed to the secondary dissociation of NO_2^*. Oh argues that the NO_2 was formed entirely in the $^2B_1$ state.

Butler etal[38,39] studied the photodissociation of CH_3NO_2 at 193 nm. They concluded that the photodissociation occurs by two channels

$CH_3NO_2 + h\nu \rightarrow CH_3 + NO_2^*\ ^2B_2$

$\rightarrow CH_3 + NO + O$

The NO + O channel occurs via the secondary dissociation of NO_2^*. They found that the anisotropy parameter for the photodissociation was $\beta=-0.3$

There has been some theoretical work done on the structure of NO_2-X compounds.[13,14,40-47] Most of this work has been done on calculations of the ground state. The generally accepted electron configuration is $1a_1^2 1b_2^2 2a_1^2 3a_1^2 2b_2^2 4a_1^2 5a_1^2 3b_2^2 1b_1^2 4b_2^2 6a_1^2 1a_2^2$. The three lowest transitions are out of the $4b_2$, $6a_1$, and $1a_2$ orbitals and into the unoccupied $3b_1$ orbital. By analogy with the diabatic correlation diagram published by Sinha[32] the $1a_2$, $4b_2$ and the excited $3b_1$ orbitals on NO_2Cl would correlate with the $1a_2$,

$4b_2$, and the excited $2b_1$ orbitals on NO_2. The $6a_1$ orbital carries the bonding on the N-Cl bond and correlates with the singly occupied $6a_1$ orbital on NO_2 and the singly occupied ∘ orbital on OH.

Different calculations have suggested different views of the NO_2Cl molecule. Destro etal[46] suggest that both N and Cl carry a positive charge implying that the ground state has charge transfer character. Kleier[14] found that R–NO_2 molecules have singlet biradical character. Marynick[44] calculated the lowest triplet levels for a series of R–NO_2 compounds. Although the calculated splitting was very sensitive to the basis set, he found that the splitting was proportional to the electronegativity of the atom attached to the nitrogen. His best calculation gave a splitting of 3.75 eV for HNO_3 and 3.99 eV for FNO_2. This implies that some of the excited molecules may have triplet character.

The best calculation to date was done by Bai and Segal[43]. They found that the first excited state was bent with the O-H bond twisted 90° from the plane of the ground state HNO_3 molecule. The lowest excited state adiabatically correlates with ground state NO_2 and the next two excited states adiabatically correlate with NO_2^* B^2B_1. This calculation was in agreement with the argument of August[34] that the forbidden electronic transition is made into a parallel vibronic transition by an out of plane bending vibration.

Frost and coworkers[48] have measured the photoelectron spectrum of NO_2Cl, NO_2F, and HNO_3. They confirm the assignments in general for HNO_3 and FNO_2. For $ClNO_2$ that the highest occupied molecular orbitals were the p_π and p_σ orbitals on the chlorine atom. These would have B_2 and B_1 symmetries respectively and would correlate to the $3b_2$ and $1b_1$ orbitals in HNO_3. These high energy nonbonding orbitals on chlorine imply the possibility of a charge transfer absorption.

Experimental

The experiment was performed on the same machine that was discussed in chapters 1 and 2. Several modifications were made to do photochemistry (figure 4). Light from a Lambda-Physik EMG-103 MSC excimer laser was focused to a .25cm x .35cm rectangular spot where it intersected the NO_2Cl beam. The experiment was performed in a coplanar geometry in which the laser intersected the molecular beam orthogonally in the plane of the detector's rotation. Two pieces of wire mesh were used in the 248 nm experiments to cut down on two photon effects. Measurements inside the machine showed that 13 mj/pulse were delivered to the scattering center. The absorption cross section at this wavelength is 1×10^{-18} cm^2.[11,12] This means that we photodissociate 17% of the molecules in the beam. At 308 nm 20 mj/pulse was focussed to a .35cm x .27cm spot. The absorption

cross section at this wavelength is 1.4 x 10^{-19} cm^2. This means we dissociate 4.6% of the molecules in the beam.

The NO_2Cl was synthesized by Daniel Oh of the Johnston group. The synthesis is described in his thesis and in reference 49. Briefly, dried HCl was passed through a mixture of 25 ml 90% nitric acid, 60 ml 95% sulfuric acid and 70 ml 30% fuming sulfuric acid. The product was collected in a trap at 196 °K. The product was distilled from 175 °K to 77 °K to remove Cl_2 the predominant impurity. For the 308 nm experiments special care was used to remove Cl_2 as Cl_2 absorbs at this wavelength and interfered with the m/e=35 signal.

The molecular beam was formed by bubbling helium through nitryl chloride held in a cold trap at -63 °C. The mixture was expanded through a heated .003" nozzle. In place of the usual defining slits a second skimmer was used to define the beam to a 2 mm diameter at the intersection region. The beam parameters were measured in the same manner as described in chapter 1. The beam conditions and parameters are shown in table 1.

A pulse from the laser controller triggered the multichannel scaler. Signal was measured at one microsecond resolution. the laser was run at 75 - 100 Hz. Typically 200,000 shots were measured at each angle and mass.

Results and Analysis

248 nm

m/e=35

The times of flight taken at m/e=35 (Cl^+) are shown in figures 6–11. The data was fit by the forward convolution method using ROTDET.FOR a specially modified version of CMLAB2.FOR[50] that was altered to analyze data taken the rotating detector geometry. The translational energy distributions, P(E)'s, are point form and freely adjustable. The angular distribution is of the form

$$T(\theta) = 1 + 2\beta P_2[\cos(\theta)]$$

where P_2 is the second legendre polynomial, θ is the angle between the electric vector of the exciting light and the recoil direction of the products in the center of mass frame of reference, and β is the anisotropy parameter and ranges from –0.5 for a perpendicular transition to +1.0 for a parallel transition.

The possible channels are listed below and in table 2. They are illustrated in figure 5.

Channel	Kcal/mole[51]
$NO_2Cl \rightarrow NO_2\ (X^2A_1) + Cl(^2P_{3/2})$	33.9
$\rightarrow NO_2\ (A^2B_2) + Cl(^2P_{3/2})$	61.8
$\rightarrow NO_2\ (B^2B_1) + Cl(^2P_{3/2})$	76.4

$\rightarrow NO\ (X^2\pi) + ClO\ (X^2\Sigma)$ 43.0

$\rightarrow NOCl\ (X) + O(^3P)$ 68.9

$\rightarrow NO\ (X^2\pi) + O(^3P) + Cl(^2P_{3/2})$ 107.1

The spin-orbit splitting of Cl is 881 cm^{-1}. This splitting cannot be resolved in this experiment

The fits to the times of flight are included in figures 6-11. The translational energy distribution P(E) is shown in figure 12. Three clear channels can be identified. The high translational energy component can be ascribed to the production of Cl atom and ground state NO_2. The bulk of the signal is ascribed to the production of Cl atom and excited NO_2. There is some structure in the excited state fit. This can be the production of the A^2B_2 and B^2B_1 states. These peaks are so strongly overlapped that they are not separated into components. Each of these times of flight has a low energy tail. This was fit with a distribution ascribed to the production of a minor O + NOCl channel. The m/e=35 (Cl+) TOF's are the best distributions to make measurements of branching ratios and energy distributions. Since the product being detected is an atom there are no complications from an internal energy dependent ionization cross section or fragmentation pattern. The quantum yield for the production of NO_2^* is 0.66. This compares favorably with the results of Oh discussed in the introduction $\Phi(NO_2^*)=0.7 \pm 0.2$. The quantum yield for ground state NO_2 is 0.32. The yield of NOCl is 0.022. The β parameters for the three channels

are 0.97, 0.95 and 0.78 respectively. These results are summarized in Table 3. The β parameters are those which allow the best fit at the most angles at m/e=35. Due to the mediocre signal to noise of the experiments the counting time at each angle was about one hour. This was longer than the lifetime of a gas fill of the laser. Since the laser power would decline significantly during the course of a measurement the integrated time of flight distributions were not reliable measurements of the angular distributions.

m/e=46 (NO_2^+)

The time of flight distributions taken at m/e=46 are shown in figures 13-17. A different P(E) (figure 18)was used to fit these distributions. This is necessary because the highly excited NO_2^* has an energy dependent fragmentation pattern. Since NO_2 produces mostly NO^+ upon electron impact ionization the NO_2^+ fraction produced is highly dependent upon internal energy. This would result in a loss of NO_2^+ from vibrationally excited NO_2.

Another factor present is the possibility of spontaneous secondary dissociation from highly excited NO_2^*

$$NO_2Cl + 248\ nm \rightarrow Cl + NO_2^* \rightarrow Cl + NO + O$$

This channel should occur for all relative translational energies below 8 kcal/mole.

m/e=30 (NO^+)

These distributions are fit with the same energy distributions and anisotropies used to fit the m/e=35 times of flight (figures 19-23). The only difference between these fits and the m/e=35 fits is that the contribution of NO_2^* has been increased by a factor of 13% to reflect the different ionization cross-sections of ground state and excited NO_2. The effect of secondary dissociation was examined at this mass. Even for the most extreme and unrealistic secondary distributions used the contribution of secondary dissociation was very small and did not change the calculated distribution. Since the energy available is very small the velocity of NO produced by secondary dissociation is not going to be very large.

m/e=16 (O^+)

The signal to noise ratio at m/e=16 was so poor that the full power of the laser was used. This would result in 84% of the molecules dissociating. The distributions are shown in figures 24-27. Their are four components in the fit. The peak is from ground state and excited NO_2. The tail is O^+ production from NOCl and the leading edge is the momentum matched oxygen atom contribution. The P(E)'s and anisotropies are the same as those used to fit m/e=35. The only change is in the relative contributions of each channel which reflects the differing ionization cross sections and fragmentation patterns of the different channels.

The leading edge of these TOF's shows the effect of two photons being absorbed. This is not a surprise as the absorption cross section of NO_2^* is expected to be quite large. Two photon effects were seen in other experiments.[15,16]

m/e=51 and m/e=65

Signal was looked for at m/e=65 which corresponds to the parent mass of NOCl but not found. An attempt was made to detect ClO^+ however no signal was seen either.

The extremely parallel nature of the NO_2 + Cl channels is difficult to explain. The transitions out of what are thought to be the three highest orbitals are either perpendicular or forbidden in C_{2v} symmetry. August[34] measured a β of 0.4, $1 > \beta > -0.5$ for HNO_3 at 280 nm. As discussed in the introduction they invoked the mediation of the out of plane bending of the excited molecule to produce a parallel vibronic transition. This cannot explain our results. The anisotropies measured are much to high to result from the deformation of the molecule. An alternative can be found in the results of Frost[48]. By measuring the photoelectron spectrum of NO_2Cl he found that the highest occupied molecular orbitals were the non-bonding p orbitals on the chlorine atom. The p_σ orbital lying in the plane of the molecule has B_2 symmetry. Excitation of one electron out of this orbital into the b_1 would result in a state of A_2 symmetry. This pure electronic transition would be forbidden. The p_π orbital which is perpendicular to the

plane of the molecule has B_1 symmetry. This excitation would lead to a state of A_1 symmetry. This would be the parallel transition that is needed to explain these results.

These considerations suggest the following picture of the 248 nm dynamics. A parallel charge transfer transition excites an electron off the chlorine atom into the antibonding orbital on NO_2. This state would have predominantly Cl^+-NO_2^- character. The excited state undergoes rapid predissociation to Cl and NO_2 (X,A,B).

These experiments suggest three new measurements to be taken. An accurate determination of the angular distribution would be useful to confirm or refute the anisotropies determined. A measurement of the m/e=16 distribution at low laser powers would be useful in confirming the presence of the O + NOCl channel at this wavelength. It would also make it easier to fit the high energy part of this distribution thus making it easier to disentangle the contributions of NOCl and NO_2^* in the m/e=30 and m/e=35 spectra. Thirdly it would be useful to study the photodissociation of NO_2F. This molecule has a similar structure to NO_2Cl and has the same number of valence electrons but the nonbonding p electrons on the fluorine atom are at a lower energy. The ordering of the orbitals for this molecule is expected to be more like that of HNO_3.

A motivation for this experiment was to provide data for comparison with photolysis induced fluorescence experiments.[15,16] The agreement

between the excited state NO_2 plus Cl energy distribution is quite good (figures 28,29). However the PIF experiments are insensitive to the production of ground state NO_2 and cannot take account of the production of other channels. It also has difficulty with the secondary dissociation of NO_2^*.

308 nm

The time of flight distributions taken at m/e=35 are shown in figures 30 through 35. The two major channels are Cl + NO_2 (X^2A_1) and Cl + NO_2^*. There is no structure present in the excited state distribution. The maximum translational energy for the excited state is 22 kcal/mole. The energy available for the production of the B^2B_1 excited state of NO_2 is 16 kcal/mole. The narrowness of the distribution suggests that most of the excited product is in this state. As in the 248 nm experiment NOCl + O occurs as a minor channel.

The P(E) used to fit these distributions is shown in figure 40. The quantum yield for the production of excited state NO_2 is 0.28. The yield for ground state NO_2 is 0.70 and the yield of NOCl is 0.015. The anisotropies of these channels are 0.6, 0.6 and 0.4 respectively. These results are summarized in table 4.

The momentum matched time of flight distributions taken at m/e=30 are shown in figures 36-39. The same translational energy distributions and anisotropies were used to fit m/e=30 data as was used to fit m/e=35 data. The relative contribution of the excited state NO_2 distribution was increased by 10%. This is very similar to the 13% enhancement used to fit the 248 nm data.

The dynamics of the photodissociation are likely to be analogous to the 280 nm photodissociation seen by August[34] and discussed by Bai[43]. A perpendicular or forbidden electronic transition becomes an allowed parallel vibronic transition. The lowest excited surface adiabatically correlates to the ground state of NO_2. Production of excited NO_2 results from excitation to the second excited surface which is called the $2^1A'$ state in HNO_3 and correlates to the B^2B_1 state of NO_2.

Conclusions

The excitation of NO_2Cl at 248 nm generates a short lived charge transfer-state that predissociates primarily to Cl atom and both ground state and excited NO_2. This charge transfer state is not seen in other NO_2–X molecules studied because of the unusually high energy of the nonbonding π electrons on the Cl atom. The 308 nm excitation on the other

and is mediated by the out of plane bending motion of the excited molecule. This photodissociation generates mainly chlorine atom and the ground and excited B^2B_1 states of NO_2

Substituent effects can have a dramatic effect on the electronic structure of X-NO_2 molecules. Different substituents alter the orbitals available for excitation and hence the change the dynamics of excited X–NO_2. The photodissociation of NO_2F would be an extremely interesting experiment to compare and contrast with these studies.

Endnotes

1. J.G. Anderson, Annual Reviews of Physical Chemistry, 38, 489, (1987)
2. J.J. Margitan, Journal of Physical Chemistry, 87, 674, (1983)
3. W.S. Smith, C.C. Chou, and F.S. Rowland, Geophysical Research Letters, 4, 517, (1977)
4. W.J. Williams, J.N. Brooks, D.G. Murray, and F.H. Murray, Journal of Atmospheric Science, 29, 1375, (1972)
5. M. Loewenstein and W.L. Starr, Geophysical Research Letters, 5, 531, (1978)
6. F.S. Rowland, J.E. Spencer, and M.J. Molina, Journal of Physical Chemistry, 80, 2711, (1976)
7. F.S. Rowland, J.E. Spencer, and M.J. Molina, Journal of Physical Chemistry, 80, 2713, (1976)
8. F.S. Rowland and M.J. Molina, Rev. of Geophys. and Space Phys., 11, 1, (1975)
9. M.T. Leu, C.L. Lin, and W.B. Demore, Journal of Physical Chemistry, 81, 190, (1977)
10. K. Endo, Nippon Kagaku Kaishi, 9, 1129, (1979)
11. A.J. Illies and G.A. Takacs Journal of Photochemistry, 6, 35, (1972)
12. H.H. Nelson, and H.S. Johnston, Journal of Physical Chemistry, 85, 3891, (1981)
13. L.E. Harris, Journal of Chemical Physics 58, 5615, (1973)

14. D.A. Kleier and M.A. Lipton, Journal of Molecular Structure (Theochem), 109, 39, (1981)

15. B.Y. Oh, Ph.D. Thesis, University of California at Berkeley, (1988)

16. W.N. Sisk, Ph.D. Thesis, University of California at Berkeley, (1990)

17. D. Husain and R.G.W. Norrish, Proceedings of the Royal Society A, 273, 165, (1963)

18. T. Berces and S. Forgeteg, Transactions of the Faraday Society, 66, 633, (1970)

19. Harold S. Johnston, Shih-Ger Chang and Gary Whitten, Journal of Physical Chemistry, 78, 1, (1974)

20. Harold S. Johnston and Richard Graham, Canadian Journal of Chemistry, 52, 1415, (1974)

21. Masako Suto and L.C. Lee, Journal of Chemical Physics, 81, 1294, (1984)

22. G.S. Jolly, D.L. Singleton, D.J. McKenney, and G. Paraskevopoulos, Journal of Chemical Physics, 79, 3162, (1983)

23. Axel Jacobs, Karl Kleinermanns, Helmut Kuge and Jürgen Wolfrum, Journal of Chemical Physics, 79, 3162, (1983)

24. Th. Papenbrock, K.K. Haak, and F. Stuhl, Ber. Bunsenges. Phys. Chem., 88, 675, (1984)

25. R.D. Kenner, F. Rohrer, Th. Papenbrock, and F. Stuhl, Journal of Chemical Physics, 90, 1294, (1986)

26. David D. Nelson Jr., Aram Schiffman, and David J. Nesbitt, Journal of Chemical Physics, 90, 10, (1989)

27. R.D. Kenner, F. Rohrer, and F. Stuhl, Chemical Physics Letters, 116, 374, (1985)

28. Amitabha Sinha, Randall L. Vander Wal, Laurie J. Butler, and F. Fleming Crim, Journal of Physical Chemistry, 91, 4645, (1987)

29. M.D. Likar, A. Sinha, T.M. Ticich, R.L. Vander Wal and F.F. Crim, Ber. Bunsenges. Phys. Chem., 92, 289, (1988)

30. Amitabha Sinha, Randall L. Vander Wal, and F. Fleming Crim, Journal of Chemical Physics, 92, 401, (1990)

31. M.D. Likar, J.E. Baggott, A. Sinha, T.M. Ticich, R.L. Vander Wal, and F. Fleming Crim, Journal of the Chemical Society, Faraday Transactions 2. 84, 1483, (1988)

32. Amitabha Sinha, Randall L. Vander Wal, and F. Fleming Crim Journal of Chemical Physics, 91, 2929, (1989)

33. Julie August, M. Brouard, M.P. Docker, A. Hodgon, C.J. Milne, and J.P. Simons, Ber. Bunsenges. Phys. Chem., 92, 264, (1988)

34. Julie August, Mark Brouard and John P. Simons, Journal of the Chemical Society, Faraday Transactions 2. 84, 587, (1988)

35. Diane Swanson, Brian Kan, and Harold S. Johnston, Journal of Physical Chemistry, 88, 3115, (1984)

36. J.R. Barker, L. Brouwer, R. Patrick, M.J. Rossi, P.L. Trevor, and D.M. Golden, International Journal of Chemical Kinetics, 17, 991, (1985)

37. Daniel Oh, Wade Sisk, Anthony Young, and Harold Johnston, Journal of Chemical Physics, 85, 7146, (1986)

38. L.J. Butler, D. Krajnovich, Y.T. Lee, G. Ondrey, and R. Bersohn, Journal of Chemical Physics, 79, 1708, (1983)

39. L.J.Butler, Ph.D. Thesis, University of California at Berkeley, (1985)

40. Kazuo Okada, Satoshi Yabushita, Kizashi Yamaguchi, and Takayuki Fueno, Chemistry Letters, 1247, (1977)

41. John E. Carpenter and Gerald Maggiora, Chemical Physics Letters, 87, 349, (1982)

42. Subhash C. Bhatia and John H Hall Jr., Journal of Chemical Physics, 82, 1191, (1984)

43. Y.Y. Bai and G.A. Segal, Journal of Chemical Physics, 56, 7479, (1990)

44. Dennis S. Marynick, Asok K. Ray, and John L. Fry, Chemical Physics Letters, 116, 429, (1985)

45. Karl Jug and Joachim Schulz, Journal of Computational Chemistry, 8, 1040, (1987)

46. Riccardo Destro, Felicita Merati, and Emanuele Ortoleva, Chemical Physics Letters, 145, 193, (1988)

47. M.P. McGrath, M.M. Francl, F.S. Rowland and W.J. Hehre, Journal of Physical Chemistry, 92, 5352, (1988)

48. D.C. Frost, S.T. Lee, C.A. McDowell, and N.P.C. Westwood, Journal of Electron Spectroscopy and Related Phenomena, 7, 331, (1975)

49. M. Volpe and H.S. Johnston, Journal of the American Chemical Society, 78, 3903, (1956)

50. X. Zhao, Ph.D. Thesis, University of California at Berkeley, (1990)

51. D.L. Baulch, R.A. Cox, R.F. Hampson Jr., J. Troe, and R.T. Watson, Journal of Physical and Chemical Reference Data, 9, 295, (1980)

Table 1

Beam Parameters

0

λ	stag. press.	bath temp.	nozz. temp.	v_0 cm/sec	$v_0/\Delta v$
248 nm	325 torr	-63°C	105°C	1.08×10^5	9.1
308 nm	325 torr	-63°C	18°C	9.76×10^4	9.4

Table 2

Possible Photodissociation Channels for NO_2Cl

Channel	Kcal/mole[51]	nm
$NO_2Cl \rightarrow NO_2 (X^2A_1) + Cl(^2P_{3/2})$	33.9	835
$\rightarrow NO_2 (A^2B_2) + Cl(^2P_{3/2})$	61.8	462
$\rightarrow NO_2 (B^2B_1) + Cl(^2P_{3/2})$	76.4	376
$\rightarrow NO (X^2\pi) + ClO (X^2\Sigma)$	43.0	665
$\rightarrow NOCl (X) + O(^3P)$	68.9	415
$\rightarrow NO (X^2\pi) + O(^3P) + Cl(^2P_{3/2})$	107.1	270

Table 3

248 nm channels

	NO_2^*	NO_2	NOCl
Φ	0.66	0.32	.022
β	0.97	0.95	0.78

Table 4

308 nm channels

	NO_2^*	NO_2	NOCl
Φ	0.28	0.70	.015
β	0.60	0.60	0.40

Figures

Figure 1: The Ground State Structure of NO_2Cl.

Figure 2: The Ultraviolet absorption Spectrum of NO_2Cl. The assignments are taken from reference 15.

Figure 3: The Translational energy distribution of Cl + NO_2^* derived from photolysis induced flourescence experiments taken from reference 16. This distribution is changed from an internal energy distribution to a translational energy distribution to facilitate comparison with time of flight (TOF) results.

Figure 4: Crossed laser-molecular beam machine used in this experiment. For more details see chapters 1 and 2 and references therein.

Figure 5: Energy Diagram of NO_2Cl. Energies are taken from reference 51.

Figure 6: Time of flight distribution taken at m/e=35 (Cl+) for photolysis at 248 nm with the detector 10 degrees from the NO_2Cl beam. The open circles are data points. The chain dashed line (leading edge) is the Cl + ground state NO_2 channel. The dashed line which makes up

the bulk of the peak is Cl + excited NO_2. The slow part of the peak is O + NOCl. The heavy straight line is the sum of the channels.

Figure 7: 248 nm m/e=35 20 degrees

Figure 8: 248 nm m/e=35 30 degrees

Figure 9: 248nm m/e=35 40 degrees

Figure 10: 248 nm m/e=35 50 degrees

Figure 11: 248 nm m/e=35 60 degrees

Figure 12: Translational energy distributions P(E) derived from m/e=35 and m/e=30 data. The distributions are normalized to have an area of one.

Figure 13: 248nm m/e=46 (NO_2^+) 10 degrees

Figure 14: 248nm m/e=46 20 degrees

Figure 15: 248nm m/e=46 30 degrees

Figure 16: 248nm m/e=46 40 degrees

Figure 17: 248 nm m/e=46 50 degrees

Figure 18: P(E)'s derived from m/e=46

Figure 19: 248nm m/e=30 (NO^+ from NO_2 fragmentation) 10 degrees

Figure 20: 248nm m/e=30 20 degrees

Figure 21: 248nm m/e=30 30 degrees

Figure 22: 248nm m/e=30 40 degrees

Figure 23: 248nm m/e=30 50 degrees

Figure 24: 248nm m/e=16 (O^+ from O atom and NO_2 and NOCl fragmentation) 10 degrees

Figure 25: 248nm m/e=16 20 degrees

Figure 26: 248nm m/e=16 30 degrees

Figure 27: 248nm m/e=16 40 degrees

Figure 28: Translational energy distributions derived from m/e=35 times of flight and from photolysis induced fluorescence. The areas under the TOF P(E) curves are normalized to the branching ratios.

Figure 29: P(E)'s derived from m/e=46 TOF and the P(E) derived from PIF.

Figure 30: 308nm m/e=35 10 degrees

Figure 31: 308nm m/e=35 20 degrees

Figure 32: 308nm m/e=35 30 degrees

Figure 33: 308nm m/e=35 40 degrees

Figure 34: 308nm m/e=35 50 degrees

Figure 35: 308nm m/e=35 60 degrees

Figure 36: 308nm m/e=30 10 degrees

Figure 37: 308nm m/e=30 20 degrees

Figure 38: 308nm m/e=30 30 degrees

Figure 39: 308nm m/e 30 40 degrees

Figure 40: Translational energy distributions derived for 308 nm photolysis from m/e=35 and m/e=30 data.

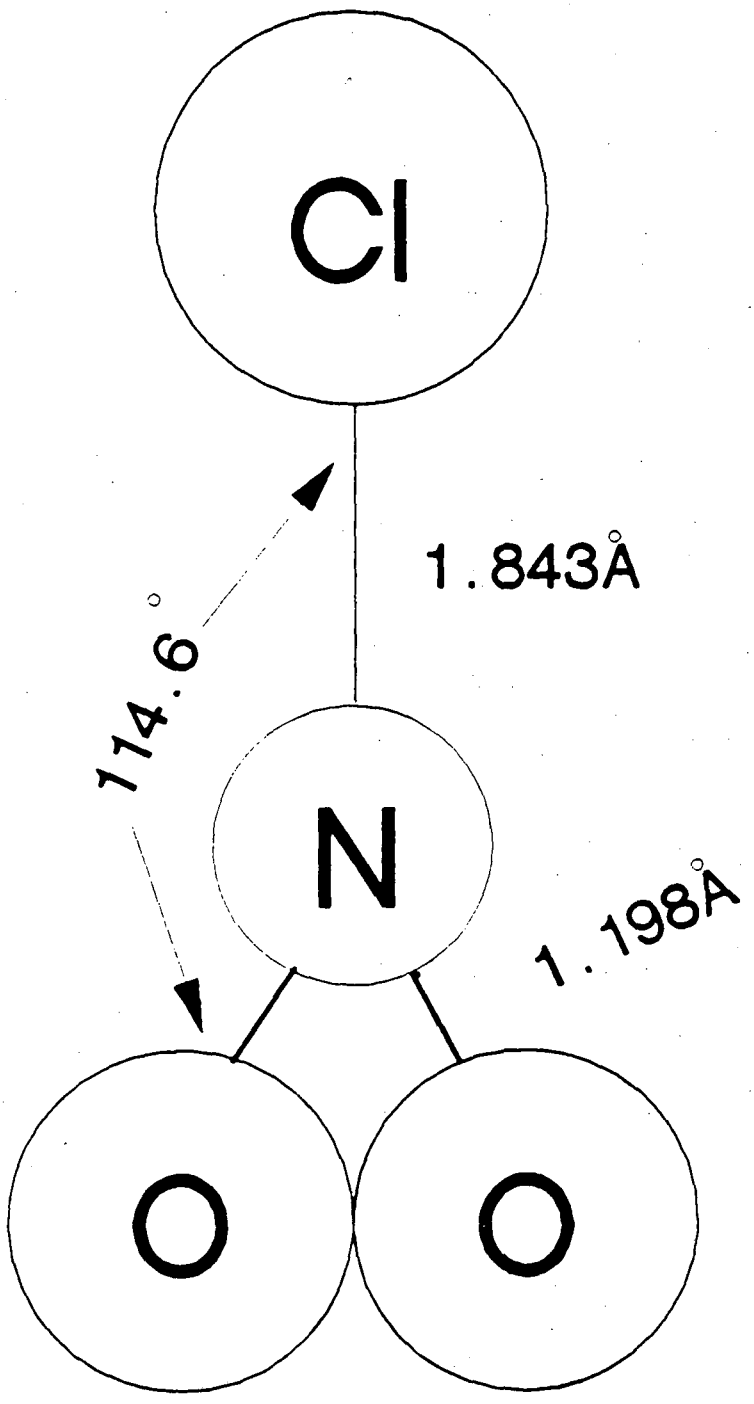

XBL 9011-3732

Figure 1

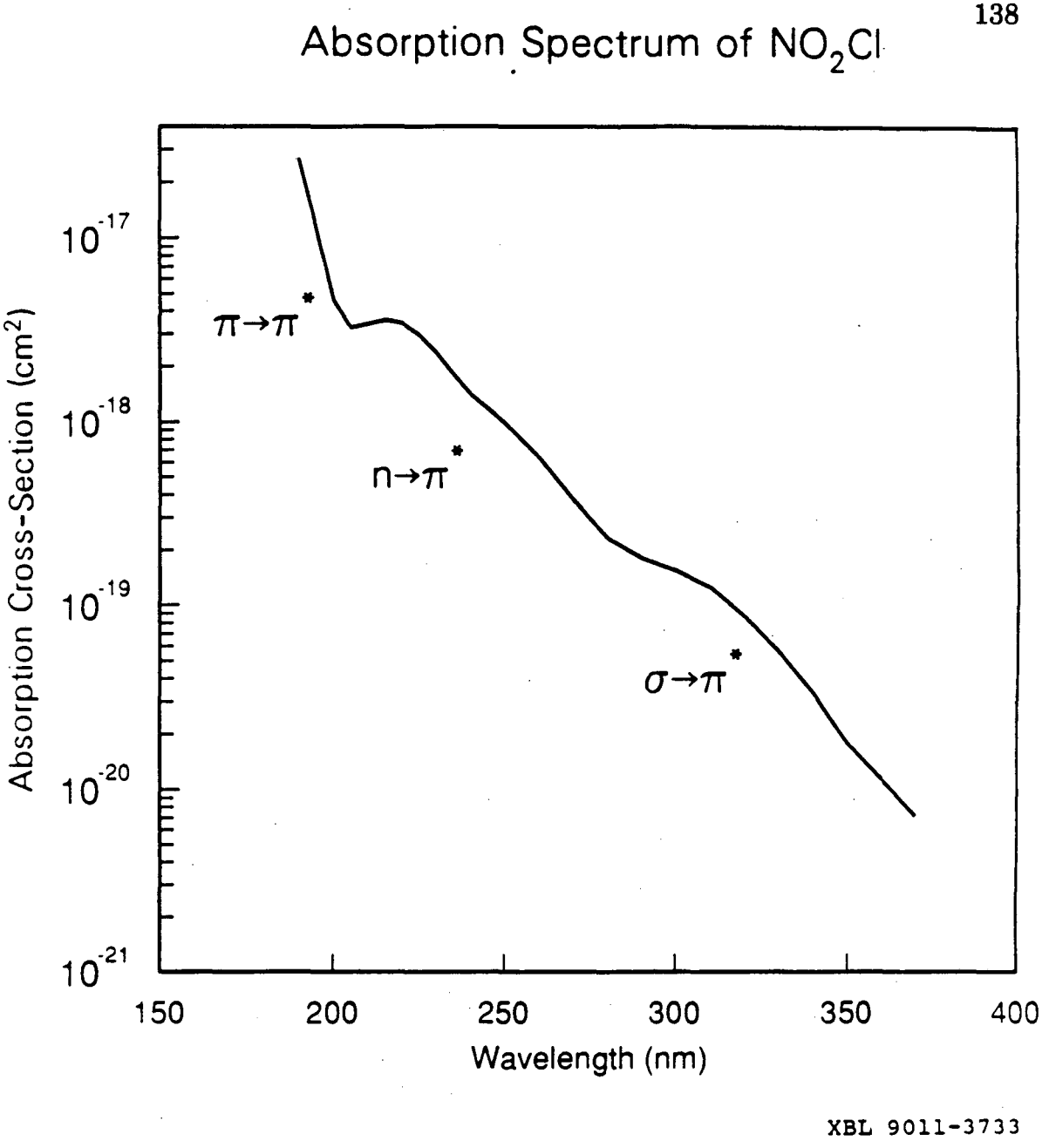
Absorption Spectrum of NO_2Cl
Absorption Cross-Section (cm^2)
10^{-17}
10^{-18}
10^{-19}
10^{-20}
10^{-21}
$\pi \rightarrow \pi^*$
$n \rightarrow \pi^*$
$\sigma \rightarrow \pi^*$
150
200
250
300
350
400
Wavelength (nm)
XBL 9011-3733

Figure 2

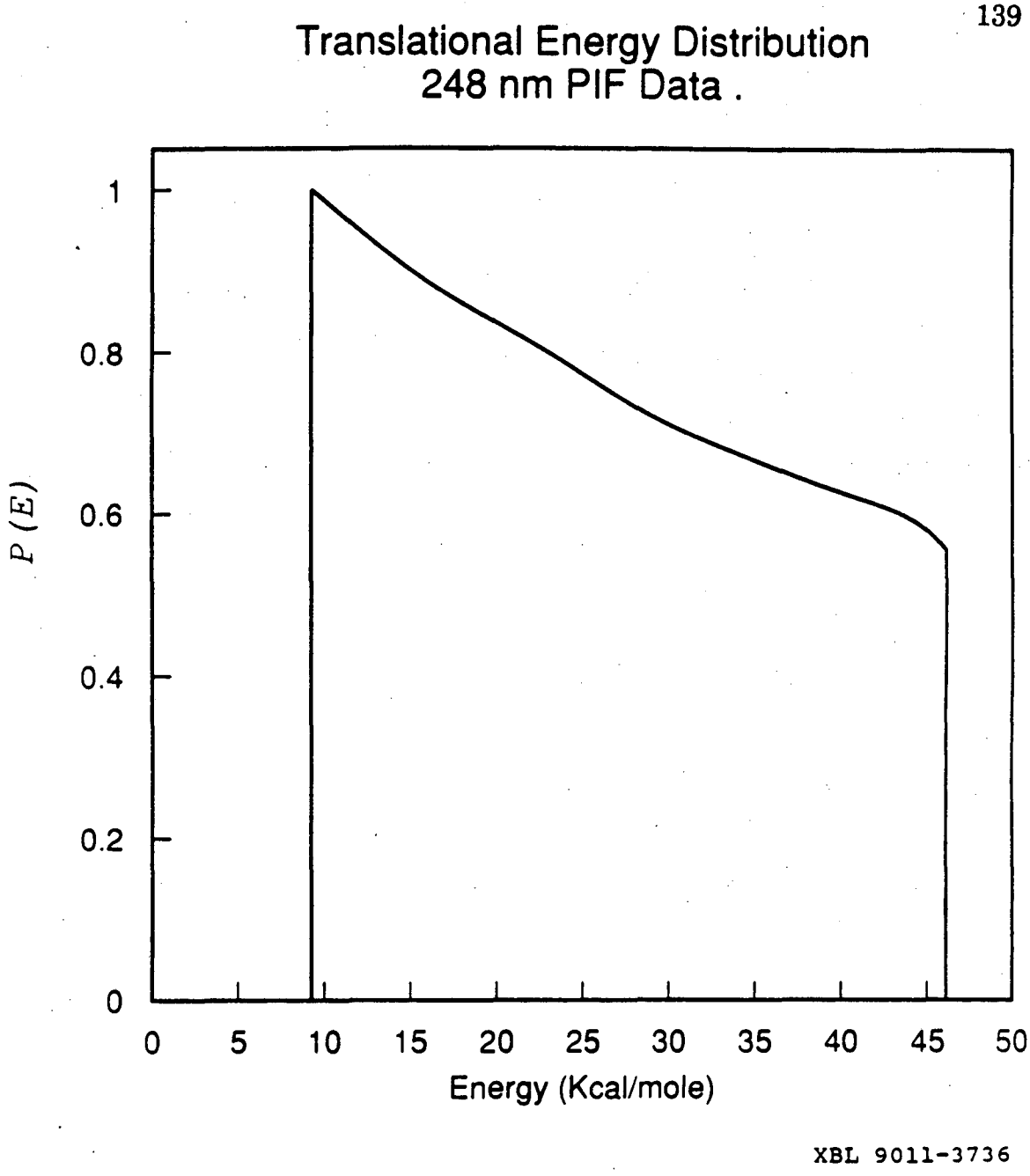
Translational Energy Distribution
248 nm PIF Data .
P (E)
1
0.8
0.6
0.4
0.2
0
0
5
10
15
20
25
30
35
40
45
50
Energy (Kcal/mole)
XBL 9011-3736

Figure 3

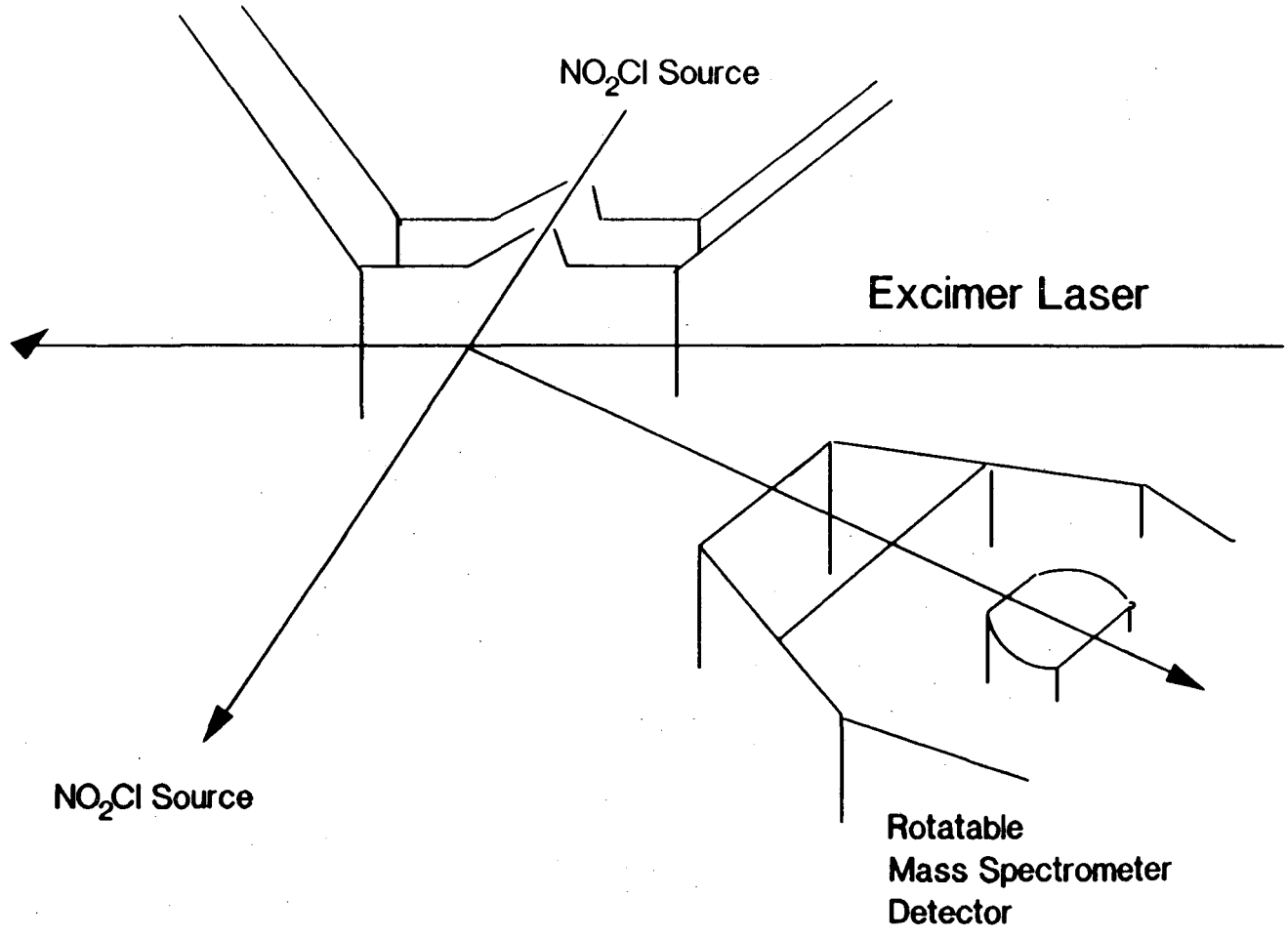

Figure 4

Crossed Laser-Molecular Beams Apparatus

XBL 9011-3735

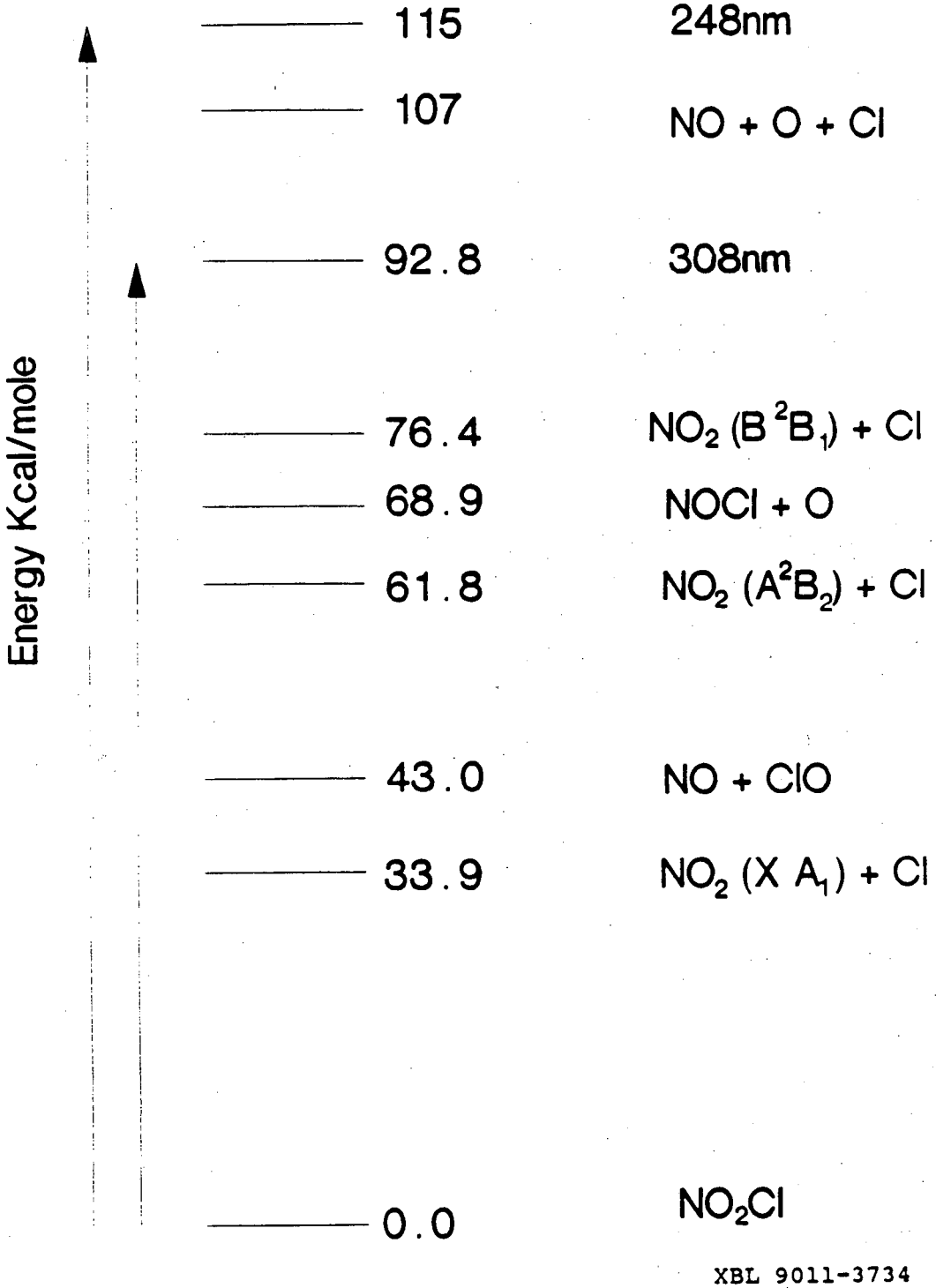
Energy Kcal/mole
115
248nm
107
NO + O + Cl
92.8
308nm
76.4
NO2 (B 2B1) + Cl
68.9
NOCl + O
61.8
NO2 (A2B2) + Cl
43.0
NO + ClO
33.9
NO2 (X A1) + Cl
0.0
NO2Cl
XBL 9011-3734

Figure 5

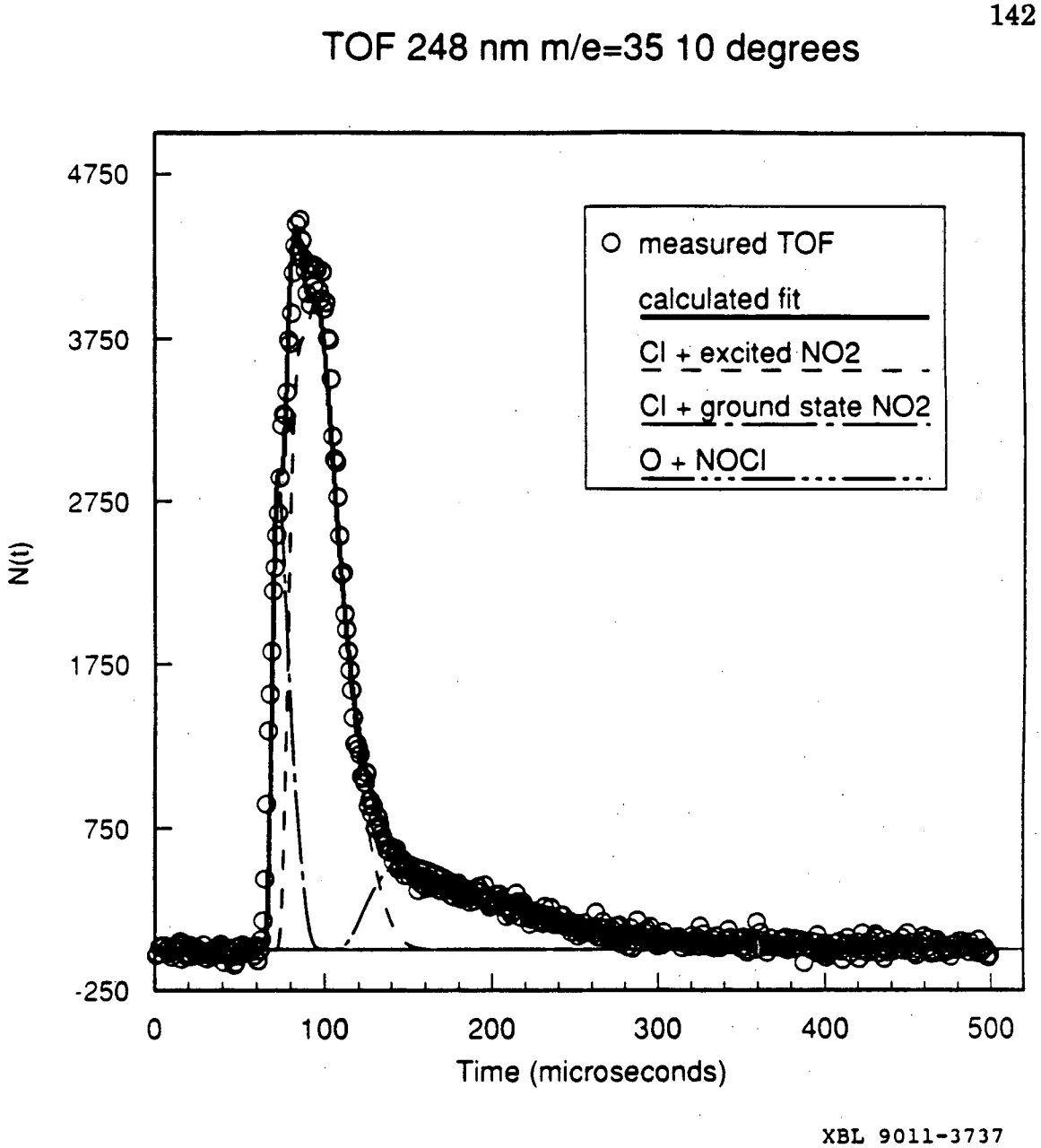
TOF 248 nm m/e=35 10 degrees
4750
3750
2750
1750
750
-250
N(t)
0
100
200
300
400
500
Time (microseconds)
measured TOF
calculated fit
Cl + excited NO2
Cl + ground state NO2
O + NOCl
XBL 9011-3737

Figure 6

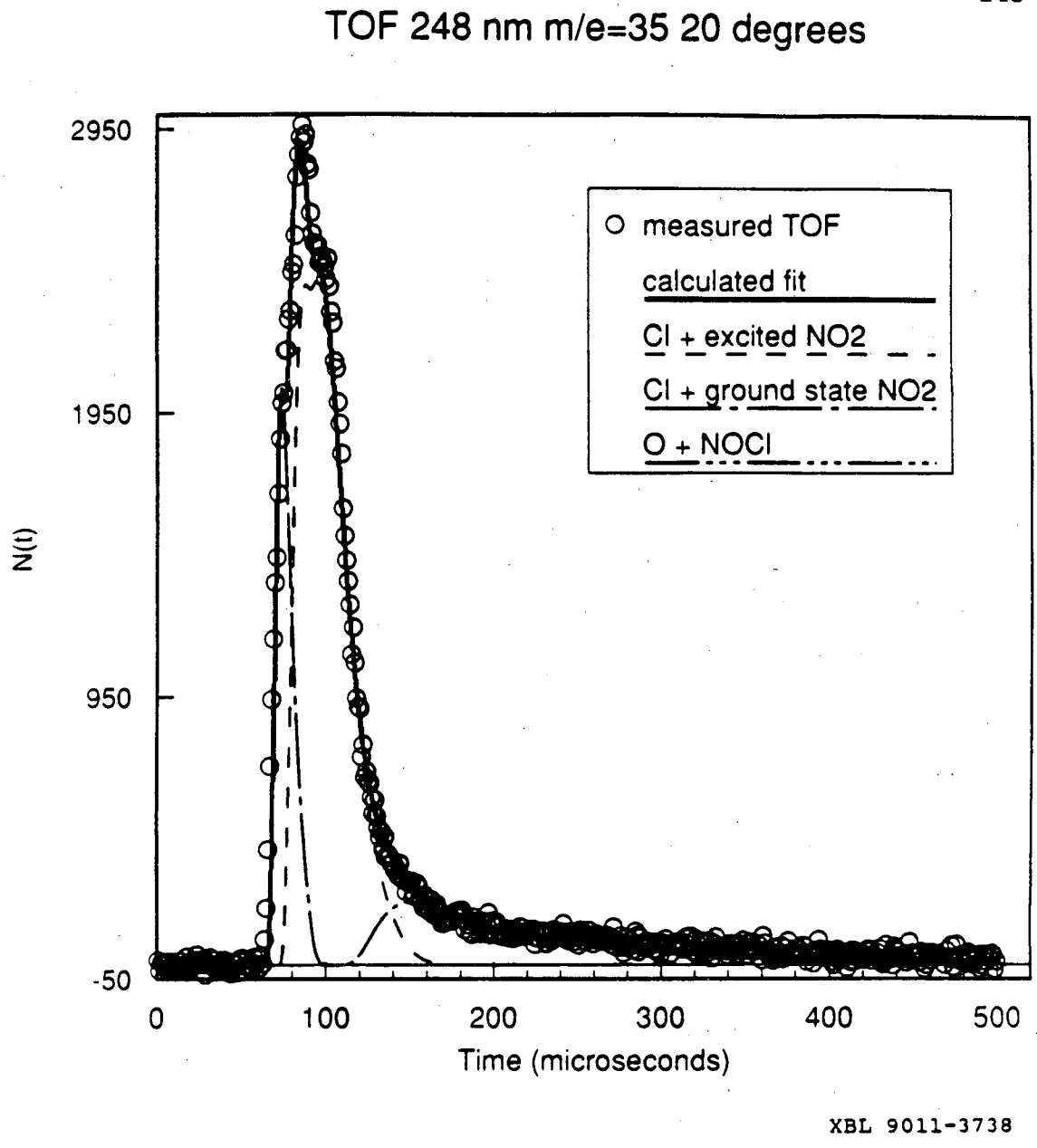
TOF 248 nm m/e=35 20 degrees
2950
1950
950
-50
N(t)
0
100
200
300
400
500
Time (microseconds)
measured TOF
calculated fit
Cl + excited NO2
Cl + ground state NO2
O + NOCl
XBL 9011-3738

Figure 7

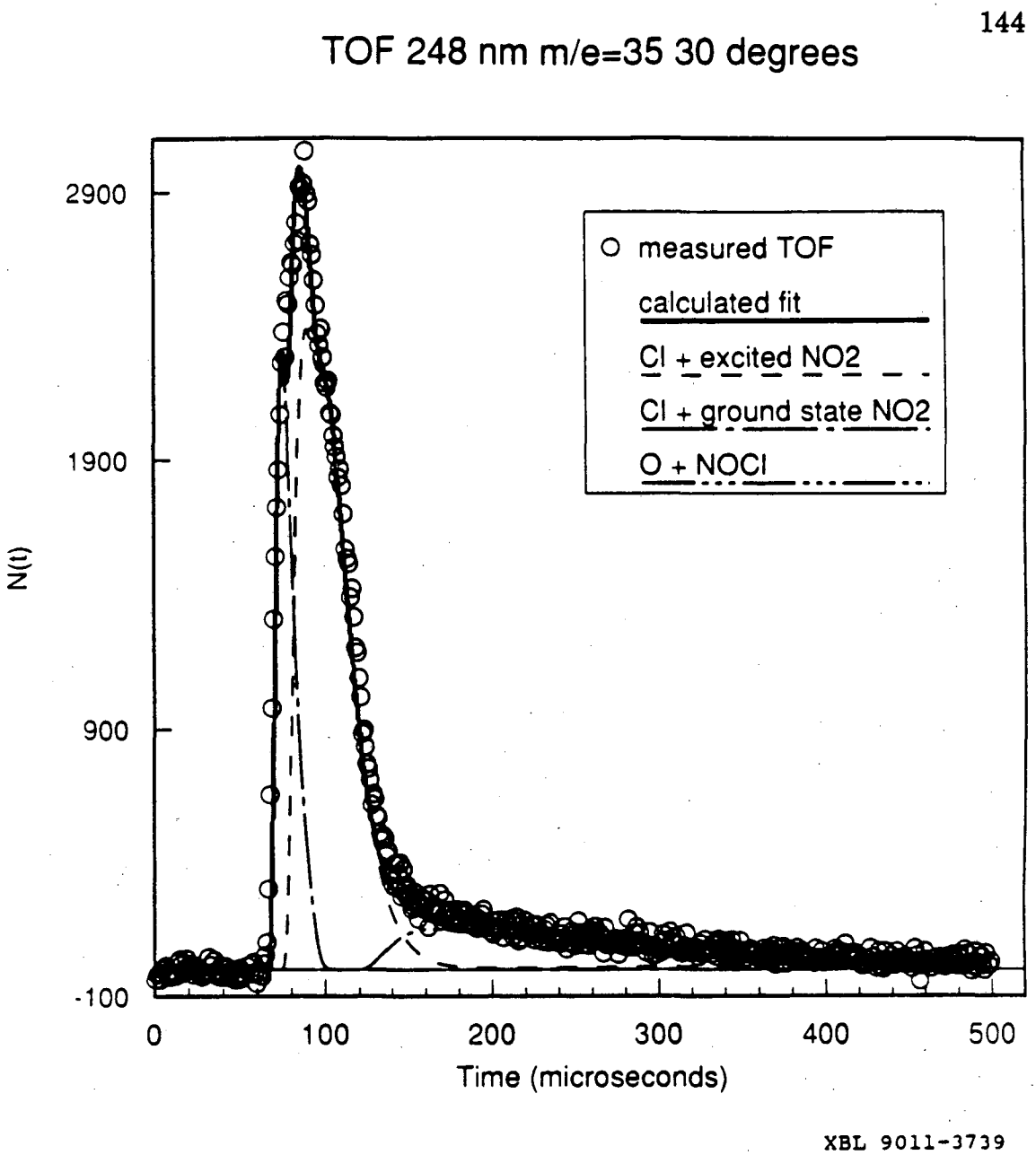
TOF 248 nm m/e=35 30 degrees
2900
1900
900
-100
N(t)
0
100
200
300
400
500
Time (microseconds)
measured TOF
calculated fit
Cl + excited NO2
Cl + ground state NO2
O + NOCl
XBL 9011-3739

Figure 8

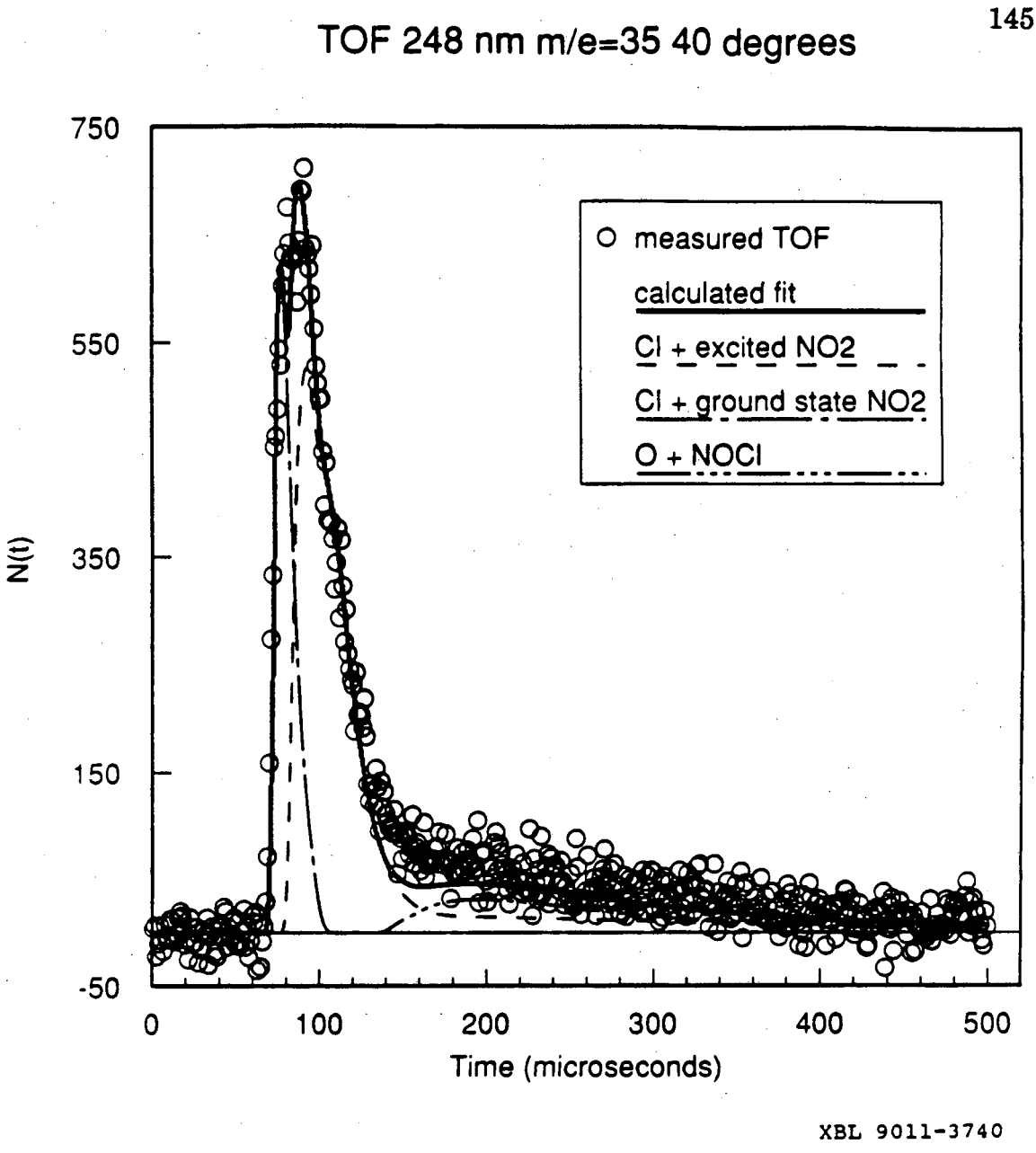
TOF 248 nm m/e=35 40 degrees
750
550
350
150
-50
N(t)
0
100
200
300
400
500
Time (microseconds)
measured TOF
calculated fit
Cl + excited NO2
Cl + ground state NO2
O + NOCl
XBL 9011-3740

Figure 9

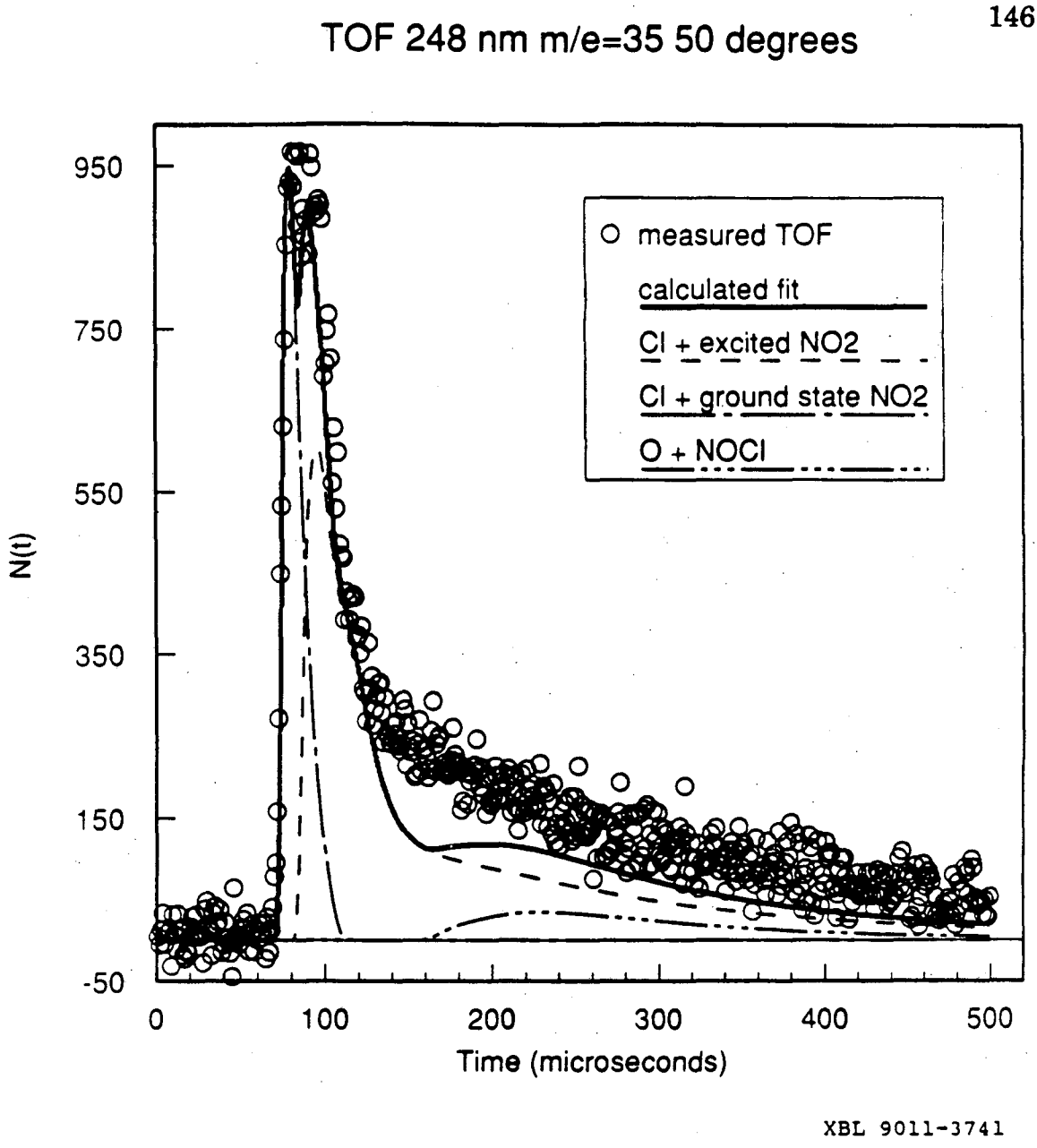
TOF 248 nm m/e=35 50 degrees
950
750
550
350
150
-50
N(t)
0
100
200
300
400
500
Time (microseconds)
measured TOF
calculated fit
Cl + excited NO2
Cl + ground state NO2
O + NOCl
XBL 9011-3741

Figure 10

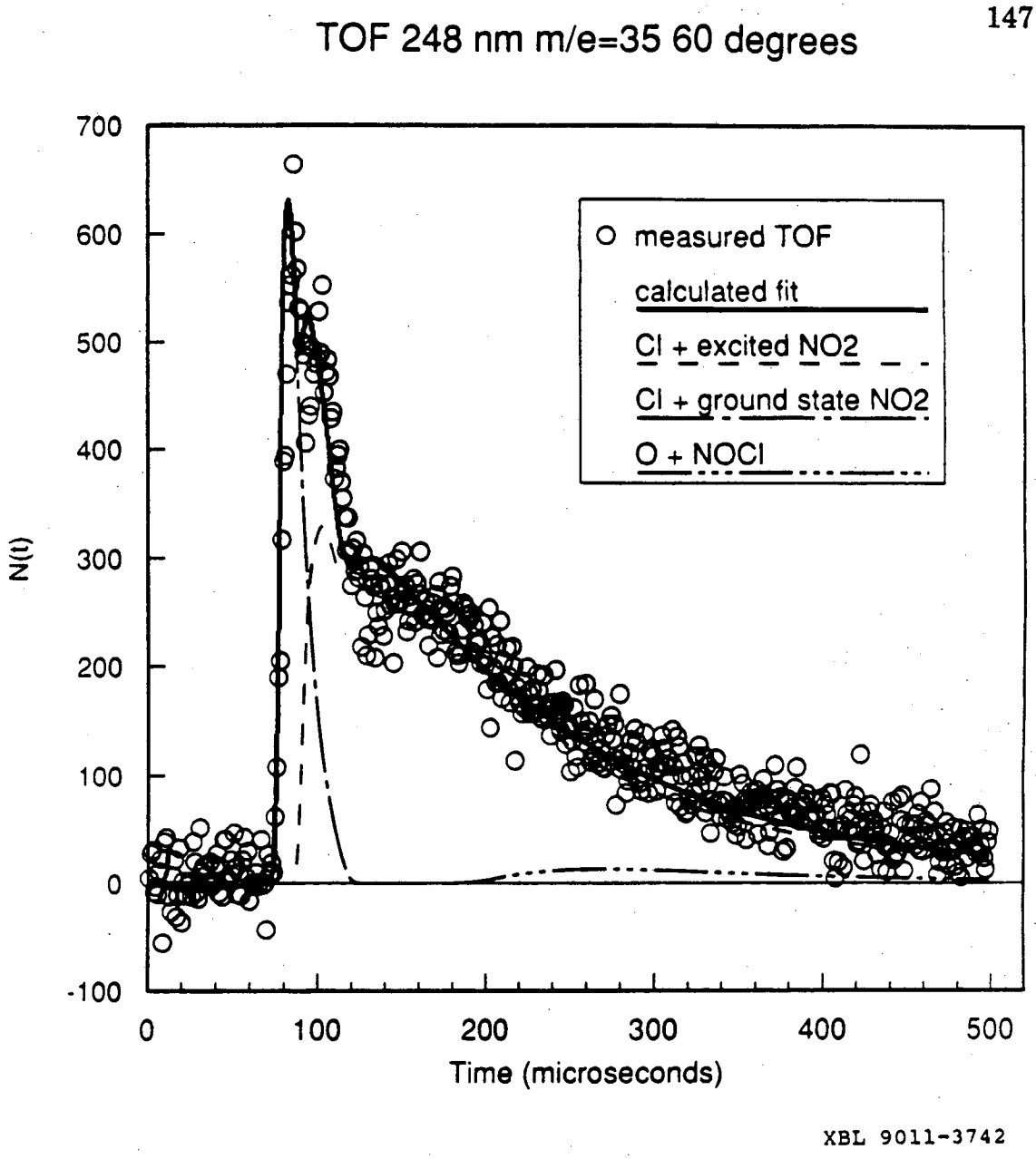
TOF 248 nm m/e=35 60 degrees
700
600
500
400
300
200
100
0
-100
N(t)
0
100
200
300
400
500
Time (microseconds)
measured TOF
calculated fit
Cl + excited NO2
Cl + ground state NO2
O + NOCl
XBL 9011-3742

Figure 11

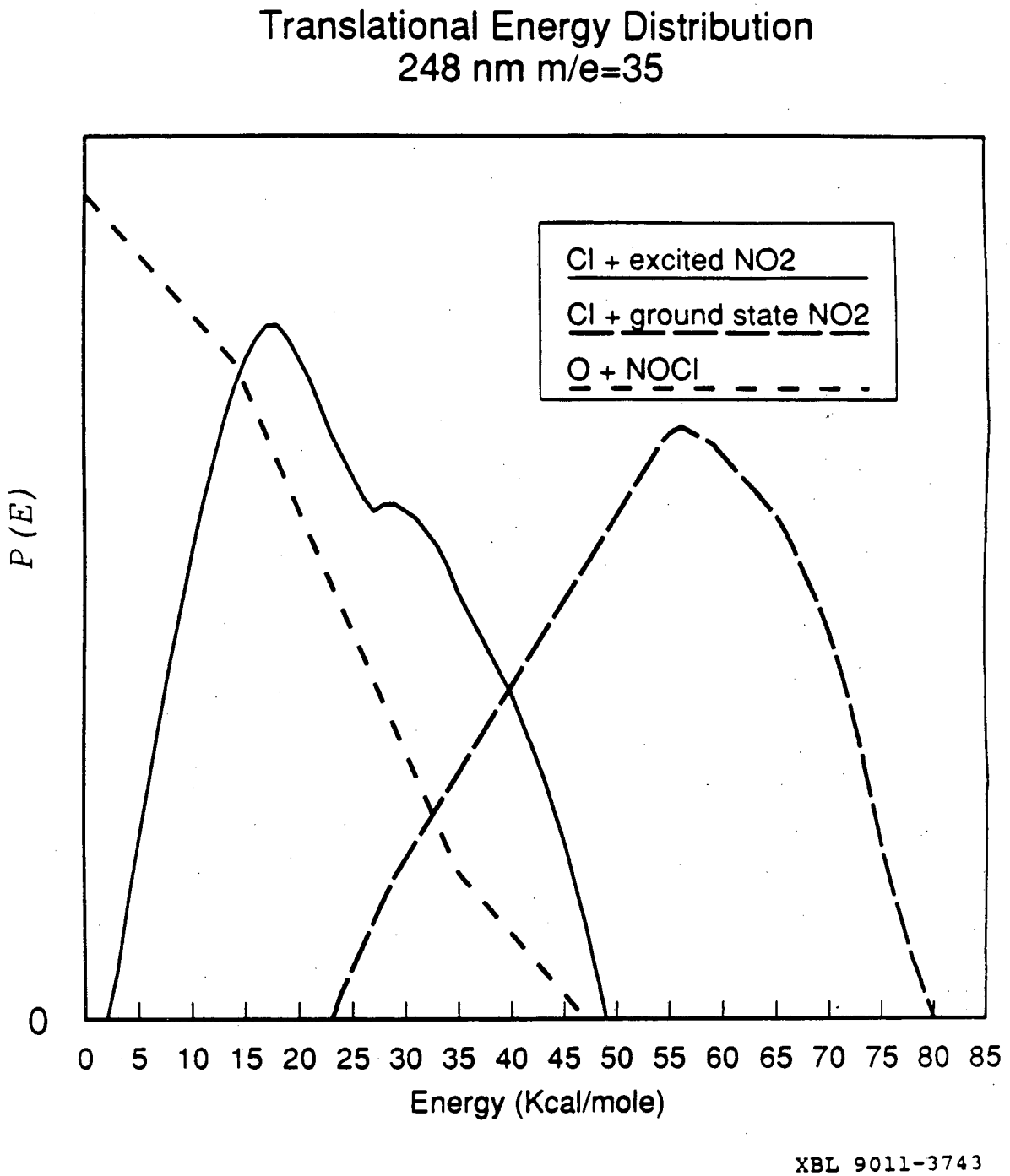
Translational Energy Distribution
248 nm m/e=35
Cl + excited NO2
Cl + ground state NO2
O + NOCl
P (E)
0
0 5 10 15 20 25 30 35 40 45 50 55 60 65 70 75 80 85
Energy (Kcal/mole)
XBL 9011-3743

Figure 12

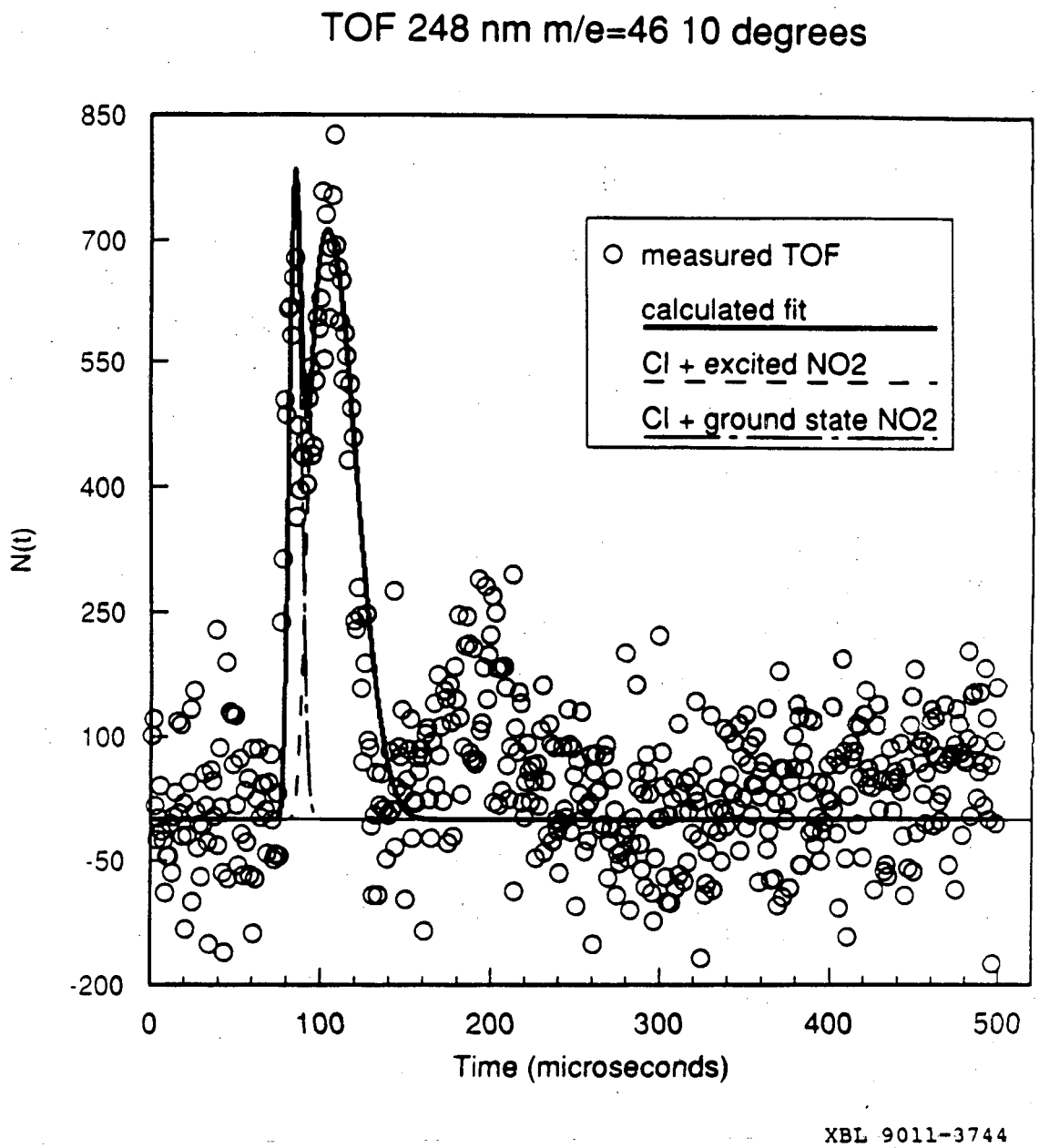
TOF 248 nm m/e=46 10 degrees
850
700
550
400
250
100
-50
-200
N(t)
0
100
200
300
400
500
Time (microseconds)
measured TOF
calculated fit
Cl + excited NO2
Cl + ground state NO2
XBL 9011-3744

Figure 13

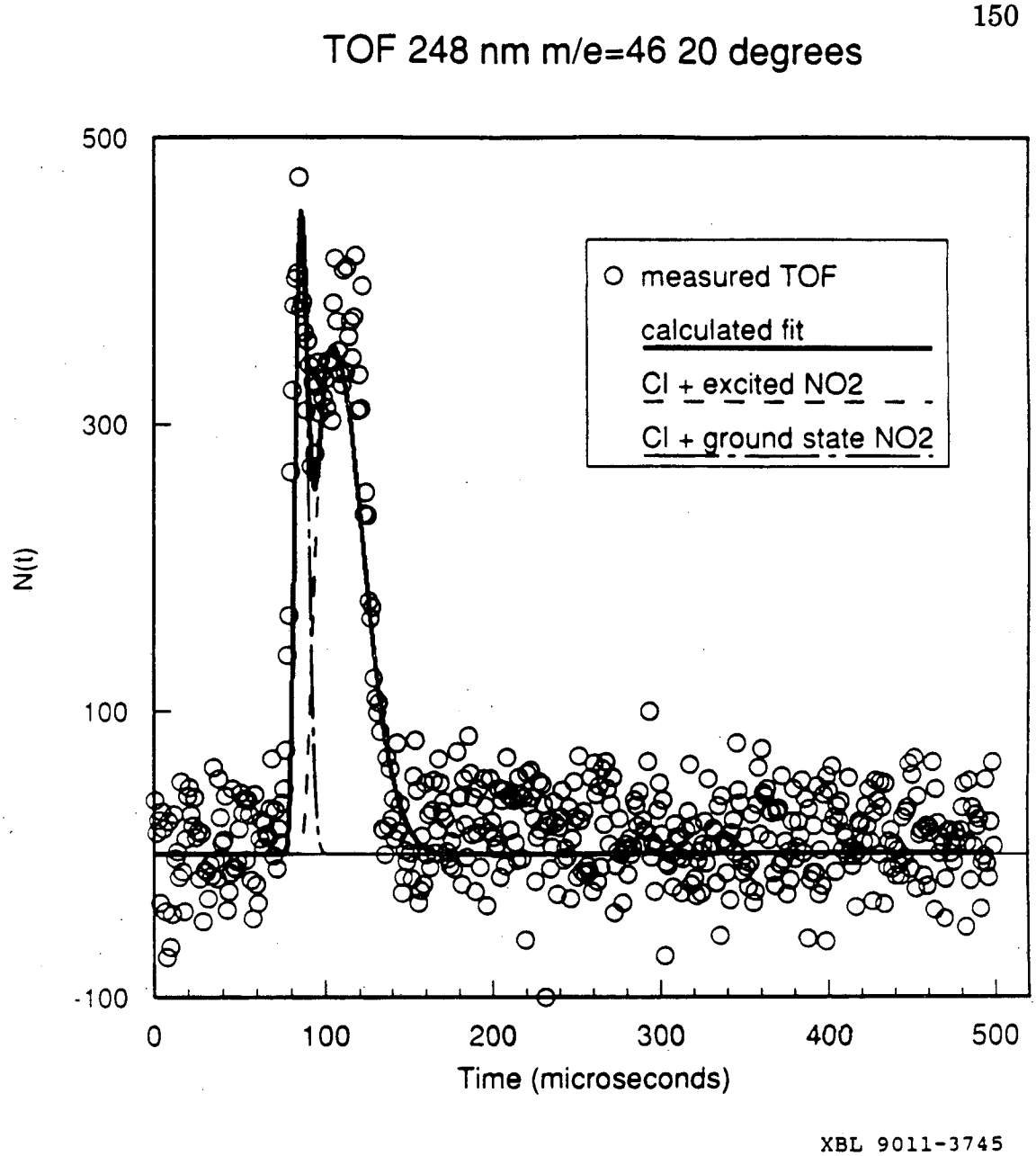
TOF 248 nm m/e=46 20 degrees
500
300
100
-100
N(t)
0
100
200
300
400
500
Time (microseconds)
measured TOF
calculated fit
Cl + excited NO2
Cl + ground state NO2
XBL 9011-3745

Figure 14

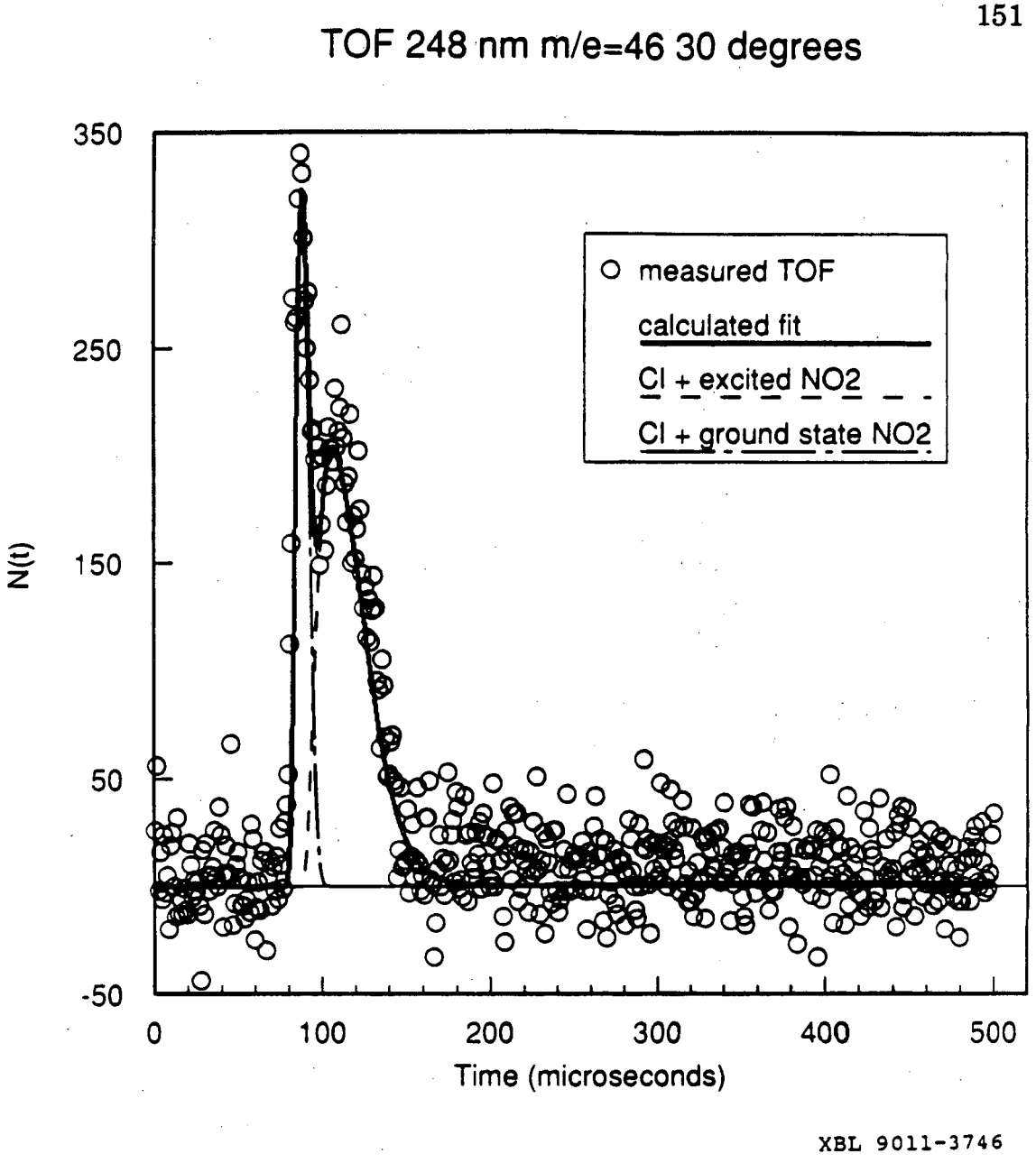
TOF 248 nm m/e=46 30 degrees
350
250
150
50
-50
N(t)
0
100
200
300
400
500
Time (microseconds)
measured TOF
calculated fit
Cl + excited NO2
Cl + ground state NO2
XBL 9011-3746

Figure 15

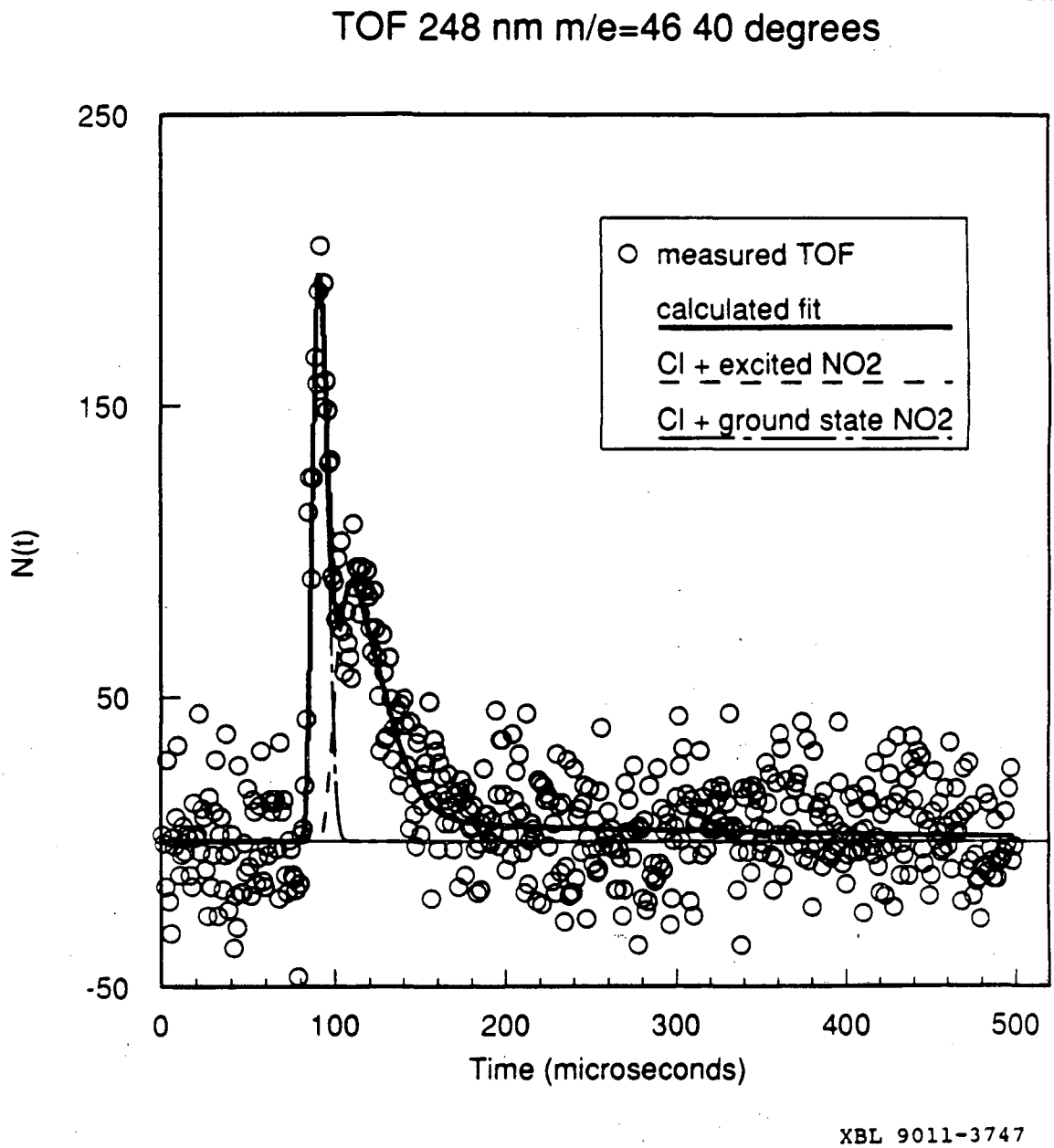
TOF 248 nm m/e=46 40 degrees
250
150
50
-50
N(t)
0
100
200
300
400
500
Time (microseconds)
measured TOF
calculated fit
Cl + excited NO2
Cl + ground state NO2
XBL 9011-3747

Figure 16

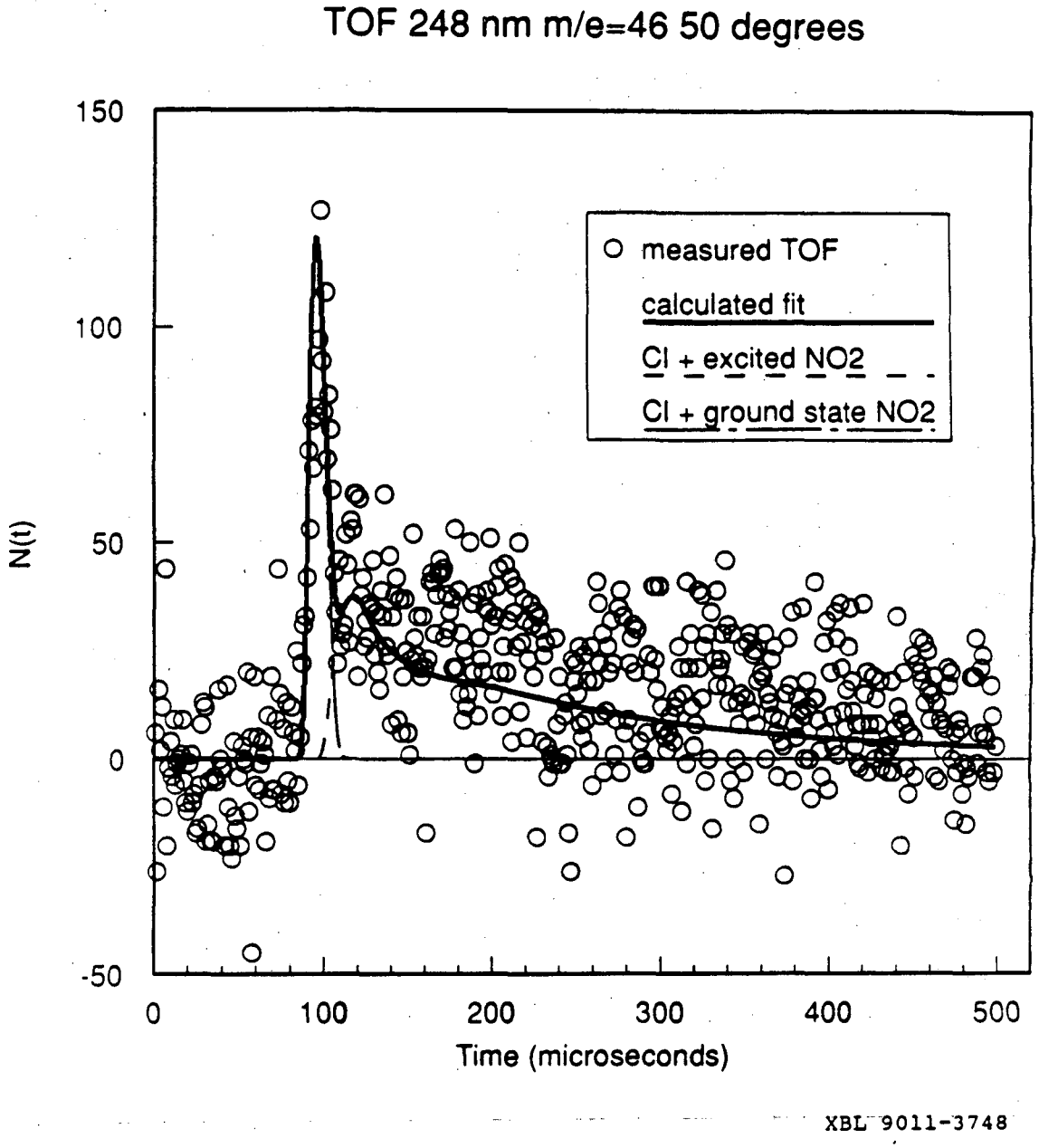
TOF 248 nm m/e=46 50 degrees
150
100
50
0
-50
N(t)
0
100
200
300
400
500
Time (microseconds)
measured TOF
calculated fit
Cl + excited NO2
Cl + ground state NO2
XBL 9011-3748

Figure 17

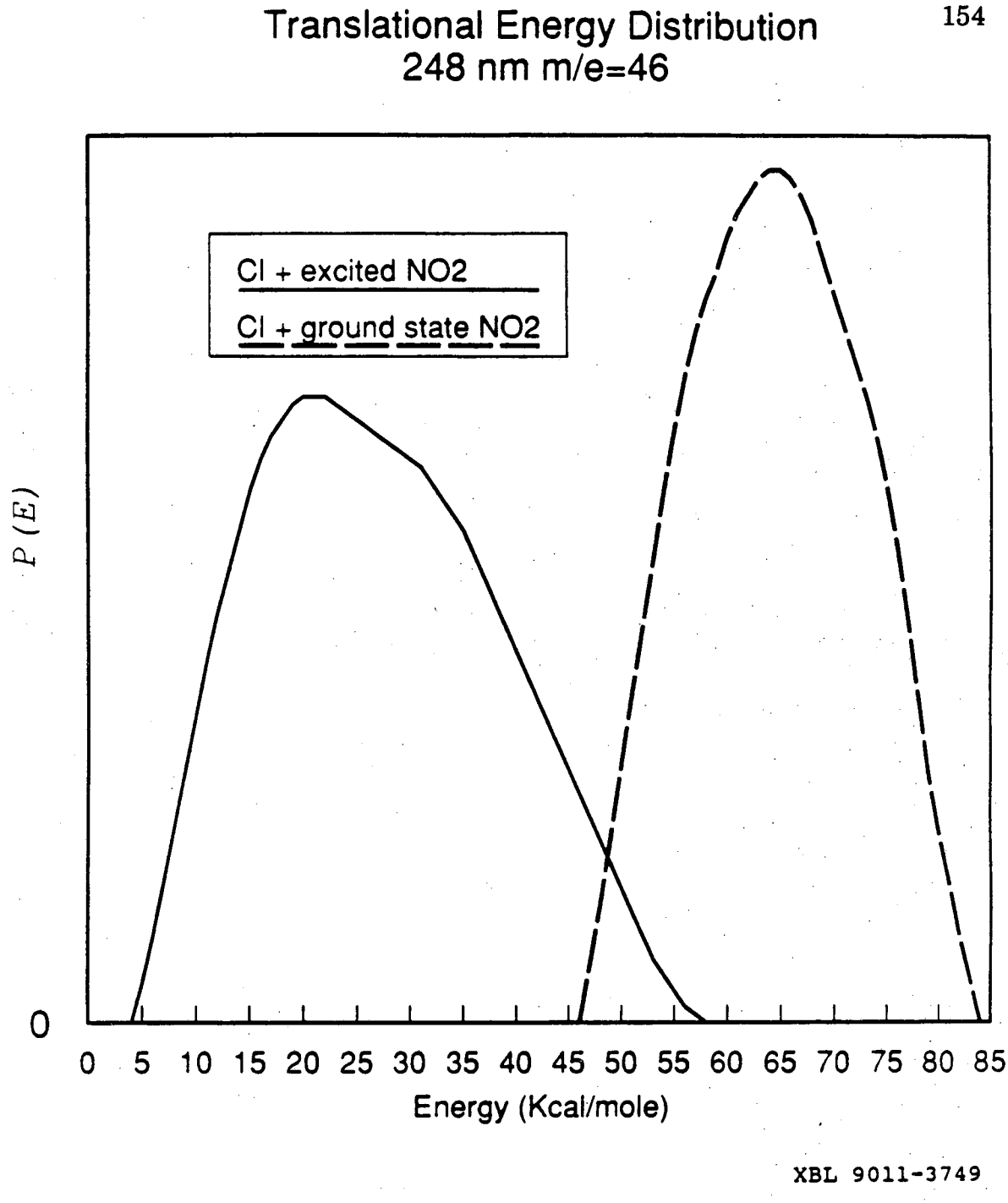
Translational Energy Distribution
248 nm m/e=46
Cl + excited NO2
Cl + ground state NO2
P (E)
0
0 5 10 15 20 25 30 35 40 45 50 55 60 65 70 75 80 85
Energy (Kcal/mole)
XBL 9011-3749

Figure 18

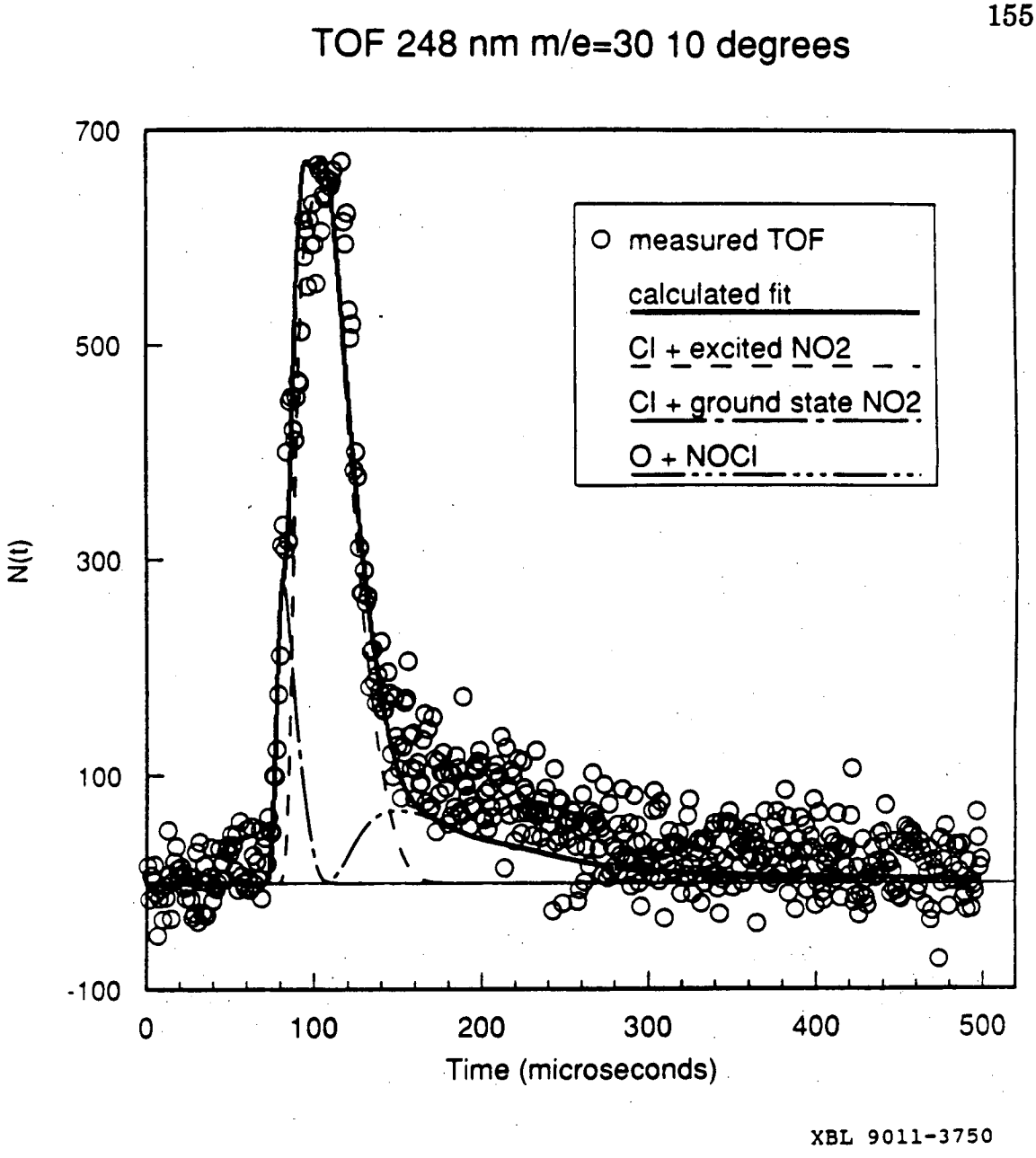
TOF 248 nm m/e=30 10 degrees
700
500
300
100
-100
N(t)
0
100
200
300
400
500
Time (microseconds)
measured TOF
calculated fit
Cl + excited NO2
Cl + ground state NO2
O + NOCl
XBL 9011-3750

Figure 19

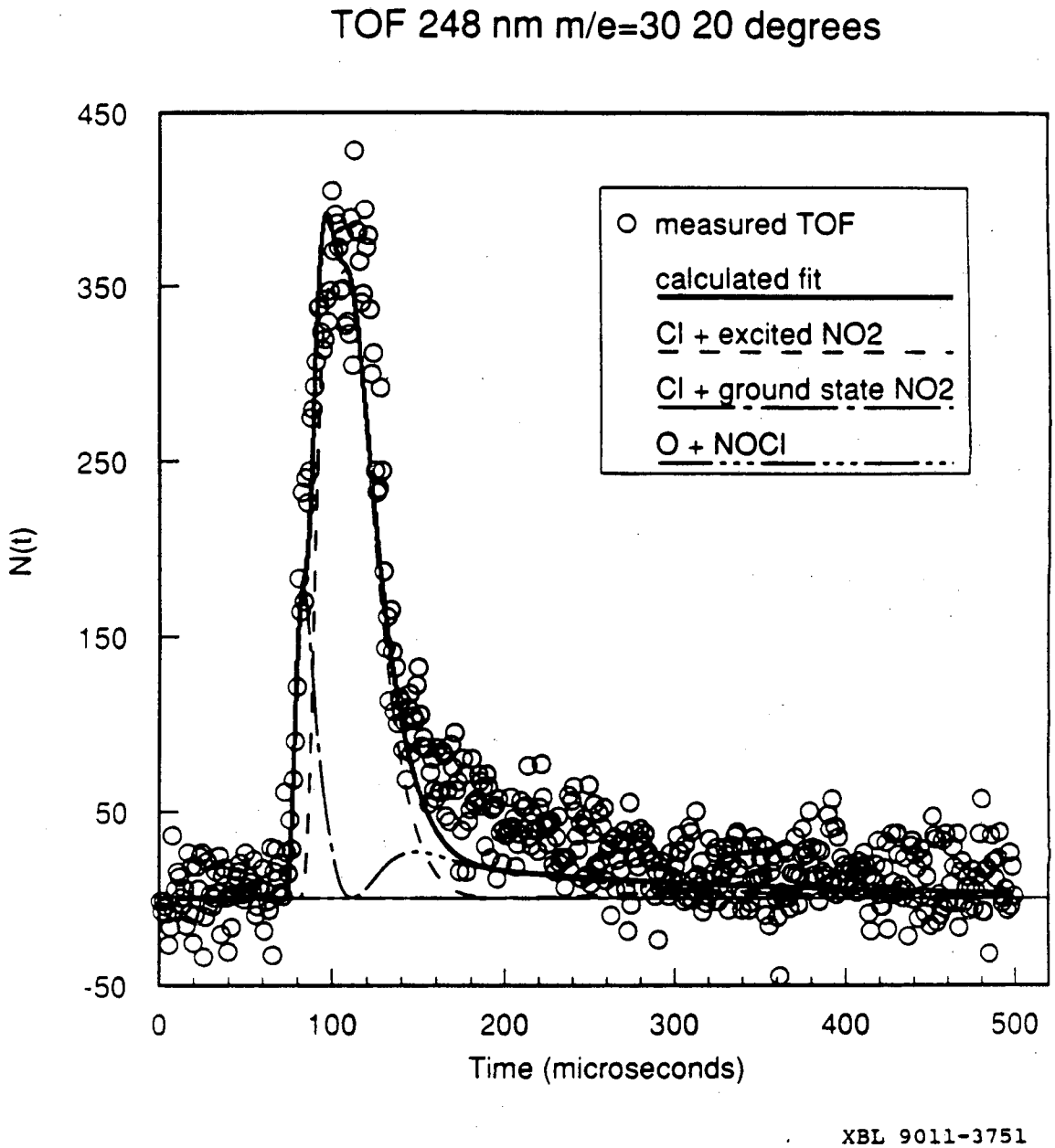
TOF 248 nm m/e=30 20 degrees
450
350
250
150
50
-50
N(t)
0
100
200
300
400
500
Time (microseconds)
measured TOF
calculated fit
Cl + excited NO2
Cl + ground state NO2
O + NOCl
XBL 9011-3751

Figure 20

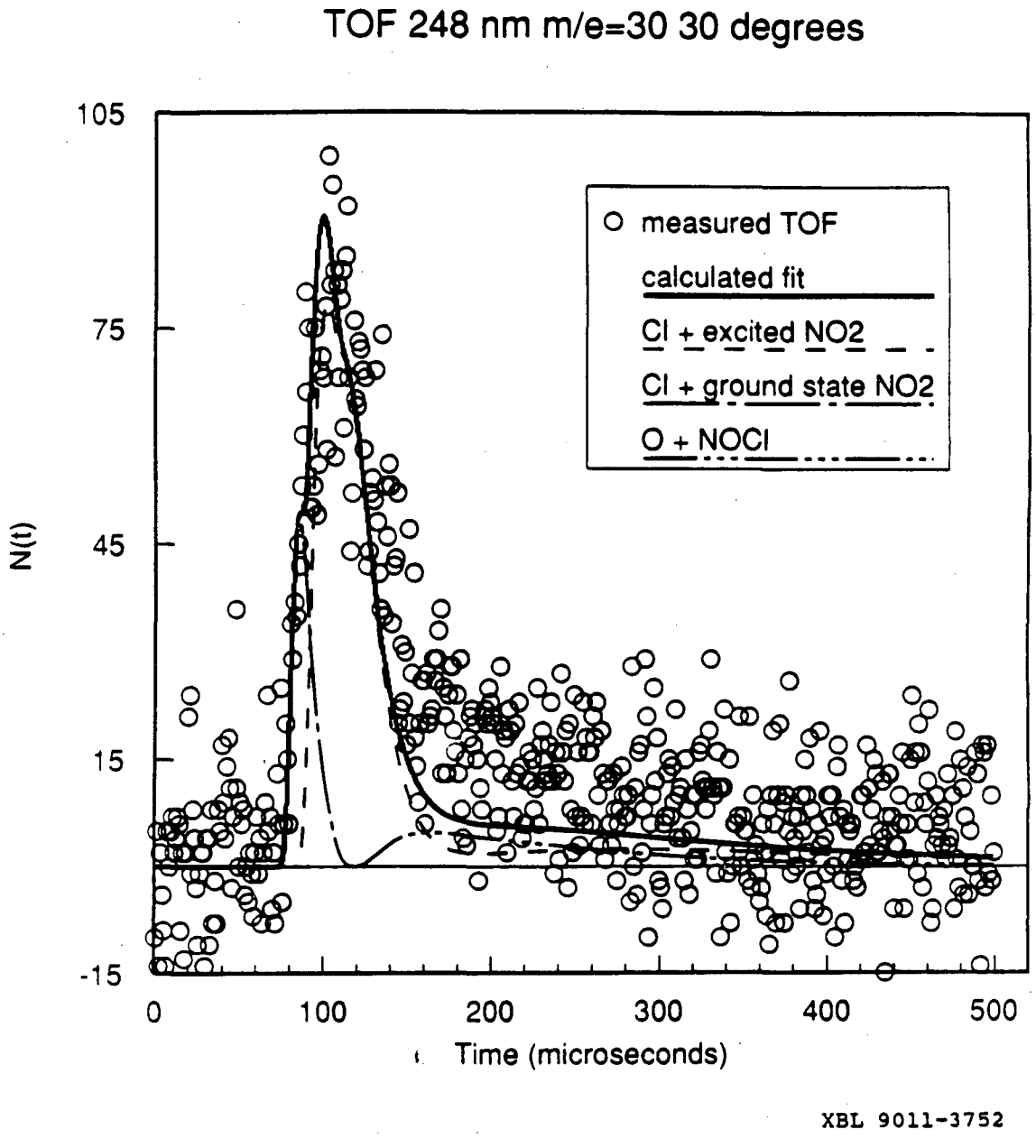
TOF 248 nm m/e=30 30 degrees
105
75
45
15
-15
N(t)
0
100
200
300
400
500
Time (microseconds)
measured TOF
calculated fit
Cl + excited NO2
Cl + ground state NO2
O + NOCl
XBL 9011-3752

Figure 21

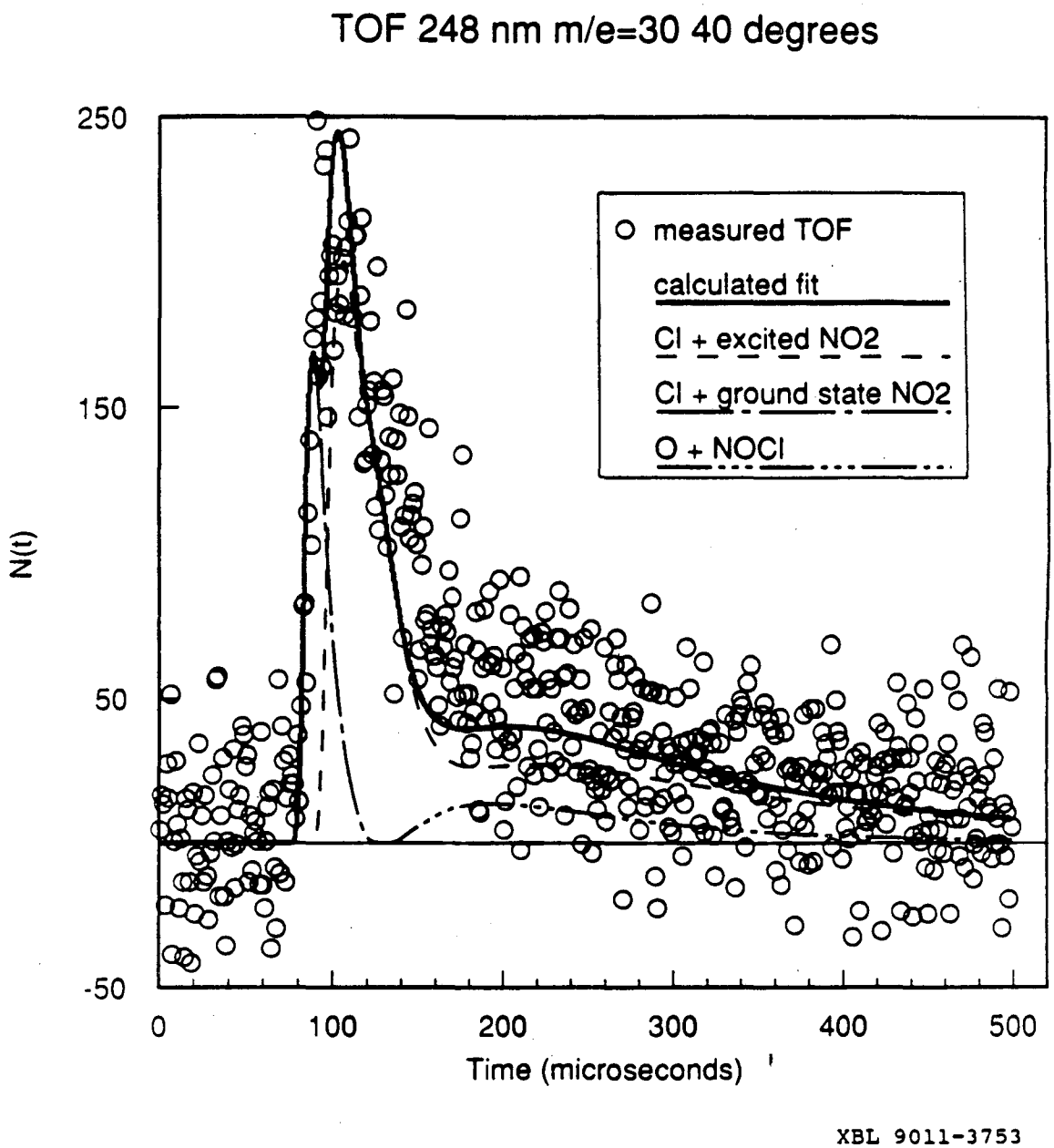
TOF 248 nm m/e=30 40 degrees
250
150
50
-50
N(t)
0
100
200
300
400
500
Time (microseconds)
measured TOF
calculated fit
Cl + excited NO2
Cl + ground state NO2
O + NOCl
XBL 9011-3753

Figure 22

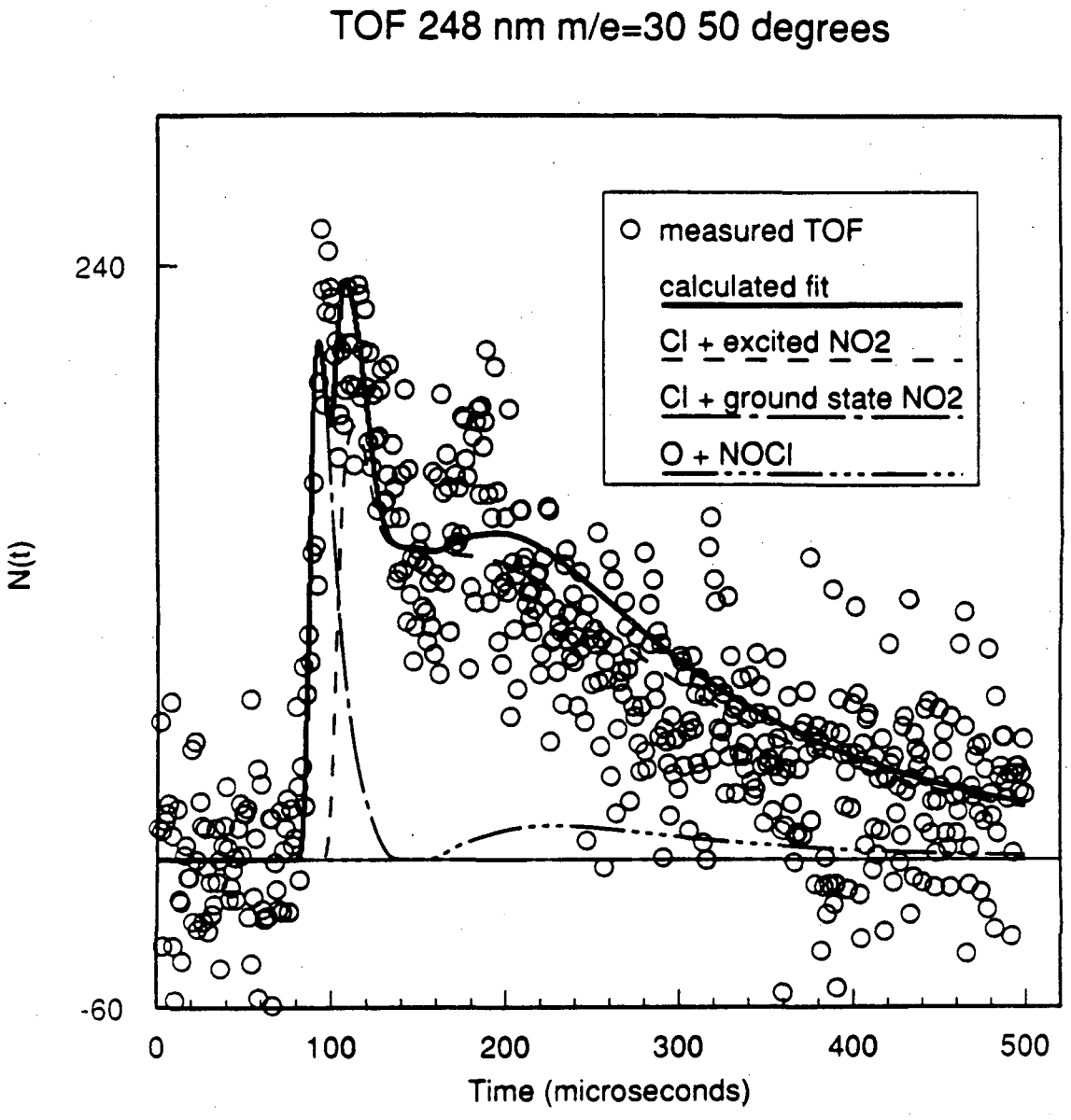
TOF 248 nm m/e=30 50 degrees
measured TOF
calculated fit
Cl + excited NO2
Cl + ground state NO2
O + NOCl
240
-60
N(t)
0
100
200
300
400
500
Time (microseconds)
XBL 9011-3754

Figure 23

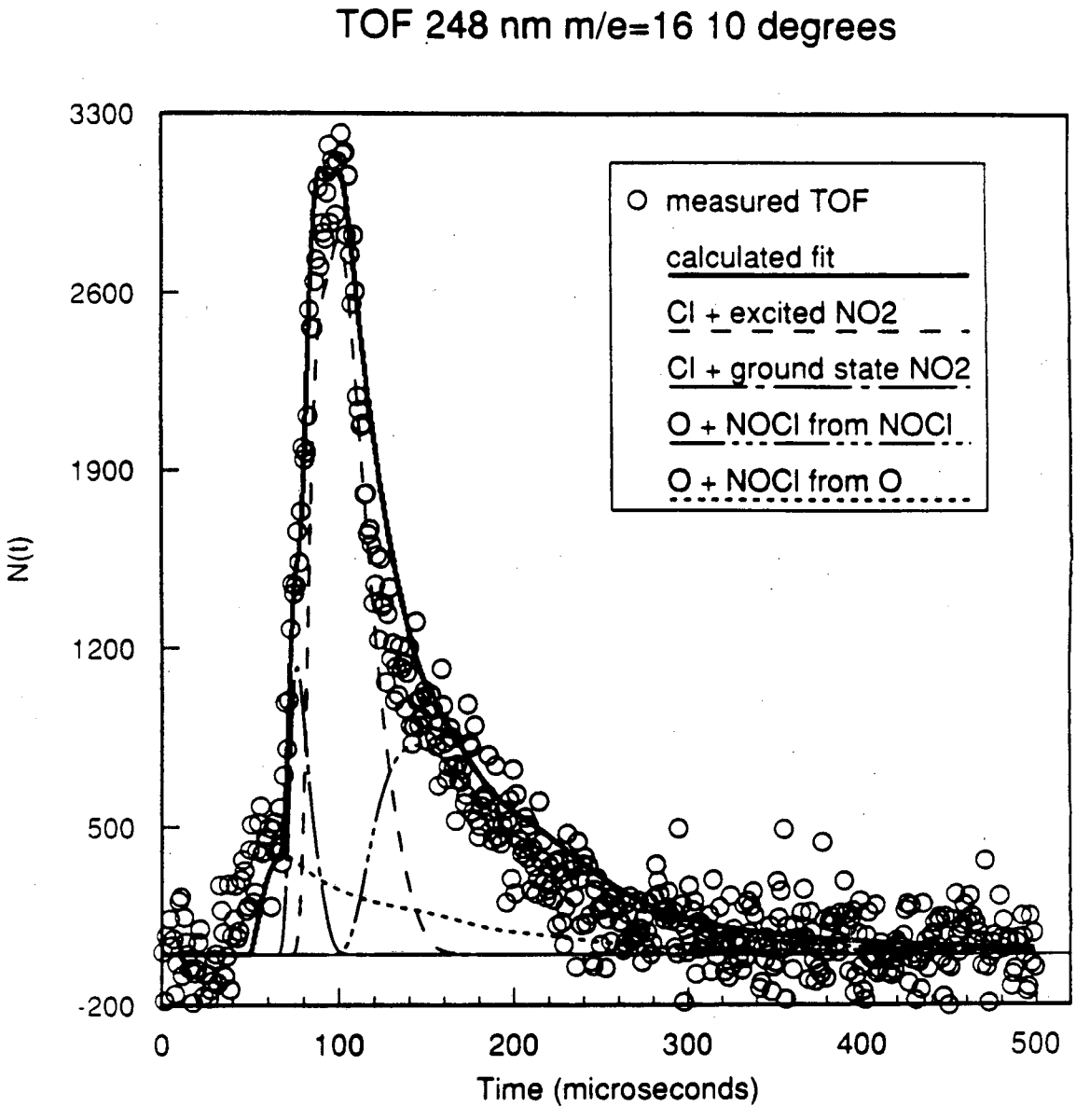
TOF 248 nm m/e=16 10 degrees
3300
2600
1900
1200
500
-200
N(t)
0
100
200
300
400
500
Time (microseconds)
measured TOF
calculated fit
Cl + excited NO2
Cl + ground state NO2
O + NOCl from NOCl
O + NOCl from O
XBL 9011-3755

Figure 24

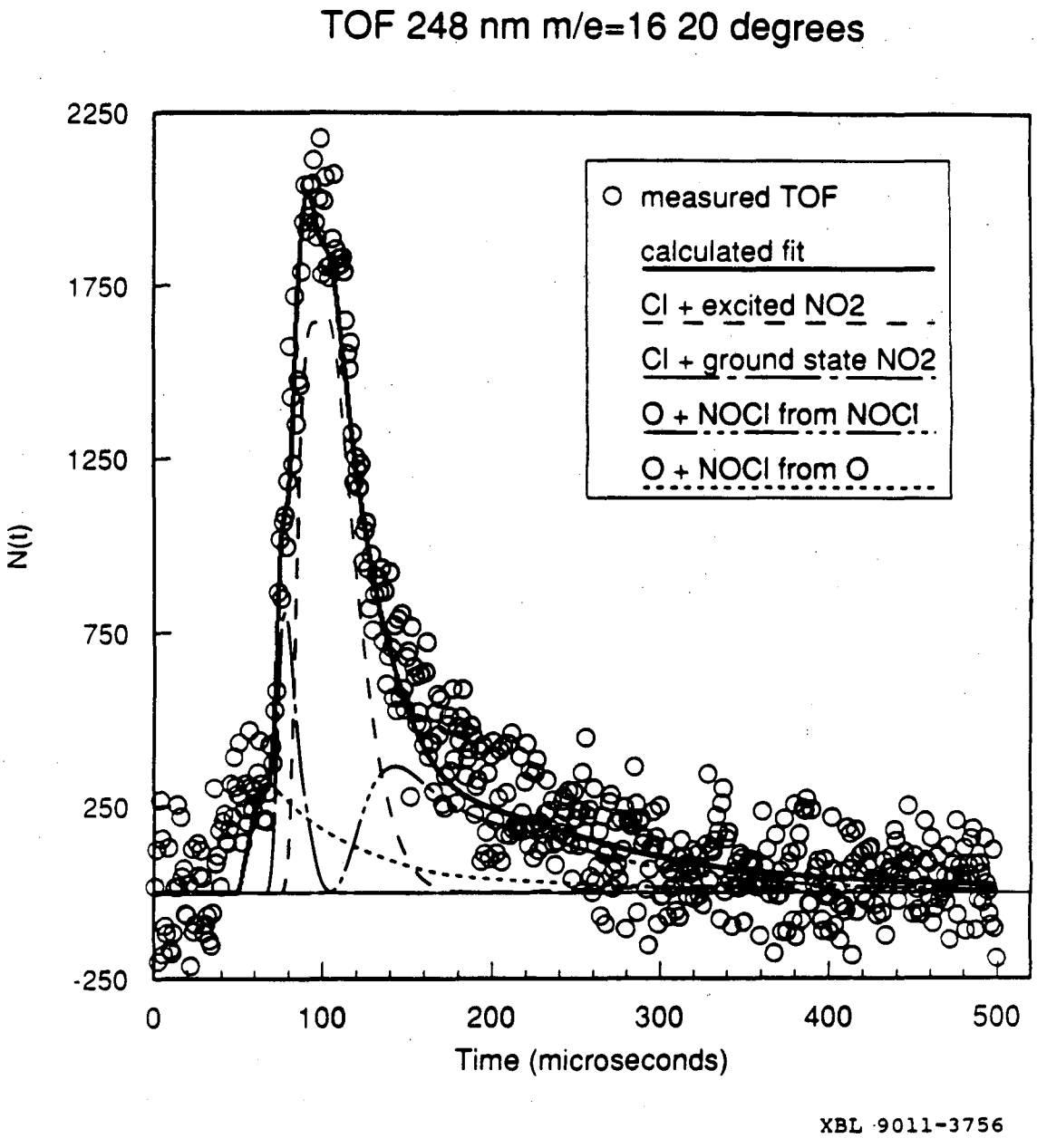
TOF 248 nm m/e=16 20 degrees
2250
1750
1250
750
250
-250
N(t)
0
100
200
300
400
500
Time (microseconds)
measured TOF
calculated fit
Cl + excited NO2
Cl + ground state NO2
O + NOCl from NOCl
O + NOCl from O
XBL 9011-3756

Figure 25

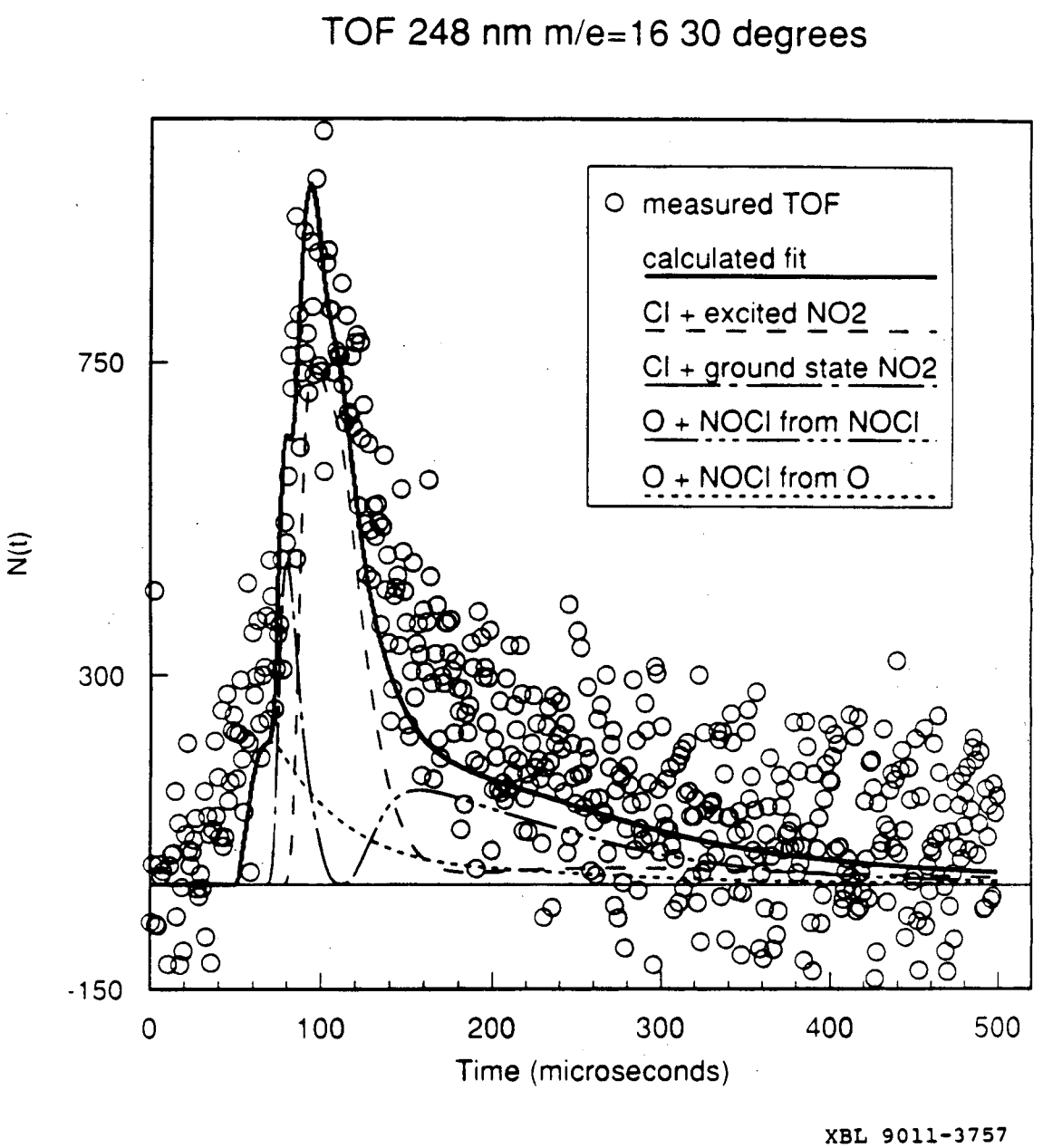
TOF 248 nm m/e=16 30 degrees
measured TOF
calculated fit
Cl + excited NO2
Cl + ground state NO2
O + NOCl from NOCl
O + NOCl from O
N(t)
750
300
-150
0
100
200
300
400
500
Time (microseconds)
XBL 9011-3757

Figure 26

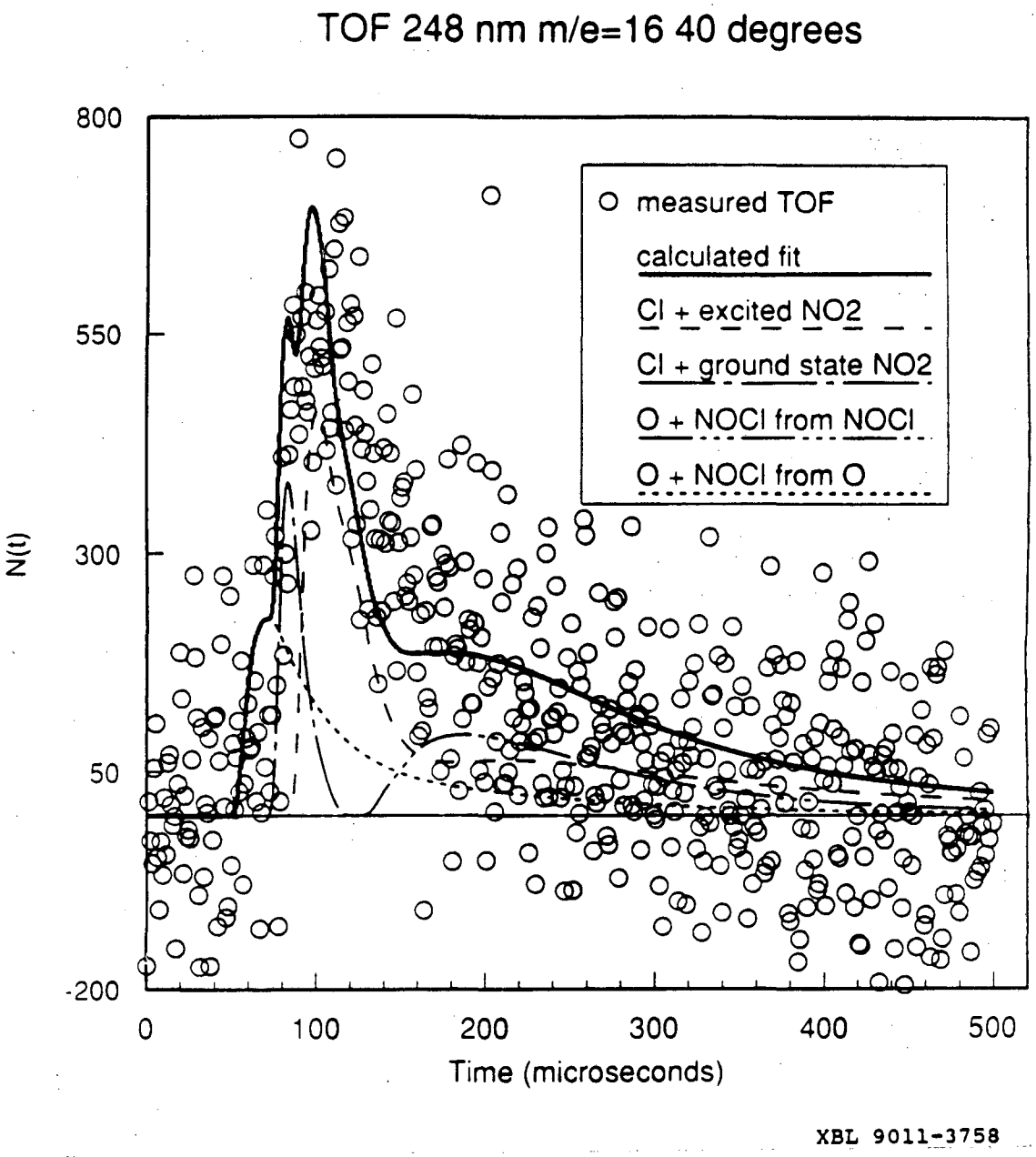
TOF 248 nm m/e=16 40 degrees
800
550
300
50
-200
N(t)
0
100
200
300
400
500
Time (microseconds)
measured TOF
calculated fit
Cl + excited NO2
Cl + ground state NO2
O + NOCl from NOCl
O + NOCl from O
XBL 9011-3758

Figure 27

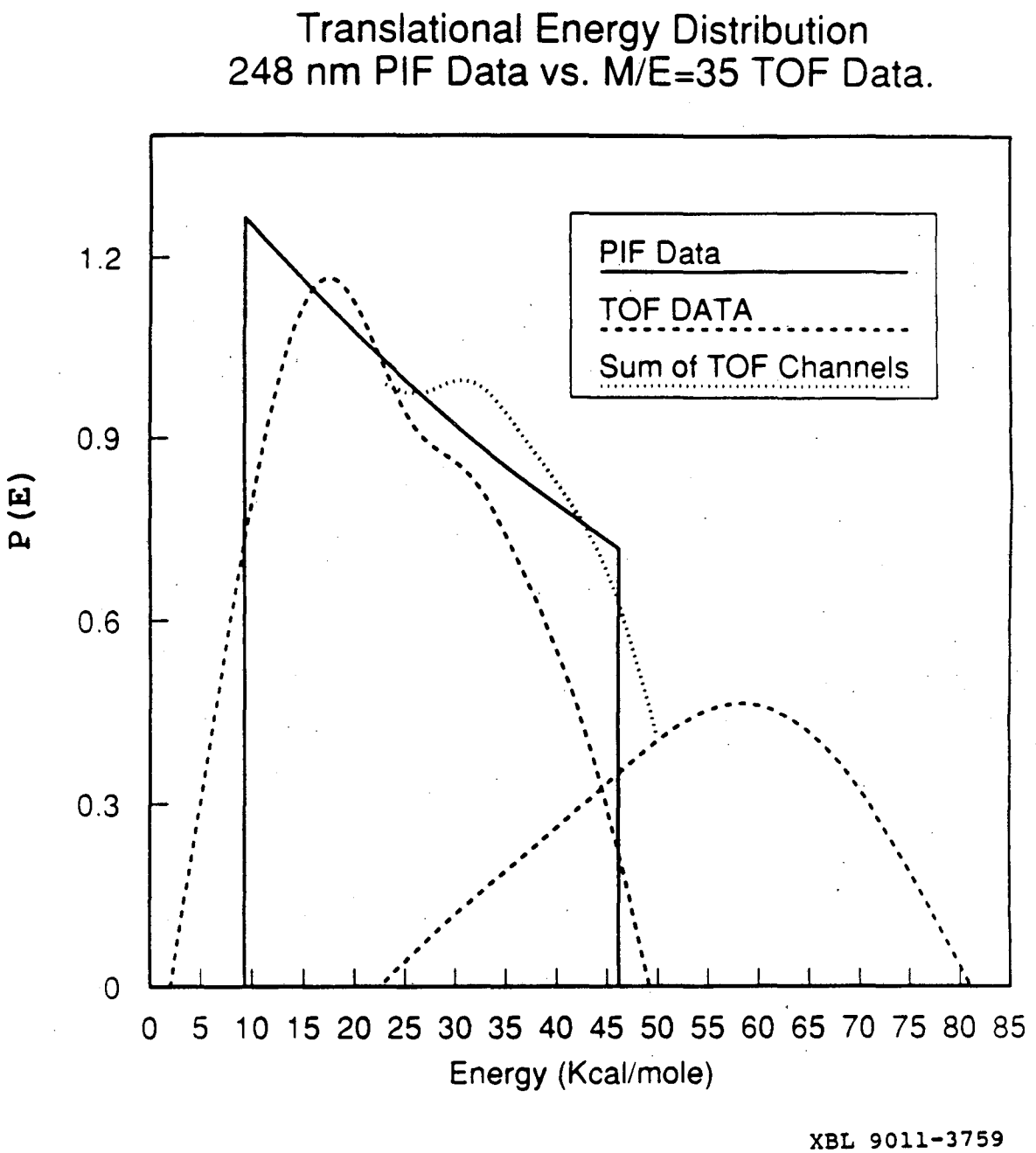
Translational Energy Distribution
248 nm PIF Data vs. M/E=35 TOF Data.
PIF Data
TOF DATA
Sum of TOF Channels
P (E)
1.2
0.9
0.6
0.3
0
0 5 10 15 20 25 30 35 40 45 50 55 60 65 70 75 80 85
Energy (Kcal/mole)
XBL 9011-3759

Figure 28

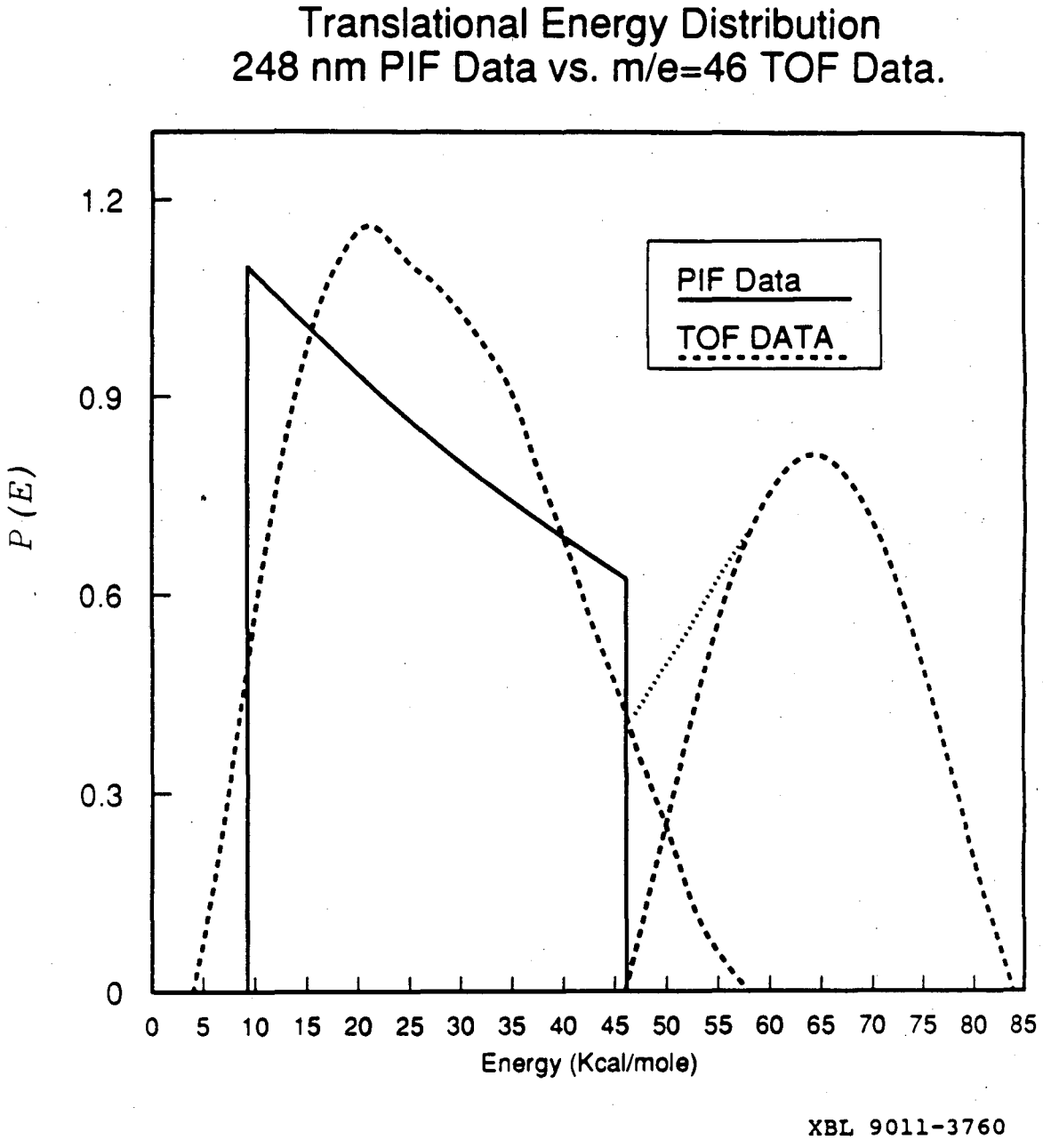
Translational Energy Distribution
248 nm PIF Data vs. m/e=46 TOF Data.
PIF Data
TOF DATA
P (E)
1.2
0.9
0.6
0.3
0
0 5 10 15 20 25 30 35 40 45 50 55 60 65 70 75 80 85
Energy (Kcal/mole)
XBL 9011-3760

Figure 29

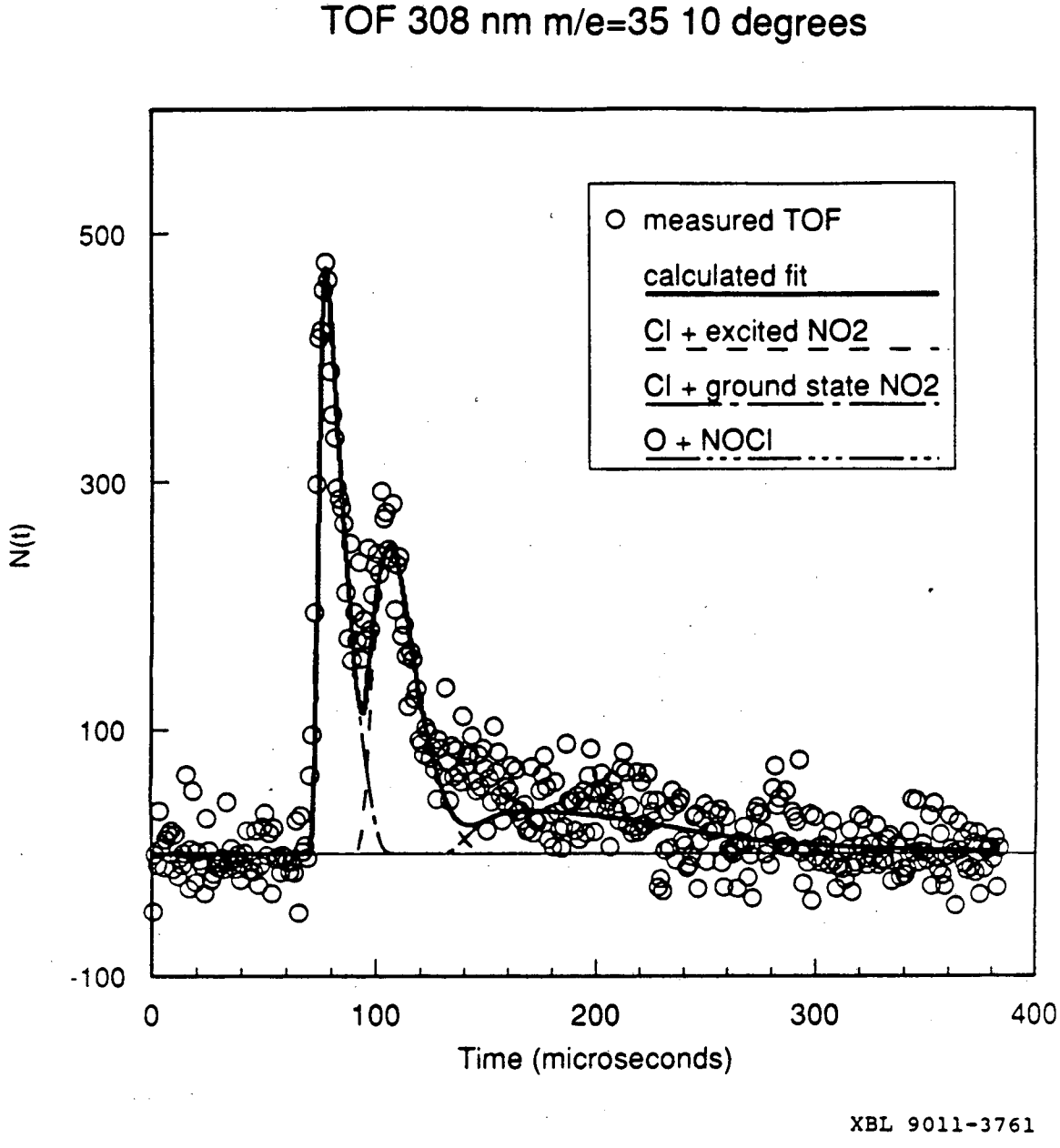
TOF 308 nm m/e=35 10 degrees
measured TOF
calculated fit
Cl + excited NO2
Cl + ground state NO2
O + NOCl
N(t)
500
300
100
-100
0
100
200
300
400
Time (microseconds)
XBL 9011-3761

Figure 30

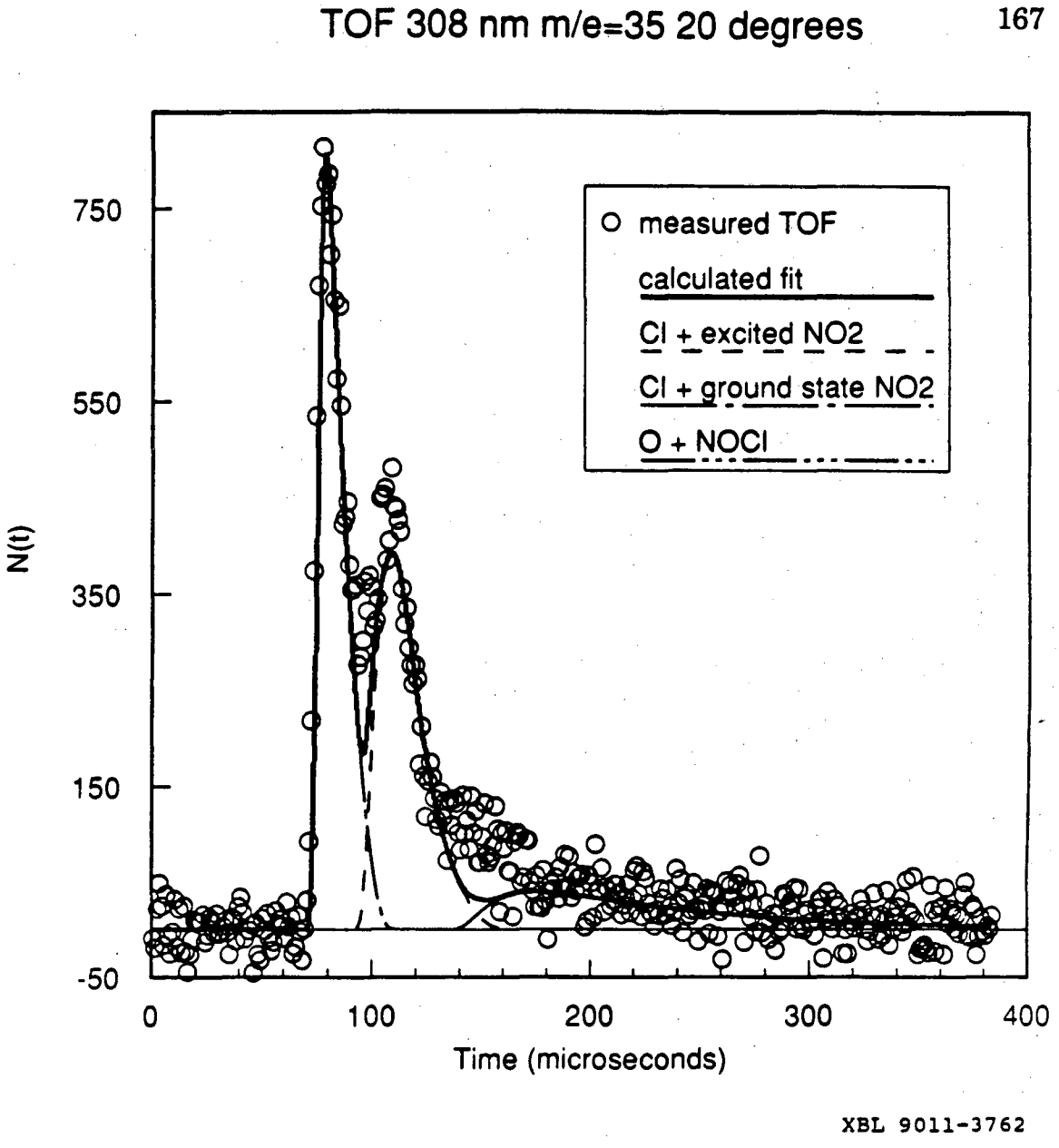
TOF 308 nm m/e=35 20 degrees
measured TOF
calculated fit
Cl + excited NO2
Cl + ground state NO2
O + NOCl
N(t)
750
550
350
150
-50
0
100
200
300
400
Time (microseconds)
XBL 9011-3762

Figure 31

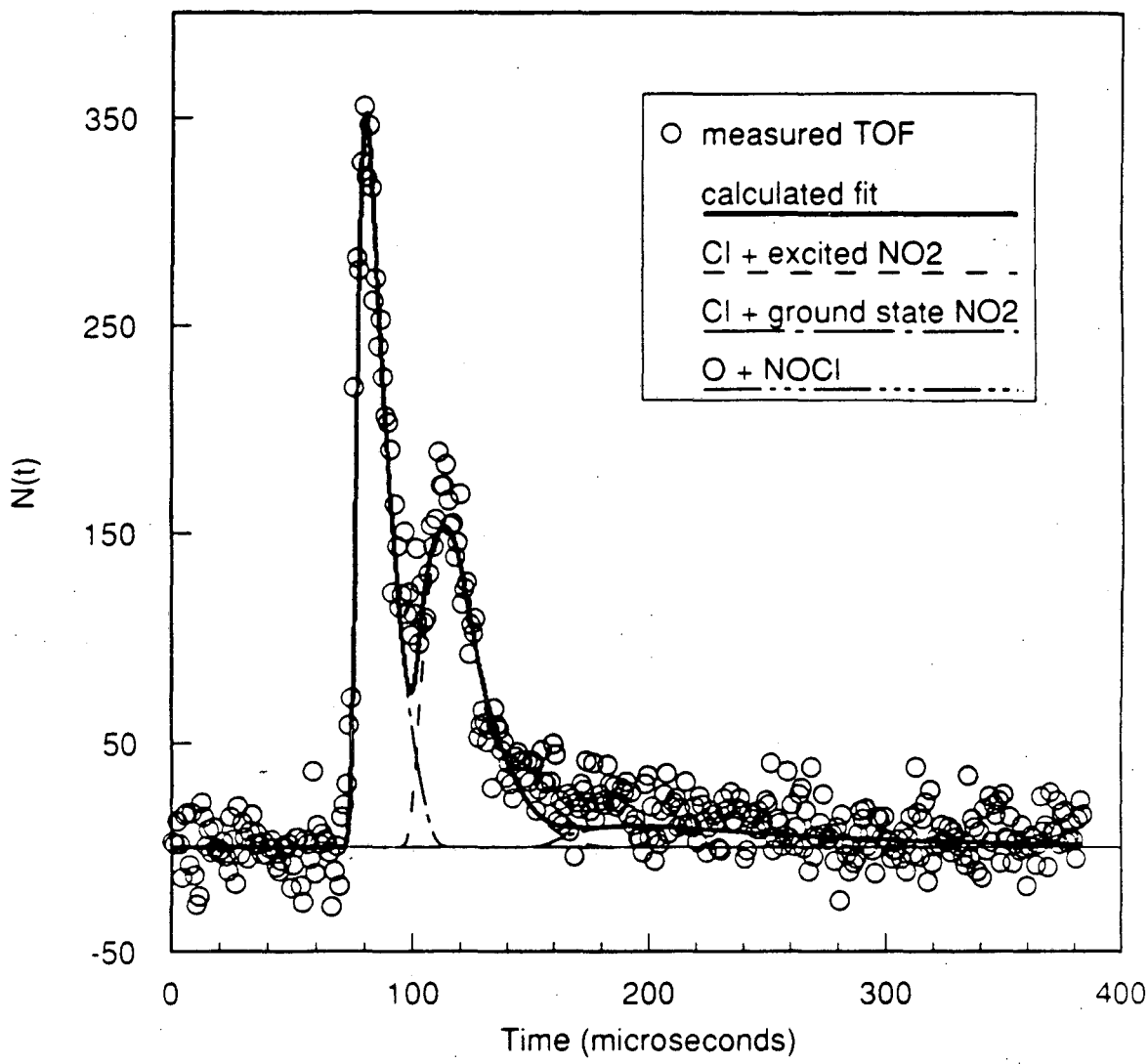
TOF 308 nm m/e=35 30 degrees
measured TOF
calculated fit
Cl + excited NO2
Cl + ground state NO2
O + NOCl
N(t)
350
250
150
50
-50
0
100
200
300
400
Time (microseconds)
XBL 9011-3763

Figure 32

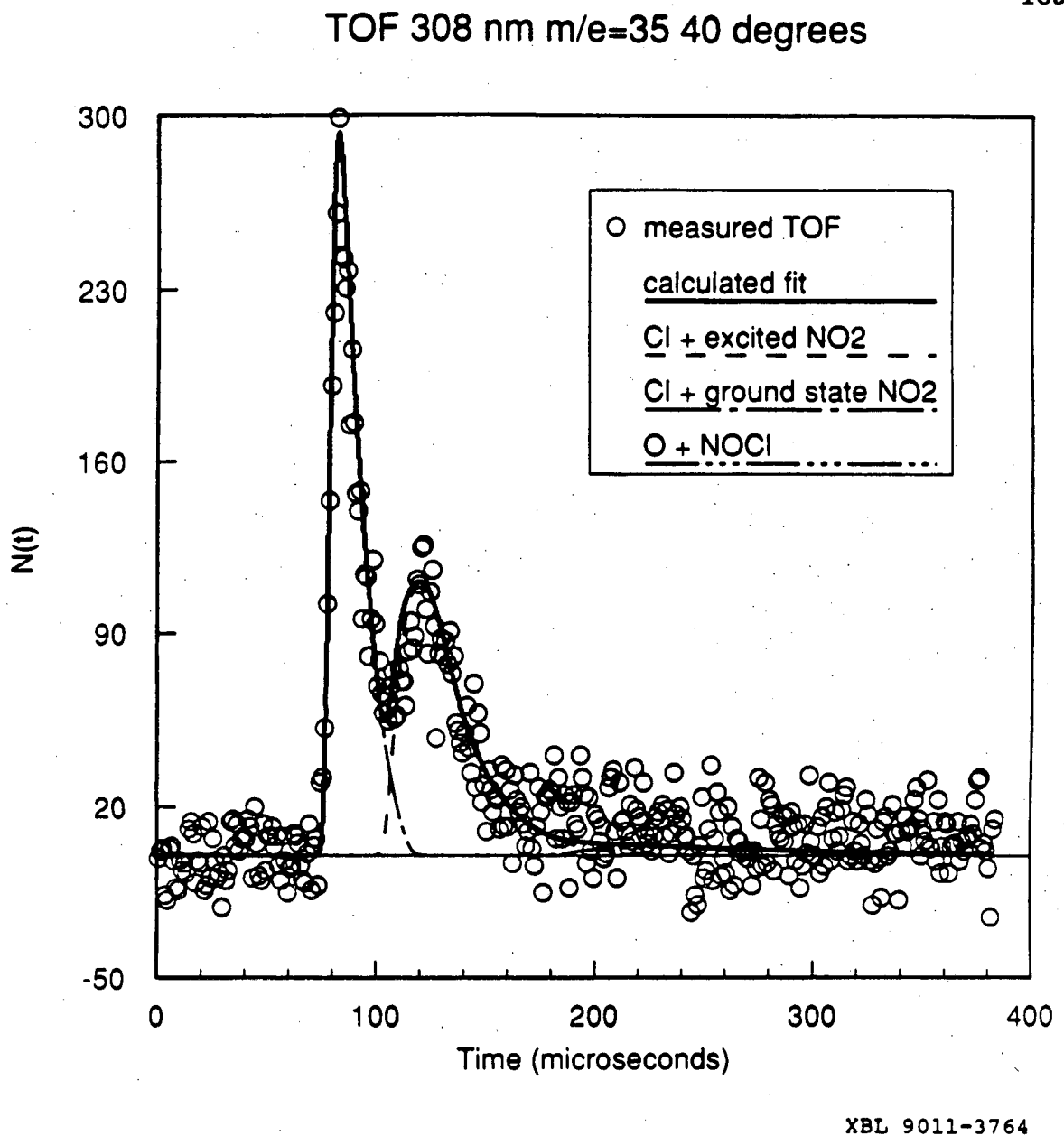
TOF 308 nm m/e=35 40 degrees
300
230
160
90
20
-50
N(t)
0
100
200
300
400
Time (microseconds)
measured TOF
calculated fit
Cl + excited NO2
Cl + ground state NO2
O + NOCl
XBL 9011-3764

Figure 33

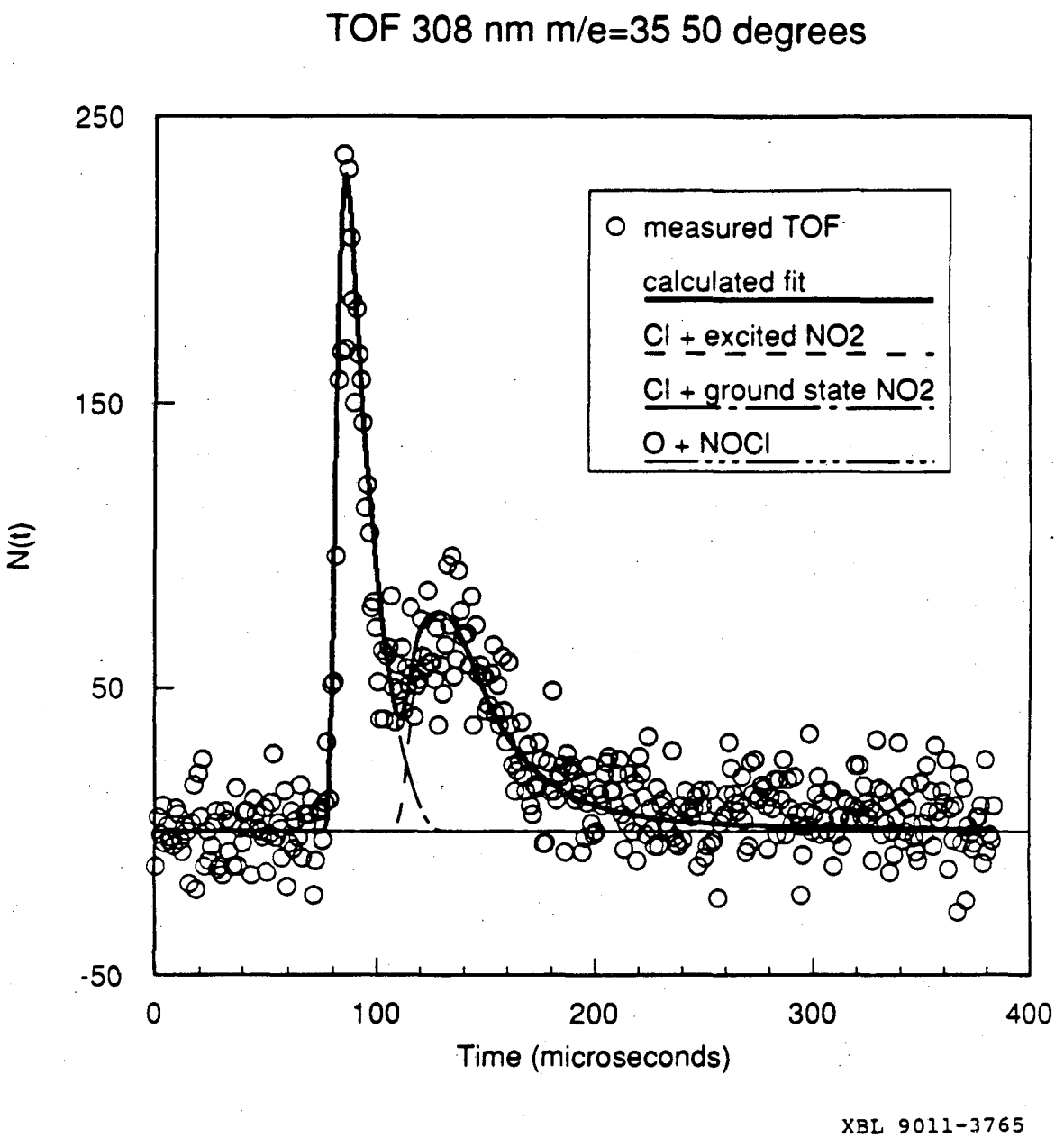
TOF 308 nm m/e=35 50 degrees
250
150
50
-50
N(t)
0
100
200
300
400
Time (microseconds)
measured TOF
calculated fit
Cl + excited NO2
Cl + ground state NO2
O + NOCl
XBL 9011-3765

Figure 34

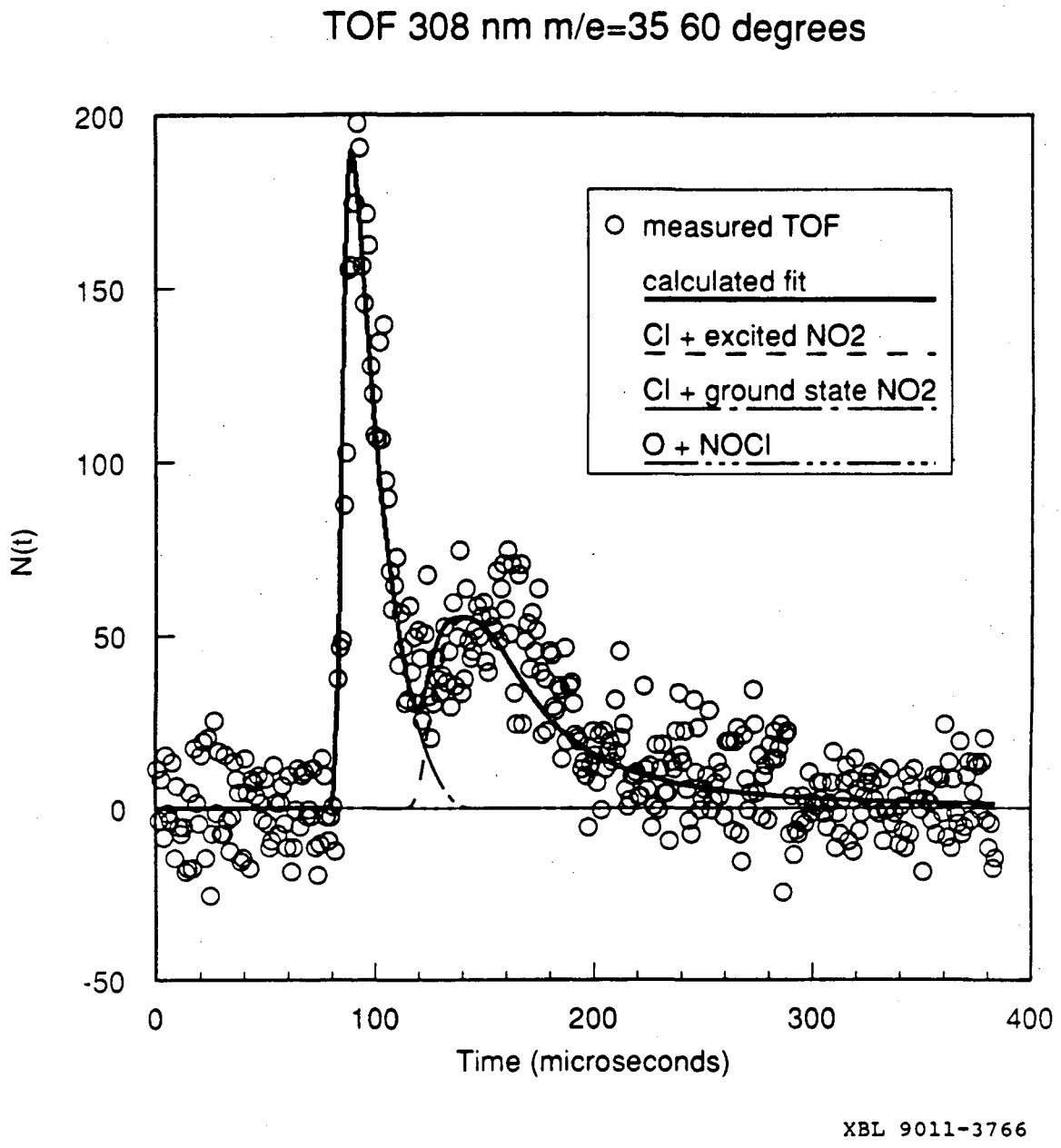
TOF 308 nm m/e=35 60 degrees
200
150
100
50
0
-50
N(t)
0
100
200
300
400
Time (microseconds)
measured TOF
calculated fit
Cl + excited NO2
Cl + ground state NO2
O + NOCl
XBL 9011-3766

Figure 35

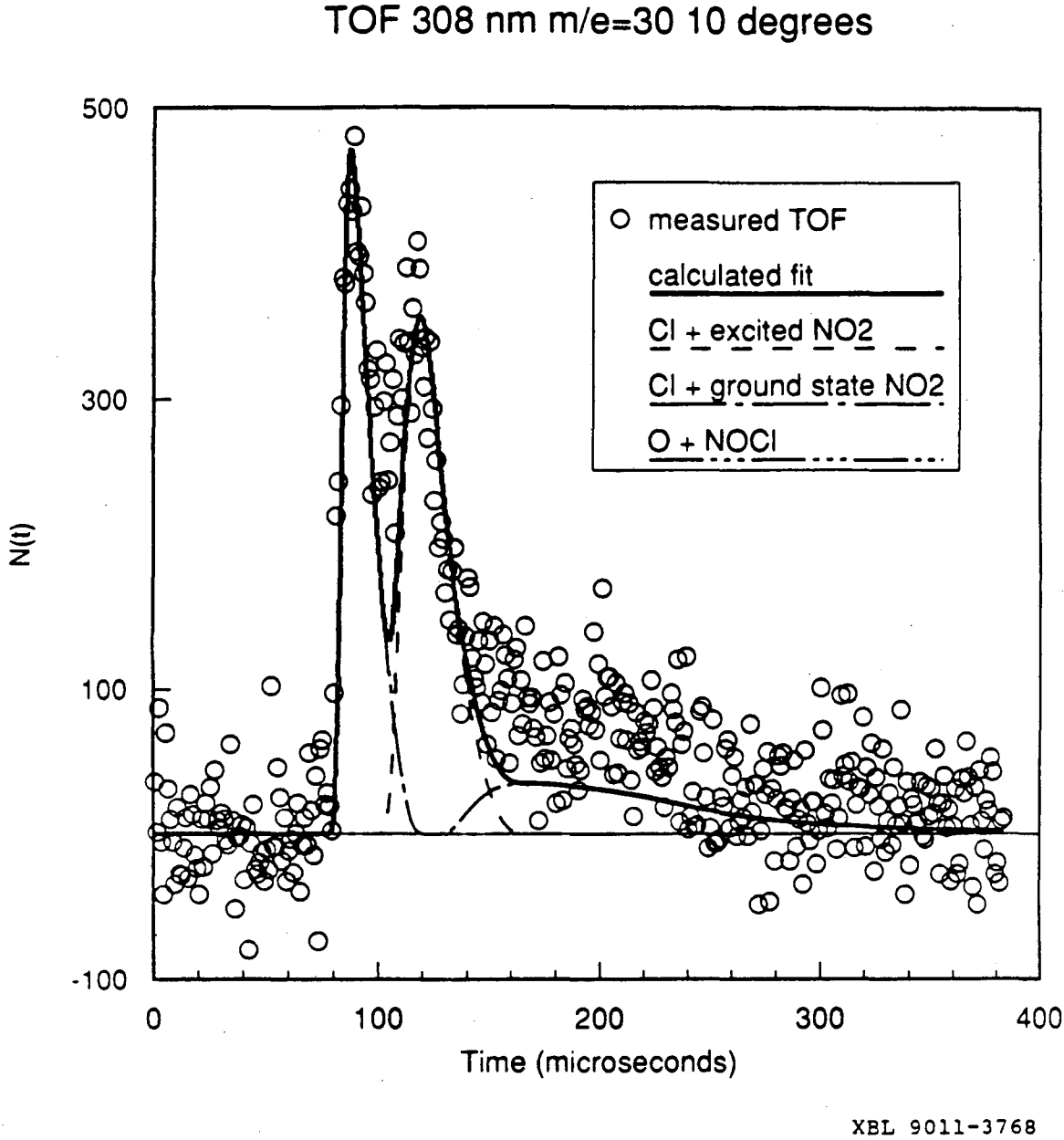
TOF 308 nm m/e=30 10 degrees
500
300
100
-100
N(t)
0
100
200
300
400
Time (microseconds)
measured TOF
calculated fit
Cl + excited NO2
Cl + ground state NO2
O + NOCl
XBL 9011-3768

Figure 36

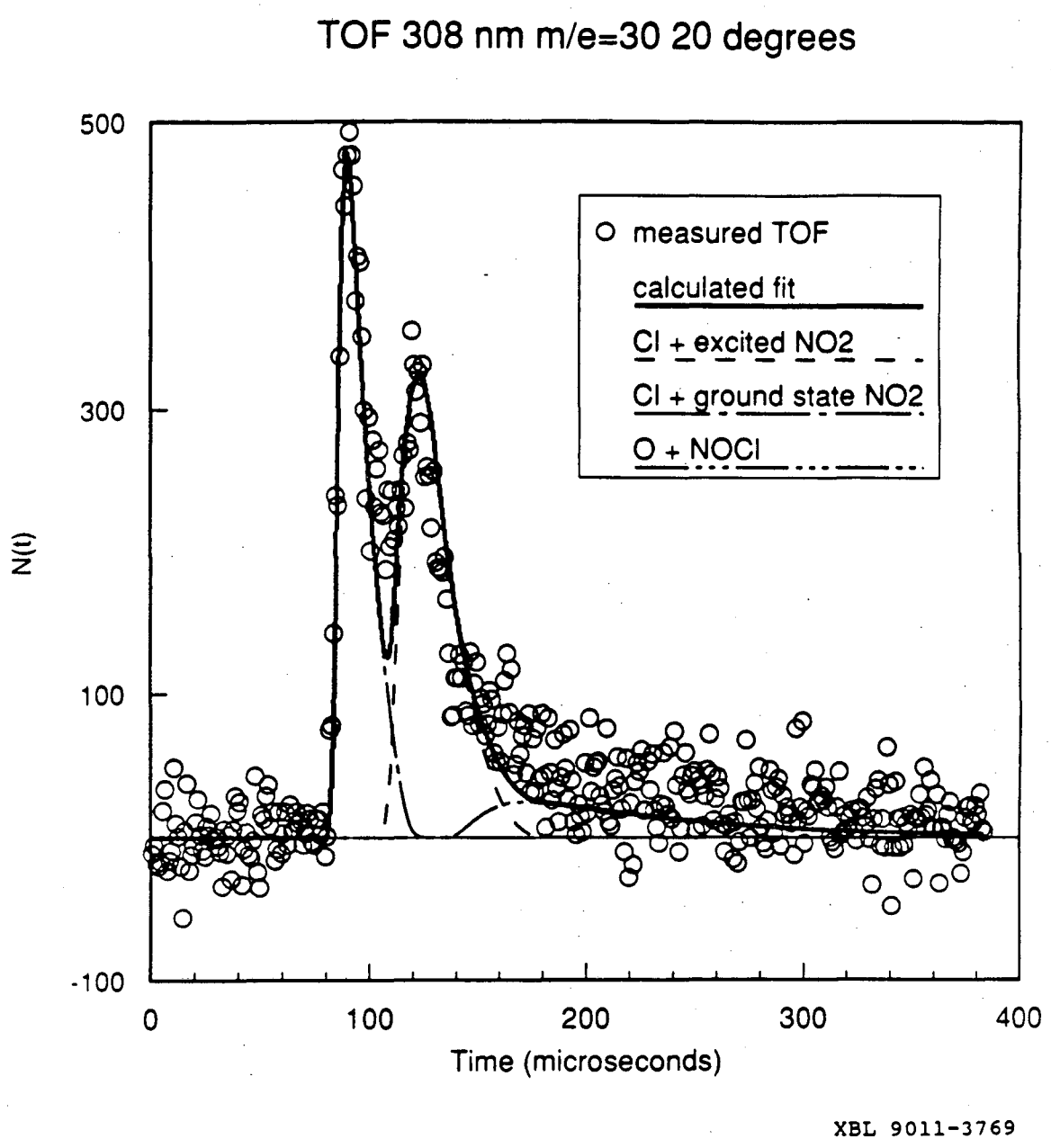
TOF 308 nm m/e=30 20 degrees
500
300
100
-100
N(t)
0
100
200
300
400
Time (microseconds)
measured TOF
calculated fit
Cl + excited NO2
Cl + ground state NO2
O + NOCl
XBL 9011-3769

Figure 37

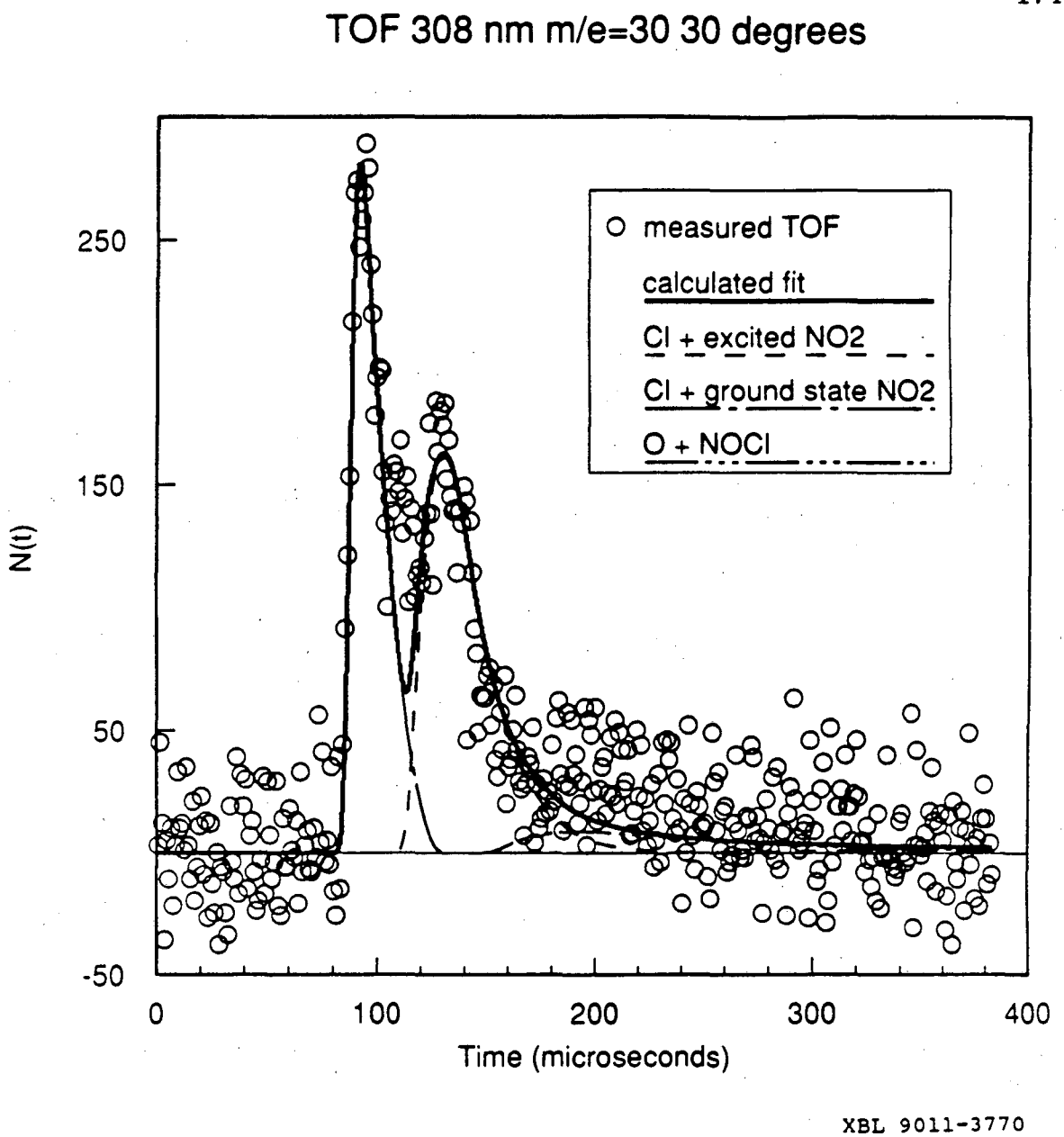
TOF 308 nm m/e=30 30 degrees
measured TOF
calculated fit
Cl + excited NO2
Cl + ground state NO2
O + NOCl
N(t)
250
150
50
-50
0
100
200
300
400
Time (microseconds)
XBL 9011-3770

Figure 38

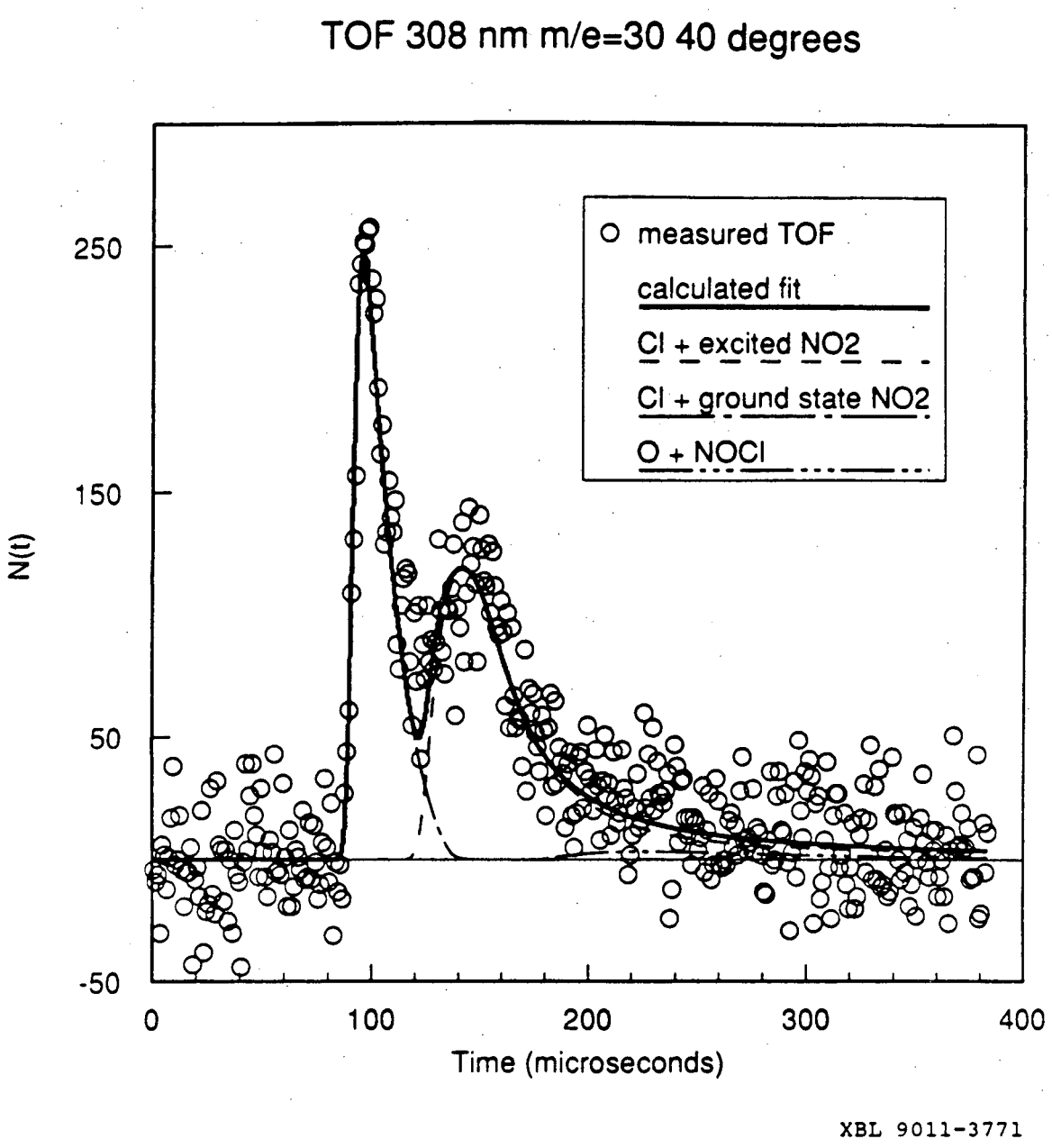
TOF 308 nm m/e=30 40 degrees
measured TOF
calculated fit
Cl + excited NO2
Cl + ground state NO2
O + NOCl
N(t)
250
150
50
-50
0
100
200
300
400
Time (microseconds)
XBL 9011-3771

Figure 39

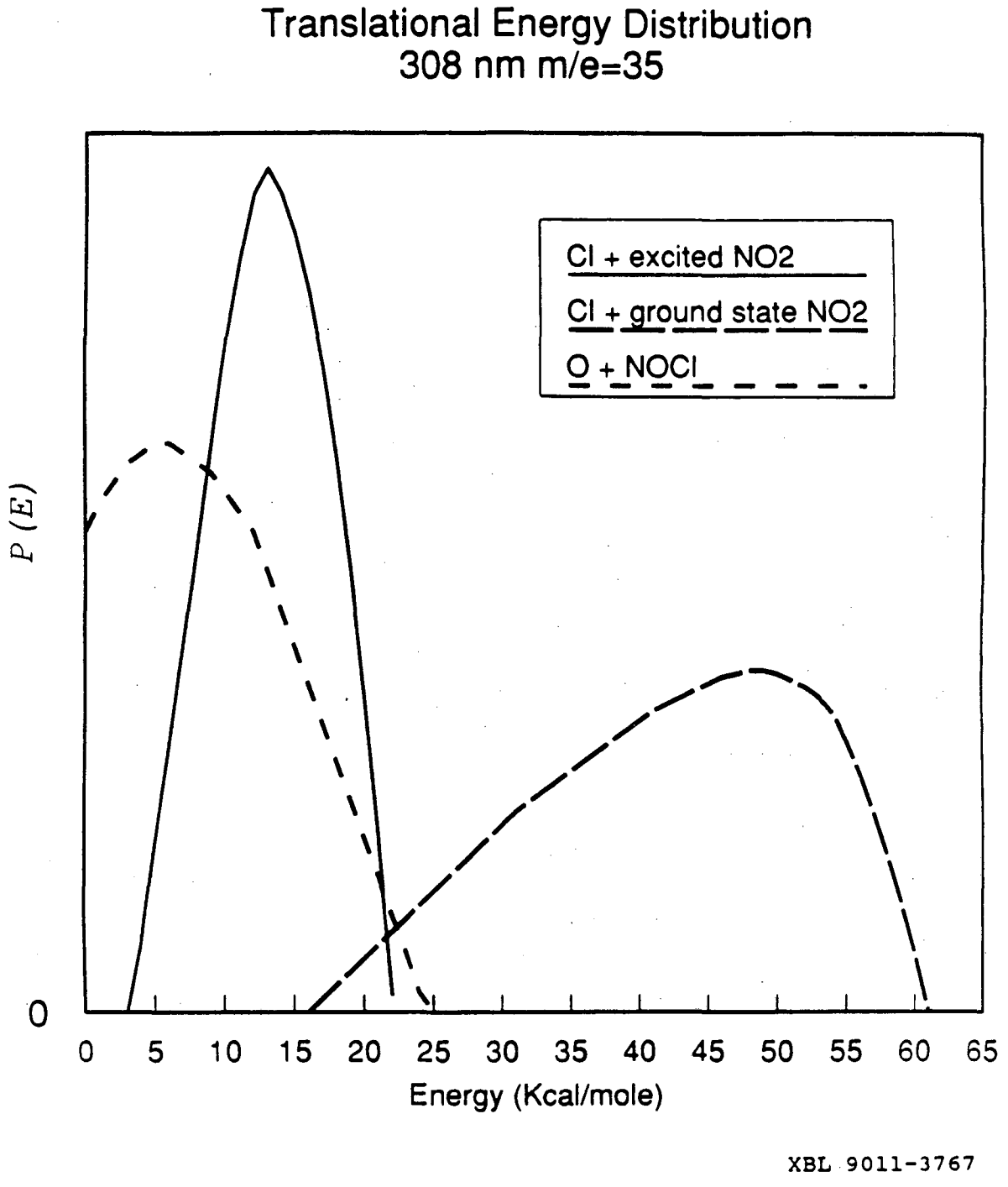
Translational Energy Distribution
308 nm m/e=35
Cl + excited NO2
Cl + ground state NO2
O + NOCl
P (E)
0
0 5 10 15 20 25 30 35 40 45 50 55 60 65
Energy (Kcal/mole)
XBL 9011-3767

Figure 40

LAWRENCE BERKELEY LABORATORY
UNIVERSITY OF CALIFORNIA
INFORMATION RESOURCES DEPARTMENT
BERKELEY, CALIFORNIA 94720